BANDPASS DEPENDENCE OF X-RAY TEMPERATURES IN GALAXY CLUSTERS

KENNETH W. CAVAGNOLO[1,2], MEGAN DONAHUE[1], G. MARK VOIT[1], AND MING SUN[1]

Draft version December 13, 2007

ABSTRACT

We explore the band dependence of the inferred X-ray temperature of the intracluster medium (ICM) for 193 well-observed ($N_{photons} > 1500$) clusters of galaxies selected from the *Chandra* Data Archive. If the hot gas in a cluster is nearly isothermal in the projected region of interest, the X-ray temperature inferred from a broad-band (0.7-7.0 keV) spectrum should be identical to the X-ray temperature inferred from a hard-band (2.0-7.0 keV) spectrum. However, if there is soft X-ray emission contributed by unresolved cooler lumps of gas or by non-thermal processes, the temperature of a best-fit single-component thermal model will be cooler for a broad-band spectrum than for a hard-band spectrum. Using this difference as a diagnostic, the ratio of hard-band and full-band temperatures may indicate soft contamination even when the X-ray spectrum itself may not have sufficient signal-to-noise to resolve multiple temperature components. To test this possible diagnostic, we extract X-ray spectra from an annular region between $R = 70$ kpc and $R = R_{2500}$, R_{5000} for each cluster in our archival sample. We compare the X-ray temperatures inferred for single-temperature fits of global spectra when the energy range of the fit is 0.7-7.0 keV (full) and when the energy range is 2.0/(1+z)-7.0 keV (hard). We find that the hard-band temperature is significantly higher, on average, than the full-band temperature. Upon further exploration, we find this ratio, $T_{HFR} = T_{2.0-7.0}/T_{0.7-7.0}$, is enhanced preferentially for clusters which are known merger systems and for clusters which are nearly isothermal. Clusters with temperature decrements in their cores (known as cool-core clusters) tend to have best-fit hard-band temperatures that are statistically consistent with their best-fit full-band temperatures. We show, using simulated spectra, that this test is sensitive to cool components with emission measures > 10% of the hot component for $2.0 \leq T_X \leq 15.0$ keV and for $z < 0.6$.

Subject headings: catalogs – galaxies: clusters: general – X-rays: galaxies: clusters – cosmology: observations – methods: data analysis

1. INTRODUCTION

Cluster mass functions and the evolution of the cluster mass function are useful for measuring cosmological parameters (e.g., Evrard (1989); Wang & Steinhardt (1998); Haiman et al. (2001); Hu (2003); Wang et al. (2004)). Cluster evolution tests the effect of dark matter and dark energy on the evolution of dark matter haloes, and therefore provides a complementary and distinct constraint on cosmological parameters to those tests which constrain them geometrically (e.g., supernovae (Riess et al. 1998, 2007) and baryon acoustic oscillations (Eisenstein et al. 2005)).

However, clusters are a useful cosmological tool only if we can infer cluster masses from observable properties such as X-ray luminosity, X-ray temperature, lensing shear, optical luminosity, or galaxy velocity dispersion. Empirically, the relationship of mass and these observable properties is well-established (Voit 2005). However, if we could identify a "2nd parameter" – possibly reflecting the degree of relaxation in the cluster – we could improve the utility of clusters as cosmological probes by parameterizing and reducing the scatter in mass-observable scaling relations.

Toward this end, we desire to understand the dynamical state of a cluster more quantitatively than simply identifying which clusters appear to be relaxed and those which appear to be unrelaxed, because most clusters are likely to have a dynamical state which is somewhere in between (O'Hara et al. 2006; Kravtsov et al. 2006). The degree to which a cluster is virialized must be quantified within simulations and then observationally calibrated with an unbiased statistical sample of clusters.

One study that examined how relaxation affects the observable properties of clusters was performed by Mathiesen & Evrard (2001) (hereafter ME01) using the ensemble of simulations by Mohr & Evrard (1997). ME01 found that most clusters which had experienced a recent merger were cooler than the cluster mass-observable scaling relations predicted. They attributed this to the presence of cool, spectroscopically unresolved accreting subclusters which introduced energy into the ICM and which have a long timescale for dissipation. The consequence was an under-prediction of cluster binding masses of $15 - 30\%$ (Mathiesen & Evrard 2001).

One method of quantifying cluster substructure – a property which results in biased cluster temperatures and therefore effects accurate cluster mass determination – employs the ratios of X-ray surface brightness moments to quantify the degree of relaxation (Buote & Tsai 1995, 1996; Jeltema et al. 2005). Although an excellent tool, power ratio suffers from being aspect dependent, much like other substructure measures such as axial ratio or centroid variation (Jeltema et al. 2007; Ventimiglia et al. 2008). ME01 found an auxiliary measure of substructure which does not depend on perspective and could be combined with power ratio, axial ratio, and centroid variation to yield a more robust metric for quantifying a cluster's degree of relaxation. They found hard-band (2.0_{rest}-9.0 keV) temperatures were $\sim 20\%$ hotter than broad-band (0.5-9.0 keV) temperatures. This can be viewed in two ways: as a cooler broad-band temperature caused by unresolved accreting cool subclusters contributing significant amounts of line emission to the soft-band ($E < 2$ keV) (an effect confirmed by Mazzotta et al. (2004) and Vikhlinin (2006) using simulated *Chandra* and *XMM-Newton* spectra), or as a hotter hard-band temperature caused by shock heating from accretion.

[1] Department of Physics and Astronomy, Michigan State University, BPS Building, East Lansing, MI 48824
[2] cavagnolo@pa.msu.edu

ME01 suggested that this temperature skewing, and consequently the fingerprint of merging, could be detected utilizing the energy resolution and soft-band sensitivity of *Chandra*. They proposed selecting a sufficiently large sample of clusters covering a broad dynamical range, fitting a single-component temperature to the hard band and full band, and then checking for a net skew above unity in the hard band to full band temperature ratio.

In this paper we present the findings of just such a temperature-ratio test using *Chandra* archival data. We find the hard-band temperature exceeds the broad-band temperature, on average, by $\sim 16\%$ in multiple flux-limited samples of X-ray clusters from the *Chandra* archive. This mean excess is weaker than the 20% predicted by ME01, but is significant at the 12σ level nonetheless. Hereafter, we refer to the hard-band to full-band temperature ratio as T_{HFR}. We also find that the non-cool core systems and mergers tend to have higher values of T_{HFR}. This study suggests that T_{HFR} is an indicator of a cluster's temporal proximity to the most recent merger event.

This paper proceeds in the following manner. In §2 we outline sample selection criteria and *Chandra* observations selected under these criteria. Data reduction and handling of the X-ray background is discussed in §3. Spectral extraction is discussed in §4 while fitting and simulated spectra are discussed in §5. Results and discussion of our analysis are presented in §6. A summary of our work is presented in §7. For this work we have assumed a flat ΛCDM Universe with cosmology $\Omega_M = 0.3$, $\Omega_\Lambda = 0.7$, and $H_0 = 70$ km s^{-1} Mpc^{-1}. All quoted uncertainties are at the 1.6σ level (90% confidence).

2. SAMPLE SELECTION

Our sample is selected from observations publicly available in the *Chandra* X-ray Telescope's Data Archive (CDA). Our initial selection pass came from the *ROSAT* Brightest Cluster Sample (Ebeling et al. 1998), RBC Extended Sample (Ebeling et al. 2000), and *ROSAT* Brightest 55 Sample (Edge et al. 1990; Peres et al. 1998). The portion of our sample at $z \gtrsim 0.4$ can also be found in a combination of the *Einstein* Extended Medium Sensitivity Survey (Gioia et al. 1990), North Ecliptic Pole Survey (Henry et al. 2006), *ROSAT* Deep Cluster Survey (Rosati et al. 1995), *ROSAT* Serendipitous Survey (Vikhlinin et al. 1998), and Massive Cluster Survey (Ebeling et al. 2001). We later extended our sample to include clusters found in the REFLEX Survey (Böhringer et al. 2004). Once we had a master list of possible targets, we cross-referenced this list with the CDA and gathered observations where a minimum of R_{5000} (defined below) is fully within the CCD field of view.

R_{Δ_c} is defined as the radius at which the average cluster density is Δ_c times the critical density of the Universe, $\rho_c = 3H_0^2/8\pi G$. For our calculations of R_{Δ_c} we adopt the relation from Arnaud et al. (2002):

$$R_{\Delta_c} = 2.71 \text{ Mpc } \beta_T^{1/2} \Delta_z^{-1/2} (1+z)^{-3/2} \left(\frac{kT_X}{10 \text{ keV}} \right)^{1/2} \quad (1)$$

$$\Delta_z = \frac{\Delta_c \Omega_M}{18\pi^2 \Omega_z}$$

$$\Omega_z = \frac{\Omega_M(1+z)^3}{[\Omega_M(1+z)^3] + [(1-\Omega_M-\Omega_\Lambda)(1+z)^2] + \Omega_\Lambda}$$

where R_{Δ_c} is in units of h_{70}^{-1}, Δ_c is the assumed density contrast of the cluster at R_{Δ_c}, and β_T is a numerically determined, cosmology-independent ($\lesssim \pm 20\%$) normalization for

the virial relation $GM/2R = \beta_T kT_{vir}$. We use $\beta_T = 1.05$ taken from Evrard et al. (1996).

The result of our CDA search is a total of 374 observations of which we use 244 for 193 clusters. The bolometric ($E = 0.1 - 100$ keV) luminosities, L_{bol}, for our sample clusters plotted as a function of redshift are shown in Figure 1. These L_{bol} values are calculated from our best-fit spectral models and are limited to the region of the spectral extraction (from $R = 70$ kpc to $R = R_{2500}$, or R_{5000} in the cases where no R_{2500} fit was possible).

Basic properties of our sample are listed in Table 1. For the sole purpose of defining extraction regions based on fixed overdensities as discussed in §4, fiducial temperatures and redshifts were taken from the Ph.D. thesis of Don Horner[3] (all redshifts confirmed with NED[4]). We will show later the *ASCA* temperatures are sufficiently close to the *Chandra* temperatures that R_{500} is reliably estimated within 20%. Note that R_{500} is only proportional to $T^{1/2}$, so a 20% error in the temperature leads to only a 10% error in R_{500}, which in turn affects our final results imperceptibly. For clusters not listed in Horner's thesis, we used a literature search to find previously measured temperatures. If no published value could be located, we measured the global temperature by recursively extracting a spectrum in the region $0.1 < r < 0.2 \, R_{500}$ fitting a temperature and recalculating R_{500}. This process was repeated until three consecutive iterations produced R_{500} values which differed by $\leq 1\sigma$. This method of temperature determination has been employed in other studies, see Sanderson et al. (2006) and Henry et al. (2006) as examples.

3. *CHANDRA* DATA

3.1. *Reprocessing and Reduction*

All datasets were reduced utilizing the *Chandra* Interactive Analysis of Observations package (CIAO) and accompanying Calibration Database (CALDB). Using CIAO v3.3.0.1 and CALDB v3.2.2, standard data analysis was followed for each observation to apply the most up-to-date time-dependent gain correction and charge transfer inefficiency (CTI) correction (when appropriate) (Townsley et al. 2000).

Point sources were identified in an exposure-corrected events file using the adaptive wavelet tool wavdetect (Freeman et al. 2002). All point sources were then visually confirmed. A 2σ region surrounding each point source was automatically output by wavdetect to define an exclusion mask. We then added regions for point sources which were missed by wavdetect and deleted regions for spuriously detected "sources". Spurious sources are typically faint CCD features (chip gaps and chip edges) not fully removed after dividing by the exposure map. This process results in an events file (at "level 2") that has been cleaned of point sources.

To check for contamination from background flares or periods of excessively high background, light curve analyses were performed using Maxim Markevitch's contributed CIAO script lc_clean.sl[5]. Periods with count rates $\geq 3\sigma$ and/or a factor ≥ 1.2 of the mean background level of the observation were removed from the GTI file. As prescribed by Markevitch's cookbook[6], ACIS front-illuminated (FI) chips were analyzed in the $0.3 - 12.0$ keV range with time bins of 259.28 sec in length, and for the ACIS back-illuminated (BI)

---

[3] http://asd.gsfc.nasa.gov/Donald.Horner/thesis.html
[4] http://nedwww.ipac.caltech.edu/
[5] http://cxc.harvard.edu/contrib/maxim/acisbg/
[6] http://cxc.harvard.edu/contrib/maxim/acisbg/COOKBOOK

chips, $2.5 - 7.0$ keV energy range with time bins of 1037.12 sec.

When a FI and BI chip were both active during an observation, we compared light curves from both chips to detect long duration, soft-flares which can go undetected on the FI chips but show up on the BI chips. While rare, this class of flare must be filtered out of the data as it introduces a spectral component which artificially increases the best-fit temperature via a high energy tail. We find evidence for a long duration soft flare in the observations of Abell 1758 (David & Kempner 2004), CL J2302.8+0844, and IRAS 09104+4109. These flares were handled by removing the time period of the flare from the GTI file.

Defining the cluster "center" is essential for the later purpose of excluding cool cores from our spectral analysis (see §4). To determine the cluster center, we calculated the centroid of the flare cleaned, point-source free level-2 events file filtered to include only photons in the $0.7 - 7.0$ keV range. Before centroiding, the events file is exposure corrected and "holes" created by excluding point sources are filled using interpolated values taken from a narrow annular region just outside the hole ("holes" are not filled during spectral extraction discussed in §4). Prior to centroiding we define the emission peak by heavily binning the image, finding the peak value within a circular region extending from the peak to the chip edge (defined by the radius R_{max}), reducing R_{max} by 5%, reducing the binning by a factor of two, and finding the peak again. This process is repeated until the image is unbinned (binning factor of one). We then return to an unbinned image with an aperture centered on the emission peak with a radius R_{max} and find the centroid using CIAO's dmstat. The centroid, (x_c, y_c), for a distribution of N good pixels with co-ordinates (x_i, y_j) and values $f(x_i, y_j)$ is defined as:

$$Q = \sum_{i,j=1}^{N} f(x_i, y_i) \qquad (2)$$

$$x_c = \frac{\sum_{i,j=1}^{N} x_i \cdot f(x_i, y_i)}{Q}$$

$$y_c = \frac{\sum_{i,j=1}^{N} y_i \cdot f(x_i, y_i)}{Q}.$$

If the centroid was within 70 kpc of the emission peak the emission peak was selected as the center, otherwise the centroid was used as the center. This selection was made to ensure all "peaky" cool cores are at the cluster center thus maximizing their exclusion later in our analysis. All cluster centers are verified by-eye.

3.2. *X-ray Background*

Because we measured a global cluster temperature, specifically looking for a temperature ratio shift in energy bands which can be contaminated by the high-energy particle background or the soft local background, it was important to carefully analyze the background and subtract it from our resulting spectra. Below we outline three steps taken in handling the background: customization of blank-sky backgrounds, re-normalization of these backgrounds for variation of hard-particle count rates, and fitting of soft background residuals.

We used the blank-sky observations of the X-ray background from Markevitch et al. (2001) and supplied within the CXC CALDB. First, we compared the flux from the diffuse soft X-ray background of the *ROSAT* All-Sky Survey (*RASS*)

combined bands $R12$, $R45$, and $R67$ to the 0.7-2.0 keV flux in each extraction aperture for each observation. *RASS* combined bands give fluxes for energy ranges of 0.12-0.28 keV, 0.47-1.21 keV, and 0.76-2.04 keV respectively corresponding to $R12$, $R45$, and $R67$. For the purpose of simplifying subsequent analysis, we discarded observations with an $R45$ flux $\geq 10\%$ of the total cluster X-ray flux.

The appropriate blank-sky dataset for each observation was selected from the CALDB, reprocessed exactly as the observation was, and then reprojected using the aspect solutions provided with each observation. For observations on the ACIS-I array, we reprojected blank-sky backgrounds for chips I0-I3 plus chips S2 and/or S3. For ACIS-S observations, we created blank-sky backgrounds only for the target chip plus chips I2 and/or I3. The additional off-aimpoint chips were included only if they were active during the observation and had available blank-sky data sets for the observation time period. Off-aimpoint chips were cleaned for point sources and diffuse sources using the method outlined in §3.1.

The additional off-aimpoint chips were included in data reduction since they contain data which is farther from the cluster center and are therefore more useful in analyzing the observation background. For observations which did not have a matching off-aimpoint blank-sky background in the CALDB a source-free region of the active chips is located and used for background normalization. To normalize the hard particle component we measured fluxes for identical regions in the blank-sky field and target field in the 9.5-12.0 keV range. The effective area of the ACIS arrays above 9.5 keV is zero and thus the collected photons there are exclusively from the particle background.

A histogram of the ratios of the 9.5-12.0 keV count rate from an observation's off-aimpoint chip to that of the observation specific blank-sky background are presented in Figure 2. The majority of the observations are in agreement to $\lesssim 20\%$ of the blank-sky background rate, which is small enough to not affect our analysis. Even so, we re-normalized all blank-sky backgrounds to match the observed background.

Normalization brings the observation background and blank-sky background into agreement for $E > 2$ keV, but even after normalization, typically, there may exist a soft excess/deficit associated with the spatially varying soft Galactic background. Following the technique detailed in Vikhlinin et al. (2005) we constructed and fit soft residuals for this component. For each observation we subtracted a spectrum of the blank-sky field from a spectrum of the off-aimpoint field to create a soft residual. The residual was fit with a solar abundance, zero redshift MeKaL model (Mewe et al. 1985, 1986; Kaastra 1992; Liedahl et al. 1995) where the normalization was allowed to be negative. The resulting best-fit temperatures for all of the soft residuals identified here were between 0.2-1.0 keV, which is in agreement with results of Vikhlinin et al. (2005). The model normalization of this background component was then scaled to the cluster sky area. The re-scaled component was included as a fixed background component during fitting of a cluster's spectra.

4. SPECTRAL EXTRACTION

The simulated spectra calculated by ME01 were analyzed in the energy ranges $0.5 - 9.0$ keV and $2.0_{rest} - 9.0$ keV, but to make a reliable comparison with *Chandra* data we restricted our focus to a full energy band, $0.7 - 7.0$ keV, and a hard energy band, $2.0_{rest} - 7.0$ keV. We excluded data below 0.7 keV to avoid the effective area and quantum efficiency varia-

tions of the ACIS detectors, and excluded energies above 7.0 keV in which diffuse source emission is dominated by the background and *Chandra*'s effective area is small. We also accounted for cosmic redshift by shifting the lower energy boundary of the hard band from 2.0 keV to $2.0/(1+z)$ keV (henceforth, assume the 2.0 keV cut is in the rest frame).

ME01 calculated the relation between $T_{0.5-9.0}$ and $T_{2.0-9.0}$ using apertures of R_{200} and R_{500} in size. While it is trivial to calculate a temperature out to R_{200} or R_{500} for a simulation, such a measurement at these scales is extremely difficult with *Chandra* observations (see Vikhlinin et al. (2005) for a detailed example). Thus, we chose to extract spectra from regions with radius R_{5000} and R_{2500} when possible. Clusters analyzed only within R_{5000} are denoted in Table 1 by a dagger.

The cores of some clusters are dominated by gas at $< T_{vir}/3$ which can greatly affect the global temperature, therefore we excised the central 70 kpc of each aperture. These excised apertures are denoted by "-CORE" in the text. Recent work by Maughan (2007) has shown excising $0.15\,R_{500}$ rather than a static 70 kpc reduces scatter in mass-observable scaling relations; but such a reduction does not affect this work as the conclusions drawn from our spectral analysis are strongly related to the uncertainties of $T_{2.0-7.0}$ and not on the best-fit value of $T_{0.7-7.0}$ where the effect of a cool core is the strongest.

Although some clusters are not circular in projection, but rather are elliptical or asymmetric, we found that assuming sphericity and extracting spectra from a circular annulus did not significantly change the best-fit values. For another such example see Bauer et al. (2005).

After defining annular apertures, we extracted source spectra from the target cluster and background spectra from the corresponding normalized blank-sky dataset. By standard CIAO means we created effective area functions (ARF files) and redistribution matrices (RMF files) for each cluster using a flux-weighted map (WMAP) across the entire extraction region. The WMAP was calculated over the energy range 0.3-2.0 keV to weight calibrations that vary as a function of position on the chip. Each spectrum was then binned to contain a minimum of 25 counts per channel.

5. SPECTRAL ANALYSIS

5.1. *Fitting*

Spectra were fit with XSPEC 11.3.2ag (Arnaud 1996) using a single-temperature MeKaL model in combination with the photoelectric absorption model WABS (Morrison & McCammon 1983) to account for Galactic absorption. Galactic absorption values, N_{HI}, are taken from Dickey & Lockman (1990). The potential free parameters of the absorbed thermal model (WABS(MeKaL)) are N_{HI}, X-ray temperature (T_X), metal abundance normalized to Solar (elemental ratios taken from Anders & Grevesse (1989)), and a normalization proportional to the integrated emission measure of the cluster. Results from the fitting are presented in Table 4 and Table 5. No systematic error is added during fitting and thus all quoted errors are statistical only. Clusters with multiple independent observations had their spectra fit simultaneously and are denoted by a dagger.

Additional statistical error was introduced into the fits because of uncertainty associated with the soft local background component discussed in §3.2. To estimate the sensitivity of our best-fit temperatures to this uncertainty, we used the differences between T_X for a model using the best-fit soft background normalization and T_X for models using $\pm1\sigma$ of the soft background normalization. The statistical uncertainty of the original fit and the additional uncertainty inferred from the range of normalizations to the soft X-ray background component were then added in quadrature to produce a final error. In all cases this additional background error on the temperature was less than 10% of the total statistical error and therefore represents a minor inflation of the error budget.

In all fits the metal abundance was a free parameter. When comparing fits with fixed Galactic column density with those where it was a free parameter, we found that neither the goodness of fit per free parameter nor the best-fit T_X were significantly different. Thus, N_{HI} was fixed at the Galactic value with the exception of three cases: Abell 399 (Sakelliou & Ponman 2004), Abell 520, and Hercules A. For these three clusters N_{HI} is a free parameter.

After fitting we rejected several datasets as their best-fit $T_{2.0-7.0}$ had no upper bound in the 90% confidence interval and thus were insufficient for our analysis. All fits for the clusters Abell 781, Abell 1682, CL J1213+0253, CL J1641+4001, IRAS 09104+4109, Lynx E, MACS J1824.3+4309, MS 0302.7+1658, and RX J1053+5735 were rejected. We also removed Abell 2550 from our sample after finding it to be a an anomalously cool ($T_X \sim 2$ keV) "cluster". In fact it is a line of sight set of groups as discussed by Martini et al. (2004).

5.2. *Simulated Spectra*

To quantify the effect a second, cooler gas component has on the fit of a single-component spectral model, we created an ensemble of simulated spectra for our entire sample using the fakeit command within XSPEC. With these simulated spectra we sought to answer the question: Given the count level in each observation of our sample, how bright must a second temperature component be for it to affect the observed temperature ratio, T_{HFR}? Put another way, we asked at what flux ratio a second gas phase skews T_{HFR} to greater than unity at the 1σ level.

We began by adding the observation-specific background to a convolved, absorbed thermal model with two temperature components for a time period equal to the observation exposure time and adding Poisson noise. For each realization of an observation's simulated spectrum we defined the primary component to have the best-fit temperature and metallicity of the $R_{2500-CORE}$ (or $R_{5000-CORE}$ if no $R_{2500-CORE}$ fit was performed), 0.7-7.0 keV fit, and we stepped the secondary component temperature over the values 0.5, 0.75, and 1.0 keV. The secondary component metallicity was fixed and set equal to the metallicity of the primary component.

We adjusted the normalization of the simulated two-component spectra to achieve equivalent count rates to those in the real spectra. We set the primary component normalization to $K_1 = \xi \cdot K_{bf}$ where K_{bf} is the best-fit normalization of the appropriate 0.7-7.0 keV fit and ξ is a preset factor having the values 0.8, 0.85, 0.9, 0.95, 0.96, 0.97, 0.98, and 0.99. The secondary component normalization was determined through an iterative process to make real and simulated spectral count rates match.

We also simulated a control sample of single-temperature models. The control sample is a simulated version of the best-fit model. This control provides us with a check of how often a hard component temperature might differ from a broad-band temperature statistically (i.e. if calibration effects are under control).

For each observation, we have 59 total simulated spectra: 35 single-temperature control spectra and 24 two-component

simulated spectra (three second temperatures, each with 8 different ξ). Our resulting simulated spectra ensemble contains 11387 spectra. After generating all the spectra we followed the same fitting routine detailed in §5.1.

There are three important results from the analysis of these simulated spectra:

1. In the control sample, a single temperature model rarely ($\sim 2\%$ of the time) gives a significantly different $T_{0.7-7.0}$ and $T_{2.0-7.0}$. The weighted average for the control sample is 1.00 with a standard deviation of ± 0.06 and an unbiased deviation of the mean of ± 0.002. The T_{HFR} distribution for the control sample also appears to have an intrinsic width which is likely associated with statistical noise of fitting in XSPEC (Dupke, private communication). This result indicates our remaining set of observations is statistically sound: that a result where T_{HFR} significantly differs from 1.0 cannot result from statistical fluctuations alone.

2. A significantly bright second temperature component – meaning $\xi \leq 0.90$ with $T_2 = 0.5, 0.75, 1.0$ keV – must be present in order to have values of $T_{HFR} > 1.1$ which we find in the real data.

3. As redshift increases gas cooler than 1.0 keV is slowly redshifted out of the observable X-ray band. As expected, we find from our simulated spectra that for $z \geq 0.6 T_{HFR}$ is, on average, no longer statistically distinguishable from unity. For the 14 clusters with $z \geq 0.6$ in our real sample we can safely conclude we are not overestimating the contribution of cool gas to the spectra and we are most likely underestimating the temperature inhomogeneity.

6. RESULTS AND DISCUSSION

6.1. *Temperature Ratios*

For each cluster we have measured a temperature ratio $T_{HFR} = T_{2.0-7.0}/T_{0.7-7.0}$. We find a clear departure of the mean T_{HFR} from unity for our entire sample at greater than 12σ. The weighted mean values for our sample are shown in Table 2. Presented in Figure 3 are the binned weighted means and raw T_{HFR} values of $R_{2500-CORE}$, $R_{5000-CORE}$, and the simulated control sample. The peculiar points with $T_{HFR} < 1$ are all statistically consistent with $T_{HFR} = 1$. In addition, ratios less than one in the real data occur at nearly the same frequency in the simulated data, $\sim 0.3\%$, suggesting that these ratios are consistent with statistical uncertainties in the data. The presence of clusters with $T_{HFR} = 1$ suggests that the calibration is not the sole reason for deviations of T_{HFR} from 1. We also find that the temperature ratio does not depend on the best-fit full-band temperature.

The uncertainty associated with each value of T_{HFR} is dominated by the larger error in $T_{2.0-7.0}$, and on average, $\Delta T_{2.0-7.0} \approx 2.3 \Delta T_{0.7-7.0}$. This error interval discrepancy naturally results from excluding the bulk of a cluster's emission which occurs below 2 keV. While choosing a temperature-sensitive cut-off energy for the hard-band (other than 2.0 keV) might maintain a more consistent error budget across our sample, we do not find any systematic trend in T_{HFR} or the associated errors with cluster temperature.

6.2. *Systematics*

In this study we have found the average value of T_{HFR} is significantly greater than one and that $\sigma_{HFR} > \sigma_{control}$, the latter result being robust against systematic uncertainties. As predicted by ME01, both of these results are expected to arise naturally from hierarchical formation of clusters. But systematic uncertainty related to *Chandra* instrumentation or other sources could shift the average value of T_{HFR} one would get from "perfect" data. In this section we consider some additional sources of uncertainty.

First, the disagreement between *XMM-Newton* and *Chandra* cluster temperatures has been noted in several independent studies, i.e. Vikhlinin et al. (2005); Snowden et al. (2007). But the source of this discrepancy is not well understood and efforts to perform cross-calibration between *XMM-Newton* and *Chandra* have thus far not been conclusive. One possible explanation is poor soft calibration of *Chandra* which may arise from a hydrocarbon contaminant on the High Resolution Mirror Assembly (HRMA) similar in nature to the contaminant on the ACIS detectors (Marshall et al. 2004). We have assessed this possibility by looking for systematic trends in T_{HFR} with time or temperature, as such a contaminant would most likely have a temperature and/or time dependence.

As noted in §6.1 and seen in Figure 3 we find no systematic trend with temperature either for the full sample or for a sub-sample of single observation clusters with $> 75\%$ of the observed flux attributable to the source (higher signal-tp-noise observations will be more effected by calibration uncertainty). Plotted in Figure 4 is T_{HFR} versus time for single observation clusters (clusters with multiple observations are fit simultaneously and any time effect would be washed out) and where the spectral flux is $> 75\%$ from the source. We find no systematic trend in T_{HFR} with time, which suggests that if T_{HFR} is affected by any contamination of *Chandra*'s HRMA, it may not be changing with time. Our conclusion on this matter is that the soft calibration uncertainty is not playing a dominant role in our results.

Aside from instrumental and calibration effects, some other possible sources of systematic error are signal-to-noise (S/N), redshift selection, and Galactic absorption. Presented in Figure 4 are these three parameters versus T_{HFR}. The trend in T_{HFR} with redshift is expected as the 2.0/(1+z) keV hard-band lower boundary nears convergence with the 0.7 keV full-band lower boundary which occurs at $z \sim 1.85$. We find no systematic trends with S/N or Galactic absorption which might occur if the skew in T_{HFR} were a consequence of poor count statistics, inaccurate Galactic absorption, or very poor calibration. Also shown in panel four of Fig. 4 is the ratio of T_{HFR} for $R_{2500-CORE}$ and $R_{5000-CORE}$. For every cluster in our sample both apertures result in T_{HFR} values which are not significantly different from one another. Our results are robust to changes in aperture size.

Also shown in Figure 4 is the ratio of *ASCA* temperatures taken from Don Horner's thesis to *Chandra* temperatures derived in this work. The spurious point below 0.5 with very large error bars is MS 2053.7-0449 which has a poorly constrained *ASCA* temperature of $10.03^{+8.73}_{-3.52}$. Our value of ~ 3.5 keV for this cluster is in agreement with the recent work of Maughan et al. (2007). Not all our sample clusters have an *ASCA* temperature, but a sufficient number (53) are available to make this comparison reliable. Apertures used in the extraction of *ASCA* spectra had no core region removed and were substantially larger than R_{2500}. *ASCA* spectra were also fit over a broader energy range (0.6-10 keV) than we use here.

Thus, we make the temperature comparison using our unexcised R_{2500}, 0.7-7.0 keV fits as these get us the closest to replicating the *ASCA* apertures and energy range. Our temperatures are in good agreement with those from *ASCA*, but we do note a trend of comparatively hotter *Chandra* temperatures for $T_{Chandra} > 10$ keV. The clusters with $T_{Chandra} > 10$ keV are Abell 1758, Abell 2163, Abell 2255, and RX J1347.5-1145.

Based on this trend, we test excluding the hottest clusters ($T_{Chandra} > 10$ keV where *ASCA* and *Chandra* disagree) from our sample. The mean temperature ratio for $R_{2500–CORE}$ remains 1.16 and the error of the mean increases from ±0.014 to ±0.015, while for $R_{5000–CORE}$ T_{HFR} increases by a negligible 0.9% to 1.15 ± 0.014. Our results are not being influenced by the inclusion of hot clusters.

6.3. *Using T_{HFR} to Select for Relaxation*

6.3.1. *Cool Core Versus Non-Cool Core*

The process of cluster formation and virialization may robustly result in the formation of a cool core (Ota et al. 2006; Burns et al. 2007). Flux-limited surveys have found the prevalence of CCs to be $34 - 60\%$ (White et al. 1997; Peres et al. 1998; Bauer et al. 2005; Chen et al. 2007) depending upon classification criteria, completeness, and possible selection biases. As discussed in §1, ME01 give us reason to believe the observed skewing of T_{HFR} to greater than unity is related to the dynamic state of a cluster. We thus sought to identify which clusters in our sample have cool cores (CC), which have (NCC), and if the presence or absence of a cool core is correlated to T_{HFR}. We also asked about the number of CC and NCC clusters as a function of T_{HFR}. Recall that we excluded the cool core itself during spectral extraction.

To identify a CC we extracted spectra for the 50 kpc region surrounding the cluster center and then defined a temperature decrement

$$T_{dec} = T_{50}/T_{cluster} \qquad (3)$$

where T_{50} is the temperature of the inner 50 kpc and $T_{cluster}$ is the $R_{2500–CORE}$ temperature (clusters without $R_{2500–CORE}$ fits were excluded from this analysis). If T_{dec} was 2σ less than unity, we defined the cluster as having a CC, otherwise the cluster was defined as NCC. We find CCs in 35% of our sample and when we lessen the significance needed for CC classification from 2σ to 1σ, we find 46% of our sample clusters have CCs. It's important to note the frequency of CCs in our study is consistent with other more detailed studies of CC/NCC populations.

When fitting for T_{50} we altered the method outlined in §5.1 to use XSPEC's modified Cash statistic (Cash 1979), cstat, on ungrouped spectra. This choice was made because the distribution of counts per bin in low count spectra is not Gaussian but instead Poisson. As a result, the best-fit temperature using χ^2 is typically cooler (Nousek & Shue 1989; Balestra et al. 2007). We have explored this systematic in ***all*** our fits and only found it to be significant in the lowest count spectra of the inner 50 kpc apertures discussed here. But for consistency, we fit all inner 50 kpc spectra using the modified Cash statistic.

With each cluster classified, we then took cuts in T_{HFR} and asked how many CC and NCC clusters were above these cuts. Figure 5 shows the normalized number of CC and NCC clusters as a function of cuts in T_{HFR}. If T_{HFR} were insensitive to the dynamical state of a cluster we expect, for normally distributed T_{HFR} values, to see the number of CC and NCC clusters decreasing in the same way. However, the number of

CC clusters falls off more rapidly than the number of NCC clusters. This effect is dramatically reduced – as expected – if the core is included. If the presence of a CC is indicative of a cluster's advancement towards complete virialization, then the significantly steeper fall-off of CC clusters as a function of T_{HFR} we observe indicates higher values of T_{HFR} are associated with a less relaxed state. This result is insensitive to our choice of significance level in the core classification.

Because of the CC/NCC definition we selected, our identification of CCs and NCCs was only as robust as the errors on T_{50} allowed. One can thus ask the question, did our loose definition bias us towards finding more NCCs than CCs? To explore this question we simulated 20 spectra for each observation following the method outlined in §5.2 for the control sample but using the inner 50 kpc spectral best-fit values as input. For each simulated spectrum we calculated a temperature decrement (Eq. 3) and re-classified the cluster as having a CC or NCC. Using the new set of mock classifications we assigned a reliability factor, ψ, to each real classification which is simply the fraction of mock classifications which agree with the real classification. A value of $\psi = 1.0$ indicates complete agreement and $\psi = 0.0$ meaning no agreement. When we removed clusters with $\psi < 0.9$ and repeated the analysis above, we found no significant change in the number of CC clusters as a function of T_{HFR}.

Recall that the coolest ICM gas is being redshifted out of the observable band as z increases and becomes a significant effect at $z \geq 0.6$ (§5.2). Thus, we are likely not detecting "weak" CCs in the highest redshift clusters of our sample and consequently these cores are classified as NCCs artificially increasing the NCC population. When we excluded the 14 clusters at $z \geq 0.6$ from this core classification analysis we found no significant change in our results.

6.3.2. *Mergers Versus Non-Mergers*

To further investigate trends in T_{HFR} we now examine a subclass of clusters with $T_{HFR} > 1.1$ at the 1σ level and which are identified in Table 3. $T_{HFR} > 1.1$ is an arbitrary threshold selected to limit the number of clusters to which we pay individual attention, but which is still representative of mid to high T_{HFR} values. All of these 29 clusters have core classifications with $\psi > 0.9$. We further define a subclass of clusters which have been identified as mergers in the literature. From Figure 6 and Table 3 we can see clusters exhibiting the highest significant values of T_{HFR} are all ongoing or recent mergers. At the 2σ level, we find increasing values of T_{HFR} favor merger systems with NCCs over relaxed, CC clusters. Mergers have left a spectroscopic imprint on the ICM which is predicted by ME01 and which we observe in our sample.

Of the 29 clusters with T_{HFR} significantly > 1.1, only six have CCs. Three of those, MKW3S, 3C 28.0, and RX J1720.1+2638 have their apertures centered on the bright, dense cores in confirmed mergers. Two more clusters, Abell 2384 and RX J1525+0958, while unconfirmed mergers have morphologies which are consistent with powerful ongoing mergers. Abell 2384 has a long gas tail extending out to a gaseous clump which has presumably passed through the cluster recently. RXJ1525 has a core which is shaped like an arrowhead and is reminiscent of the bow shock seen in 1E0657-56. Abell 907 is the remaining CC of the six listed. It has no signs of being a merger system but the highly compressed surface brightness contours to the west of the core are indicative of a prominent cold front which are tell-tale signs of a subcluster merger event (Markevitch & Vikhlinin 2007).

The unclassified systems – RX J0439.0+0715, MACS J2243.3-0935, MACS J0547.0-3904, ZWCL 1215, MACS J2311+0338, and Abell 267 – have NCCs and X-ray morphologies consistent with an ongoing or post-merger scenario. Two clusters, Abell 1204 and MACS J1427.6-2521, show no signs of recent or ongoing merger activity, however, they reside at the bottom of the arbitrary T_{HFR} cut, and as evidenced by Abell 401 and Abell 1689, exceptional spherical symmetry is no guarantee of relaxation.

7. SUMMARY AND CONCLUSIONS

We have explored the band dependence of the inferred X-ray temperature of the ICM for 193 well-observed ($N_{counts} > 1500$) clusters of galaxies selected from the *Chandra* Data Archive.

We extracted spectra from the annulus between $R = 70$ kpc and $R = R_{2500}$, R_{5000} for each cluster. We compared the X-ray temperatures inferred for single-component fits to global spectra when the energy range of the fit was 0.7-7.0 keV (full) and when the energy range was $2.0/(1 + z)$-7.0 keV (hard). We found that, on average, the hard-band temperature is significantly higher than the full-band temperature. For the $R_{2500\text{–}CORE}$ aperture we measured a weighted average of $T_{HFR} = 1.16$ with $\sigma = \pm 0.10$ and $\sigma_{mean} = \pm 0.01$, for the $R_{5000\text{–}CORE}$ aperture, $T_{HFR} = 1.14$ with $\sigma = \pm 0.12$ and $\sigma_{mean} = \pm 0.01$. We also found no systematic trends which could explain either the deviation from unity of T_{HFR} or the dispersion in T_{HFR}.

In addition, we simulated an ensemble of 11387 observation specific and control spectra. From analysis of these simulations we found the observational scatter, σ_{HFR}, is consistent with the presence of unresolved cool ($T_X < 1.0$ keV) gas, and we also found the observational scatter is greater than the statistical scatter, $\sigma_{control}$. As discussed in ME01 both of these results are consistent with the process of hierarchical cluster formation.

Upon further exploration, we found that T_{HFR} is enhanced preferentially for clusters which are known merger systems and for clusters which have non-cool cores. Clusters with temperature decrements in their cores (known as cool-core clusters) tend to have best-fit hard-band temperatures that are statistically consistent with their best-fit full-band temperatures. The correlation of T_{HFR} with the type of cluster core is insensitive to our choice of classification scheme and is robust against redshift effects.

Our results therefore qualitatively support ME01, and T_{HFR} might be useful for quantifying the degree of cluster relaxation/virialization. A robust test for this prediction can be made with simulations by tracking T_{HFR} during hierarchical assembly of a cluster. If T_{HFR} is tightly correlated with a cluster's degree of relaxation then along with other methods of substructure measure, such as moment analysis and centroid shift, one can assemble a powerful metric for predicting (and therefore reducing) a cluster's expected deviation from mean mass-scaling relations. The task of reducing scatter in scaling relations is of the utmost importance if we are to reliably and accurately measure the mass of clusters using observables as a surrogate. The ultimate goal being the use of large-scale structure growth as an additional tight constraint in cosmological studies.

REFERENCES

Anders, E., & Grevesse, N. 1989, Geochim. Cosmochim. Acta, 53, 197

Andersson, K. E., & Madejski, G. M. 2004, ApJ, 607, 190

Arnaud, K. A. 1996, in ASP Conf. Ser. 101: Astronomical Data Analysis Software and Systems V, ed. G. H. Jacoby & J. Barnes, 17–+

Arnaud, M., Aghanim, N., & Neumann, D. M. 2002, A&A, 389, 1

Bagchi, J., Durret, F., Neto, G. B. L., & Paul, S. 2006, Science, 314, 791

Balestra, I., Tozzi, P., Ettori, S., Rosati, P., Borgani, S., Mainieri, V., Norman, C., & Viola, M. 2007, A&A, 462, 429

Bauer, F. E., Fabian, A. C., Sanders, J. S., Allen, S. W., & Johnstone, R. M. 2005, MNRAS, 359, 1481

Bliton, M., Rizza, E., Burns, J. O., Owen, F. N., & Ledlow, M. J. 1998, MNRAS, 301, 609

Böhringer, H., Schuecker, P., Guzzo, L., Collins, C. A., Voges, W., Cruddace, R. G., Ortiz-Gil, A., Chincarini, G., De Grandi, S., Edge, A. C., MacGillivray, H. T., Neumann, D. M., Schindler, S., & Shaver, P. 2004, A&A, 425, 367

Buote, D. A., & Tsai, J. C. 1995, ApJ, 452, 522

—. 1996, ApJ, 458, 27

Burns, J. O., Hallman, E. J., Gantner, B., Motl, P. M., & Norman, M. L. 2007, ArXiv e-prints, 708

Burns, J. O., Roettiger, K., Pinkney, J., Perley, R. A., Owen, F. N., & Voges, W. 1995, ApJ, 446, 583

Cash, W. 1979, ApJ, 228, 939

Chen, Y., Reiprich, T. H., Böhringer, H., Ikebe, Y., & Zhang, Y.-Y. 2007, A&A, 466, 805

Dahle, H., Kaiser, N., Irgens, R. J., Lilje, P. B., & Maddox, S. J. 2002, ApJS, 139, 313

David, L. P., & Kempner, J. 2004, ApJ, 613, 831

Dickey, J. M., & Lockman, F. J. 1990, ARA&A, 28, 215

Ebeling, H., Edge, A. C., Allen, S. W., Crawford, C. S., Fabian, A. C., & Huchra, J. P. 2000, MNRAS, 318, 333

Ebeling, H., Edge, A. C., Bohringer, H., Allen, S. W., Crawford, C. S., Fabian, A. C., Voges, W., & Huchra, J. P. 1998, MNRAS, 301, 881

Ebeling, H., Edge, A. C., & Henry, J. P. 2001, ApJ, 553, 668

Edge, A. C., Stewart, G. C., Fabian, A. C., & Arnaud, K. A. 1990, MNRAS, 245, 559

Eisenstein, D. J., Zehavi, I., Hogg, D. W., Scoccimarro, R., Blanton, M. R., Nichol, R. C., Scranton, R., Seo, H.-J., Tegmark, M., Zheng, Z., Anderson, S. F., Annis, J., Bahcall, N., Brinkmann, J., Burles, S., Castander, F. J., Connolly, A., Csabai, I., Doi, M., Fukugita, M., Frieman, J. A., Glazebrook, K., Gunn, J. E., Hendry, J. S., Hennessy, G., Ivezić, Z., Kent, S., Knapp, G. R., Lin, H., Loh, Y.-S., Lupton, R. H., Margon, B., McKay, T. A., Meiksin, A., Munn, J. A., Pope, A., Richmond, M. W., Schlegel, D., Schneider, D. P., Shimasaku, K., Stoughton, C., Strauss, M. A., SubbaRao, M., Szalay, A. S., Szapudi, I., Tucker, D. L., Yanny, B., & York, D. G. 2005, ApJ, 633, 560

Ettori, S., & Lombardi, M. 2003, A&A, 398, L5

Evrard, A. E. 1989, ApJ, 341, L71

Evrard, A. E., Metzler, C. A., & Navarro, J. F. 1996, ApJ, 469, 494

Feretti, L., Boehringer, H., Giovannini, G., & Neumann, D. 1997, A&A, 317, 432

Freeman, P. E., Kashyap, V., Rosner, R., & Lamb, D. Q. 2002, ApJS, 138, 185

Gioia, I. M., Maccacaro, T., Geller, M. J., Huchra, J. P., Stocke, J., & Steiner, J. E. 1982, ApJ, 255, L17

Gioia, I. M., Maccacaro, T., Schild, R. E., Wolter, A., Stocke, J. T., Morris, S. L., & Henry, J. P. 1990, ApJS, 72, 567

Girardi, M., Fadda, D., Escalera, E., Giuricin, G., Mardirossian, F., & Mezzetti, M. 1997, ApJ, 490, 56

Gómez, P. L., Hughes, J. P., & Birkinshaw, M. 2000, ApJ, 540, 726

Govoni, F., Taylor, G. B., Dallacasa, D., Feretti, L., & Giovannini, G. 2001, A&A, 379, 807

Gutierrez, K., & Krawczynski, H. 2005, ApJ, 619, 161

Haiman, Z., Mohr, J. J., & Holder, G. P. 2001, ApJ, 553, 545

Hallman, E. J., & Markevitch, M. 2004, ApJ, 610, L81

Henry, J. P., Mullis, C. R., Voges, W., Böhringer, H., Briel, U. G., Gioia, I. M., & Huchra, J. P. 2006, ApJS, 162, 304

Hu, W. 2003, Phys. Rev. D, 67, 081304

Jeltema, T. E., Canizares, C. R., Bautz, M. W., & Buote, D. A. 2005, ApJ, 624, 606

Jeltema, T. E., Hallman, E. J., Burns, J. O., & Motl, P. M. 2007, ArXiv e-prints, 708

Kaastra, J. S. 1992

Kempner, J. C., Sarazin, C. L., & Markevitch, M. 2003, ApJ, 593, 291

Kravtsov, A. V., Vikhlinin, A., & Nagai, D. 2006, ApJ, 650, 128

Krempec-Krygier, J., & Krygier, B. 1999, Acta Astronomica, 49, 403

Liedahl, D. A., Osterheld, A. L., & Goldstein, W. H. 1995, ApJ, 438, L115

Markevitch, M., Forman, W. R., Sarazin, C. L., & Vikhlinin, A. 1998, ApJ, 503, 77

Markevitch, M., & Vikhlinin, A. 2007, Phys. Rep., 443, 1

Markevitch, M., Vikhlinin, A., & Mazzotta, P. 2001, ApJ, 562, L153

Marshall, H. L., Tennant, A., Grant, C. E., Hitchcock, A. P., O'Dell, S. L., & Plucinsky, P. P. 2004, in Presented at the Society of Photo-Optical Instrumentation Engineers (SPIE) Conference, Vol. 5165, X-Ray and Gamma-Ray Instrumentation for Astronomy XIII. Edited by Flanagan, Kathryn A.; Siegmund, Oswald H. W. Proceedings of the SPIE, Volume 5165, pp. 497-508 (2004)., ed. K. A. Flanagan & O. H. W. Siegmund, 497–508

Martini, P., Kelson, D. D., Mulchaey, J. S., & Athey, A. 2004, in Clusters of Galaxies: Probes of Cosmological Structure and Galaxy Evolution, ed. J. S. Mulchaey, A. Dressler, & A. Oemler

Mathiesen, B. F., & Evrard, A. E. 2001, ApJ, 546, 100

Maughan, B. J. 2007, ArXiv Astrophysics e-prints

Maughan, B. J., Jones, C., Forman, W., & Van Speybroeck, L. 2007, ArXiv Astrophysics e-prints

Mazzotta, P., Markevitch, M., Vikhlinin, A., Forman, W. R., David, L. P., & VanSpeybroeck, L. 2001, ApJ, 555, 205

Mazzotta, P., Rasia, E., Moscardini, L., & Tormen, G. 2004, MNRAS, 354, 10

Mercurio, A., Massarotti, M., Merluzzi, P., Girardi, M., La Barbera, F., & Busarello, G. 2003, A&A, 408, 57

Mewe, R., Gronenschild, E. H. B. M., & van den Oord, G. H. J. 1985, A&AS, 62, 197

Mewe, R., Lemen, J. R., & van den Oord, G. H. J. 1986, A&AS, 65, 511

Mohr, J. J., & Evrard, A. E. 1997, ApJ, 491, 38

Morrison, R., & McCammon, D. 1983, ApJ, 270, 119

Nousek, J. A., & Shue, D. R. 1989, ApJ, 342, 1207

O'Hara, T. B., Mohr, J. J., Bialek, J. J., & Evrard, A. E. 2006, ApJ, 639, 64

Ota, N., Kitayama, T., Masai, K., & Mitsuda, K. 2006, ApJ, 640, 673

Peres, C. B., Fabian, A. C., Edge, A. C., Allen, S. W., Johnstone, R. M., & White, D. A. 1998, MNRAS, 298, 416

Riess, A. G., Filippenko, A. V., Challis, P., Clocchiatti, A., Diercks, A., Garnavich, P. M., Gilliland, R. L., Hogan, C. J., Jha, S., Kirshner, R. P., Leibundgut, B., Phillips, M. M., Reiss, D., Schmidt, B. P., Schommer, R. A., Smith, R. C., Spyromilio, J., Stubbs, C., Suntzeff, N. B., & Tonry, J. 1998, AJ, 116, 1009

Riess, A. G., Strolger, L.-G., Casertano, S., Ferguson, H. C., Mobasher, B., Gold, B., Challis, P. J., Filippenko, A. V., Jha, S., Li, W., Tonry, J., Foley, R., Kirshner, R. P., Dickinson, M., MacDonald, E., Eisenstein, D., Livio, M., Younger, J., Xu, C., Dahlén, T., & Stern, D. 2007, ApJ, 659, 98

Rosati, P., della Ceca, R., Burg, R., Norman, C., & Giacconi, R. 1995, ApJ, 445, L11

Sakelliou, I., & Ponman, T. J. 2004, MNRAS, 351, 1439

Sanderson, A. J. R., Ponman, T. J., & O'Sullivan, E. 2006, MNRAS, 1068

Smith, G. P., Kneib, J.-P., Smail, I., Mazzotta, P., Ebeling, H., & Czoske, O. 2005, MNRAS, 359, 417

Snowden, S. L., Mushotzky, R. M., Kuntz, K. D., & Davis, D. S. 2007, ArXiv e-prints, 710

Teague, P. F., Carter, D., & Gray, P. M. 1990, ApJS, 72, 715

Townsley, L. K., Broos, P. S., Garmire, G. P., & Nousek, J. A. 2000, ApJ, 534, L139

Tucker, W., Blanco, P., Rappoport, S., David, L., Fabricant, D., Falco, E. E., Forman, W., Dressler, A., & Ramella, M. 1998, ApJ, 496, L5+

Ventimiglia, D., Voit, G. M., Borgani, S., & Donahue, M. 2008, ApJ Submitted

Vikhlinin, A. 2006, ApJ, 640, 710

Vikhlinin, A., Markevitch, M., Murray, S. S., Jones, C., Forman, W., & Van Speybroeck, L. 2005, ApJ, 628, 655

Vikhlinin, A., McNamara, B. R., Forman, W., Jones, C., Quintana, H., & Hornstrup, A. 1998, ApJ, 502, 558

Voit, G. M. 2005, Reviews of Modern Physics, 77, 207

Wang, L., & Steinhardt, P. J. 1998, ApJ, 508, 483

Wang, S., Khoury, J., Haiman, Z., & May, M. 2004, Phys. Rev. D, 70, 123008

White, D. A., Jones, C., & Forman, W. 1997, MNRAS, 292, 419

Yang, Y., Huo, Z., Zhou, X., Xue, S., Mao, S., Ma, J., & Chen, J. 2004, ApJ, 614, 692

Yuan, Q.-R., Yan, P.-F., Yang, Y.-B., & Zhou, X. 2005, Chinese Journal of Astronomy and Astrophysics, 5, 126

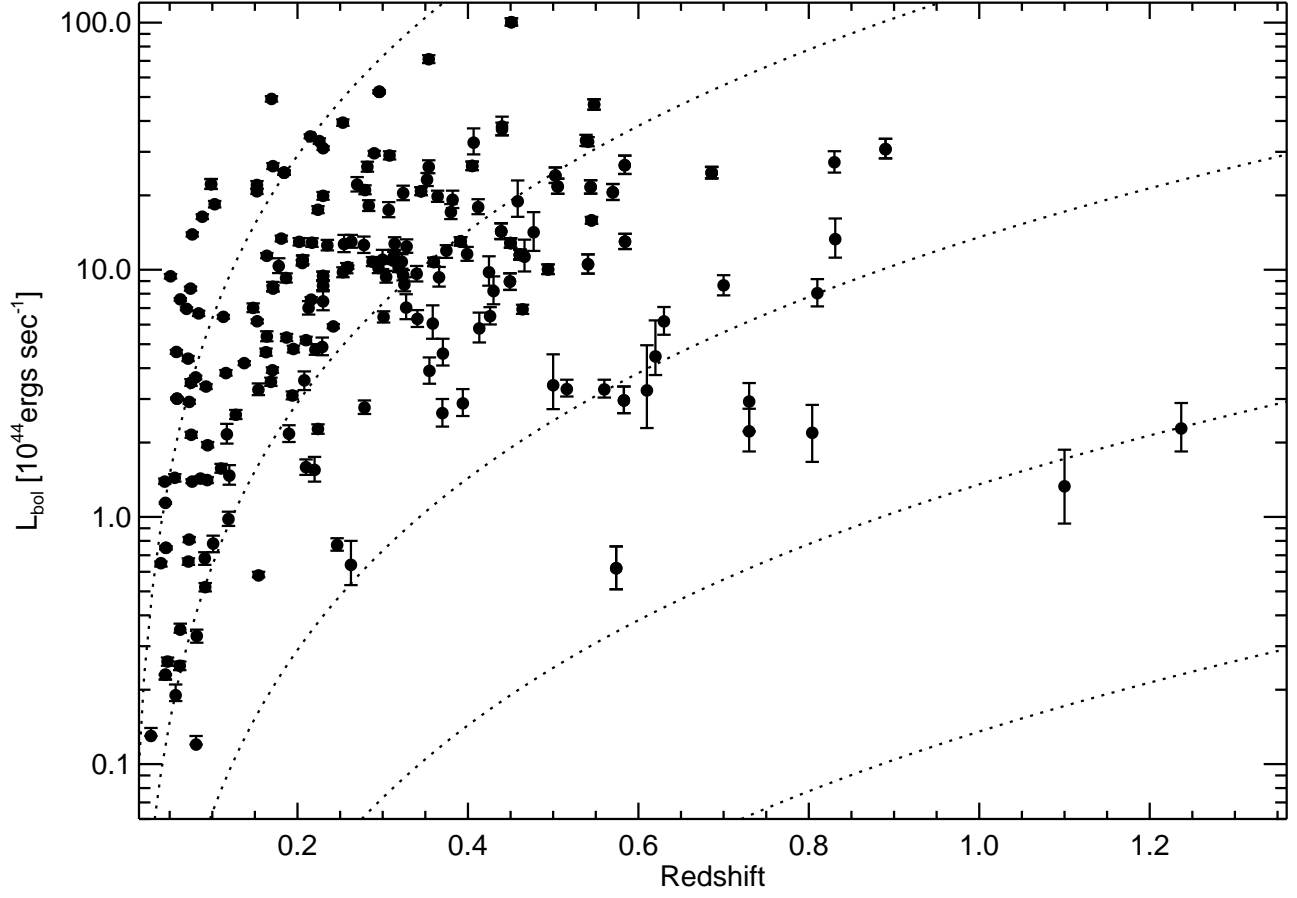FIG. 1.— Bolometric luminosity ($E = 0.1 - 100$ keV) plotted as a function of redshift for the full sample. L_{bol} values are limited to the region of spectral extraction R=$R_{2500-CORE}$ (or R=$R_{5000-CORE}$ for clusters without $R_{2500-CORE}$ fits). Dotted lines represent constant fluxes of 3.0×10^{-15}, 10^{-14}, 10^{-13}, and 10^{-12} ergs sec^{-1} cm^{-2}.
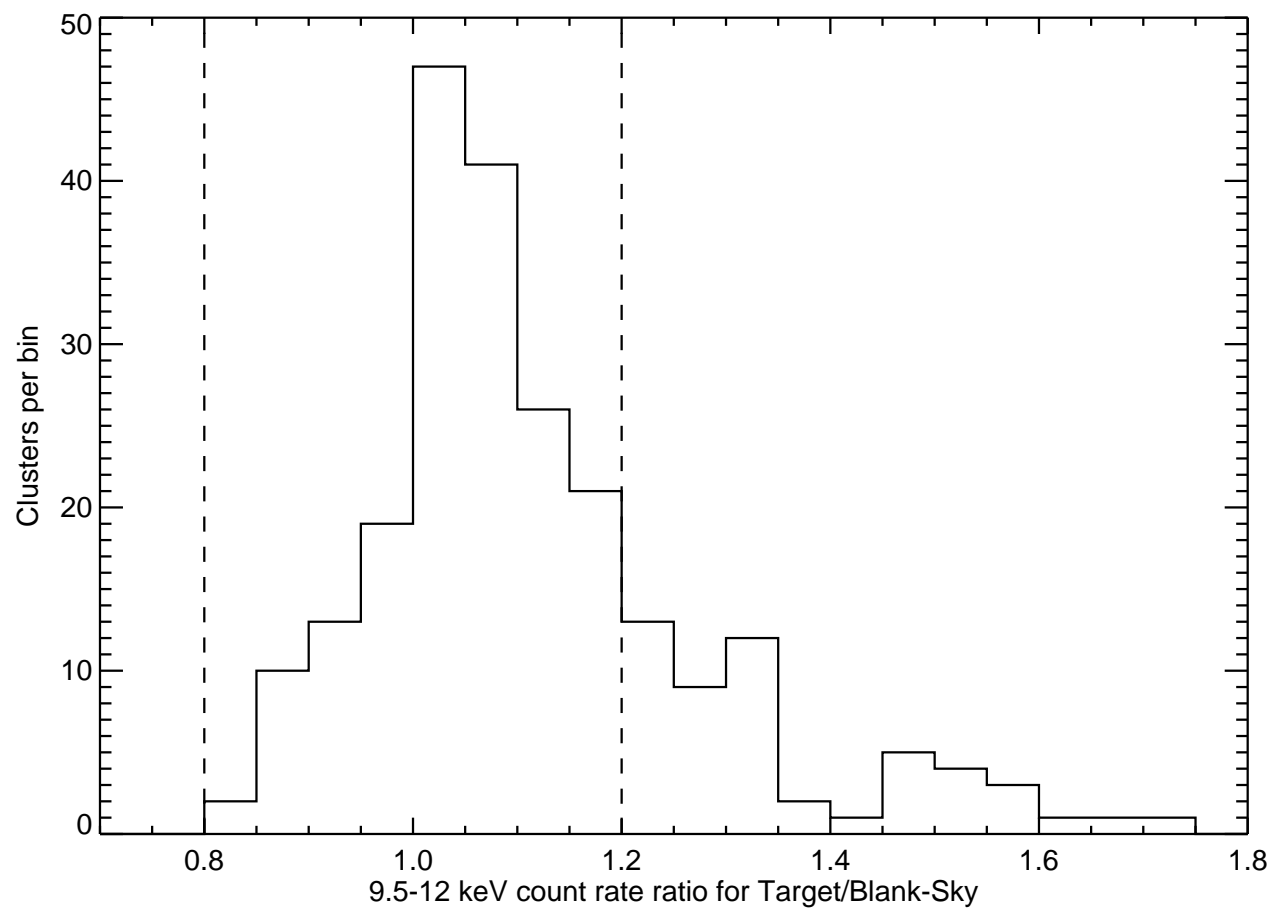
Cavagnolo et al.

Fig. 2.— Ratio of target field and blank-sky field count rates in the 9.5-12.0 keV band for each observation. Vertical dashed lines represent ±20% of unity.
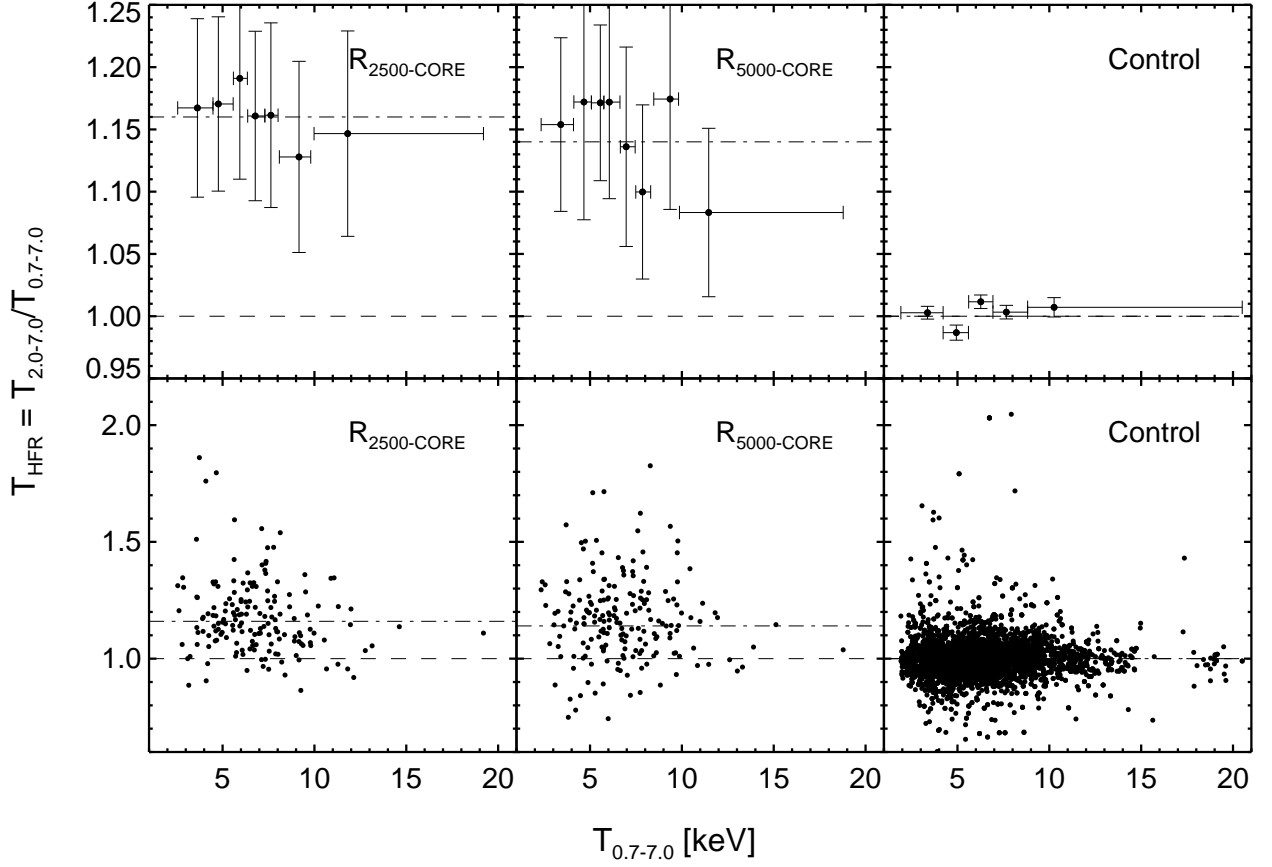
FIG. 3.— Best-fit temperatures for the hard bandpass, $T_{2.0-7.0}$, divided by the full bandpass, $T_{0.7-7.0}$ plotted against the full bandpass temperature. For binned data, each bin contains 25 clusters, with the exception of the highest temperature bins which contains 16 and 17 for $R_{2500-CORE}$ and $R_{5000-CORE}$, respectively. The simulated data bins contain 1000 clusters with the last bin having 780 clusters. The line of equality is shown as a dashed line and the weighted mean for the full sample is shown as a dashed-dotted line. Error bars are omitted in the unbinned data for clarity. Note the net skewing of T_{HBR} to greater than unity for both apertures with no such trend existing in the simulated data.
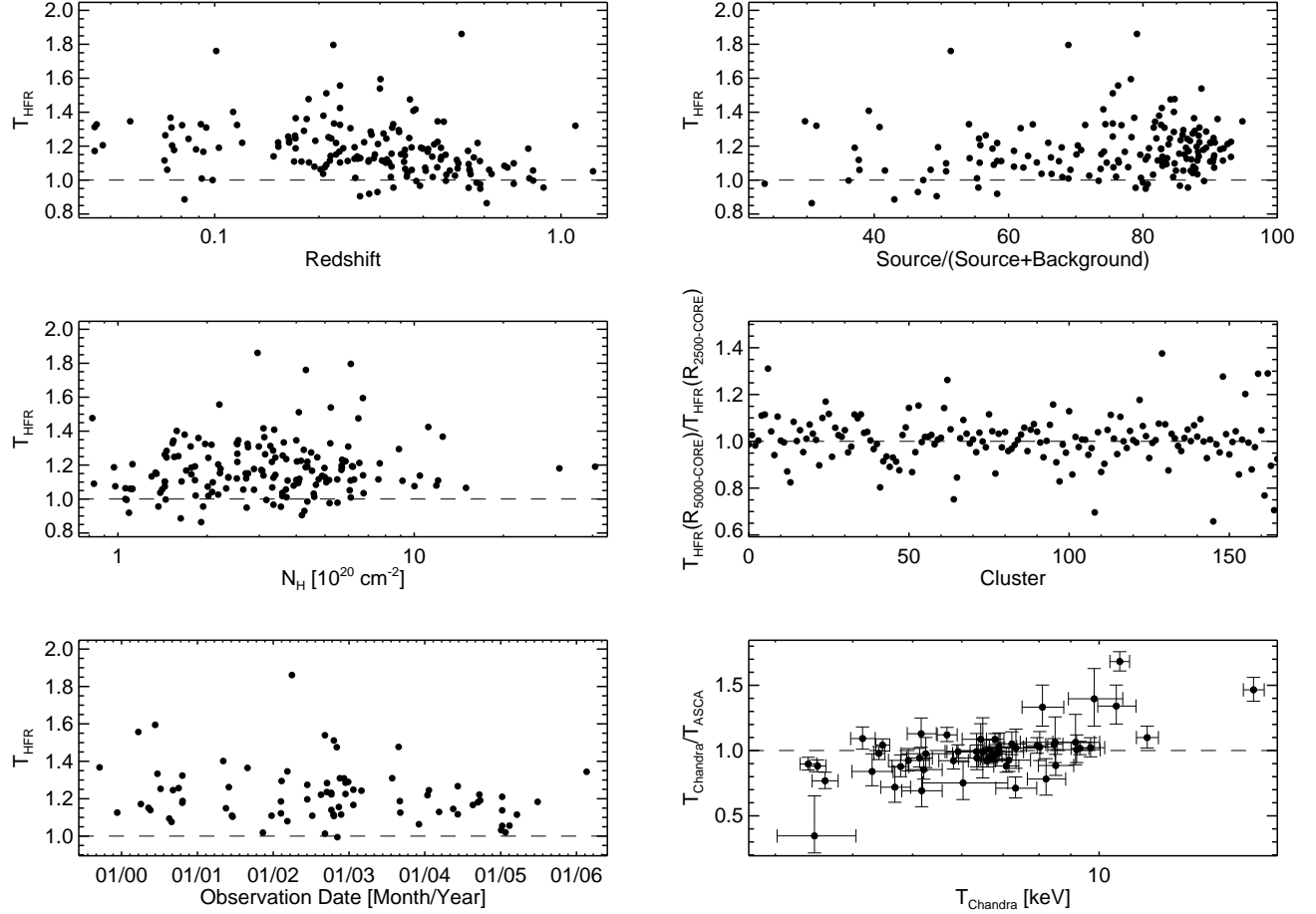
FIG. 4.— Plotted are possible sources of systematics. Error bars have been omitted in all plots for clarity. The line of equality is shown as a dashed line in all plots. *(Upper-left:)* T_{HBR} versus redshift for the entire sample. The trend in T_{HBR} with redshift is expected as the $T_{2.0-7.0}$ lower boundary nears convergence with the $T_{0.7-7.0}$ lower boundary which occurs at $z \sim 1.85$. Weighted values of T_{HBR} are consistent with unity at $z \sim 0.6$. *(Upper-right:)* T_{HBR} versus percentage of spectrum flux which is attributed to the source. We find no trend with signal-to-noise which would suggest calibration uncertainty is playing a major role in our results. *(Middle-left:)* T_{HBR} versus Galactic column density. We find no trend in absorption which would result if N_{HI} values are inaccurate or if we had improperly accounted for local soft contamination. *(Middle-right:)* Ratio of T_{HBR} for our two physically motivated apertures, $R_{2500-CORE}$ and $R_{5000-CORE}$. Error bars are omitted for clarity as they all cross the line of equality. *(Lower-left:)* T_{HBR} plotted versus observation start date. The plotted points are culled from the full sample and represent only clusters which have a single observation and where the spectral flux is > 75% from the source. We note no systematic trend with time which suggests any contamination of *Chandra*'s HRMA may not be changing with time. *(Lower-right:)* Ratio of *Chandra* temperatures derived in this work to *ASCA* temperatures taken from Don Horner's thesis. We note a trend of comparatively hotter *Chandra* temperatures for clusters > 10 keV, otherwise our derived temperatures are in good agreement with those of *ASCA*.
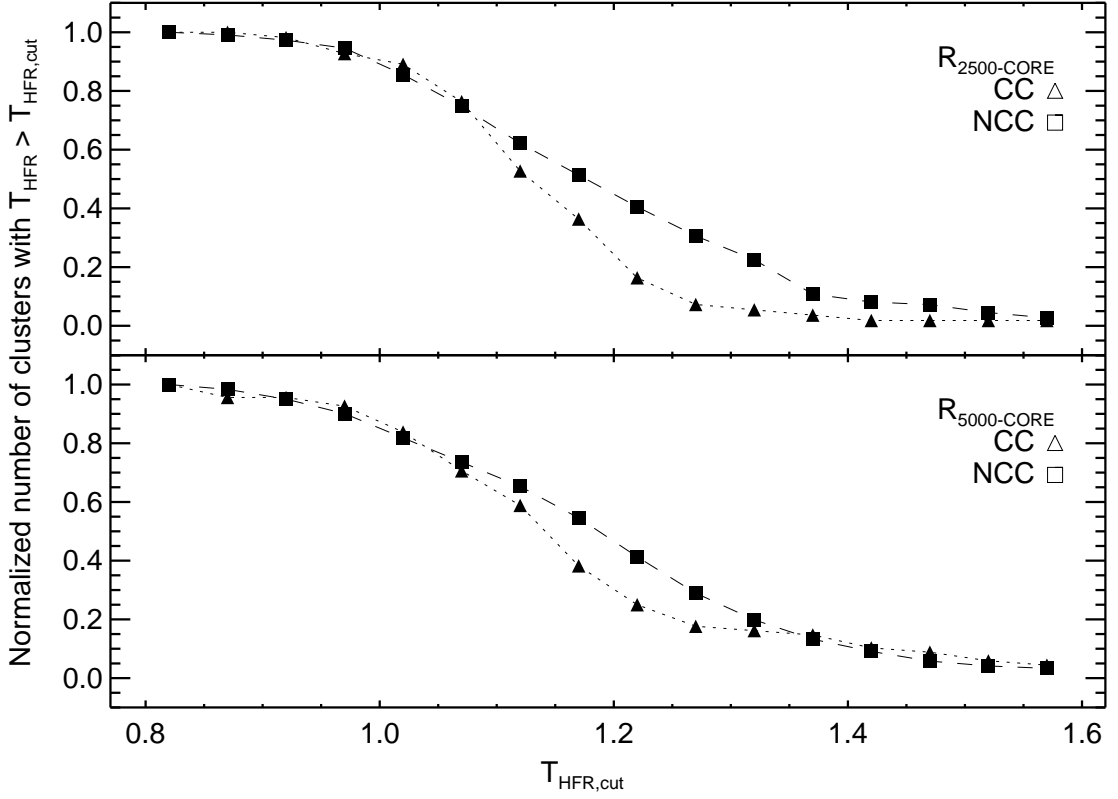
FIG. 5.— Plotted is the normalized number of cool-core (CC) and non-cool core (NCC) clusters as a function of cuts in T_{HBR}. We have defined a cluster as having a cool core (CC) when the temperature for the 50 kpc region around the cluster center divided by the temperature for $R_{2500–CORE}$ is less than 1 at the 2σ level. We then take cuts in T_{HBR} at the 1σ level and ask how many CC and NCC clusters are above these cuts. The number of CC clusters falls off more rapidly than NCC clusters in this classification scheme suggesting higher values of T_{HBR} prefer less relaxed systems which do not have cool cores. This result is insensitive to our choice of significance level in both the CC classification and T_{HBR} cuts.
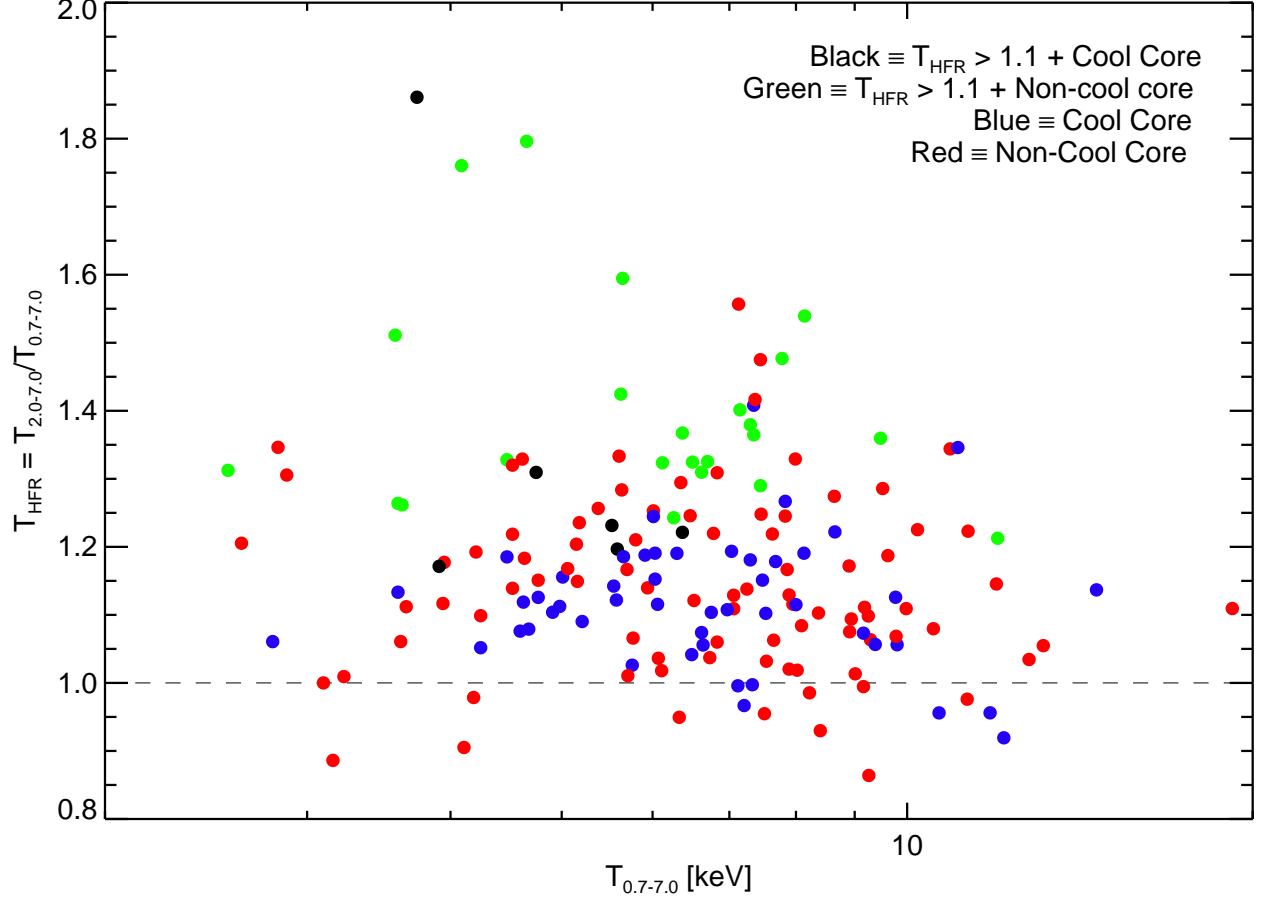
FIG. 6.— T_{HBR} plotted against $T_{0.7-7.0}$ for our sample. Points are color coded based two criteria: 1) presence of a cool core (CC) and 2) value of T_{HBR} value. Black points are clusters with a CC and T_{HBR} significantly greater than 1.1. Green points are NCC clusters with T_{HBR} significantly greater than 1.1. Blue points are CC clusters and red are NCC clusters. We have found most, if not all, of the clusters with high T_{HBR} ($\gtrsim 1.1$) (green points) are on-going or recent mergers.

TABLE 1
SUMMARY OF SAMPLE

Cluster	Obs.ID	R.A. hr:min:sec	Dec. ° : ′ : ″	ExpT ksec	Mode	ACIS	z	$L_{bol.}$ 10^{44} ergs s^{-1}
(1)	(2)	(3)	(4)	(5)	(6)	(7)	(8)	(9)
1E0657 56	3184	06:58:29.627	-55:56:39.79	87.5	VF	I3	0.296	52.48
1E0657 56	5356	06:58:29.619	-55:56:39.35	97.2	VF	I2	0.296	52.48
1E0657 56	5361	06:58:29.670	-55:56:39.80	82.6	VF	I3	0.296	52.48
1RXS J2129.4-0741	3199	21:29:26.274	-07:41:29.18	19.9	VF	I3	0.570	20.58
1RXS J2129.4-0741	3595	21:29:26.281	-07:41:29.36	19.9	VF	I3	0.570	20.58
2PIGG J0011.5-2850	5797	00:11:21.623	-28:51:14.44	19.9	VF	I3	0.075	2.15
2PIGG J0311.8-2655 †	5799	03:11:33.904	-26:54:16.48	39.6	VF	I3	0.062	0.25
2PIGG J2227.0-3041	5798	22:27:54.560	-30:34:34.84	22.3	VF	I2	0.073	0.81
3C 220.1	839	09:32:40.218	+79:06:29.46	18.9	F	S3	0.610	3.25
3C 28.0	3233	00:55:50.401	+26:24:36.47	49.7	VF	I3	0.195	4.78
3C 295	2254	14:11:20.280	+52:12:10.55	90.9	VF	I3	0.464	6.92
3C 388	5295	18:44:02.365	+45:33:29.31	30.7	VF	I3	0.092	0.52
4C 55.16	4940	08:34:54.923	+55:34:21.15	96.0	VF	S3	0.242	5.90
ABELL 0013 †	4945	00:13:37.883	-19:30:09.10	55.3	VF	S3	0.094	1.41
ABELL 0068	3250	00:37:06.309	+09:09:32.28	10.0	VF	I3	0.255	12.70
ABELL 0119 †	4180	00:56:15.150	-01:14:59.70	11.9	VF	I3	0.044	1.39
ABELL 0168	3203	01:14:57.909	+00:24:42.55	40.6	VF	I3	0.045	0.23
ABELL 0168	3204	01:14:57.925	+00:24:42.73	37.6	VF	I3	0.045	0.23
ABELL 0209	3579	01:31:52.565	-13:36:38.79	10.0	VF	I3	0.206	10.96
ABELL 0209	522	01:31:52.595	-13:36:39.25	10.0	VF	I3	0.206	10.96
ABELL 0267	1448	01:52:29.181	+00:57:34.43	7.9	F	I3	0.230	8.62
ABELL 0267	3580	01:52:29.180	+00:57:34.23	19.9	VF	I3	0.230	8.62
ABELL 0370	515	02:39:53.169	-01:34:36.96	88.0	F	S3	0.375	11.95
ABELL 0383	2321	02:48:03.364	-03:31:44.69	19.5	F	S3	0.187	5.32
ABELL 0399	3230	02:57:54.931	+13:01:58.41	48.6	VF	I0	0.072	4.37
ABELL 0401	518	02:58:56.896	+13:34:14.48	18.0	F	I3	0.074	8.39
ABELL 0478	6102	04:13:25.347	+10:27:55.62	10.0	VF	I3	0.088	16.39
ABELL 0514	3578	04:48:19.229	-20:30:28.79	44.5	VF	I3	0.072	0.66
ABELL 0520	4215	04:54:09.711	+02:55:23.69	66.3	VF	I3	0.202	12.97
ABELL 0521	430	04:54:07.004	-10:13:26.72	39.1	VF	S3	0.253	9.77
ABELL 0586	530	07:32:20.339	+31:37:58.59	10.0	VF	I3	0.171	8.54
ABELL 0611	3194	08:00:56.832	+36:03:24.09	36.1	VF	S3	0.288	10.78
ABELL 0644 †	2211	08:17:25.225	-07:30:40.03	29.7	VF	I3	0.070	6.95
ABELL 0665	3586	08:30:59.231	+65:50:37.78	29.7	VF	I3	0.181	13.37
ABELL 0697	4217	08:42:57.549	+36:21:57.65	19.5	VF	I3	0.282	26.10
ABELL 0773	5006	09:17:52.566	+51:43:38.18	19.8	VF	I3	0.217	12.87
ABELL 0781	534	09:20:25.431	+30:30:07.56	9.9	VF	I3	0.298	0.00
ABELL 0907	3185	09:58:21.880	-11:03:52.20	48.0	VF	I3	0.153	6.19
ABELL 0963	903	10:17:03.744	+39:02:49.17	36.3	F	S3	0.206	10.65
ABELL 1063S	4966	22:48:44.294	-44:31:48.37	26.7	VF	I3	0.354	71.09
ABELL 1068 †	1652	10:40:44.520	+39:57:10.28	26.8	F	S3	0.138	4.19
ABELL 1201 †	4216	11:12:54.489	+13:26:08.76	39.7	VF	S3	0.169	3.52
ABELL 1204	2205	11:13:20.419	+17:35:38.45	23.6	VF	I3	0.171	3.92
ABELL 1361 †	2200	11:43:39.827	+46:21:21.40	16.7	F	S3	0.117	2.16
ABELL 1423	538	11:57:17.026	+33:36:37.44	9.8	VF	I3	0.213	7.01
ABELL 1651	4185	12:59:22.830	-04:11:45.86	9.6	VF	I3	0.084	6.66
ABELL 1664 †	1648	13:03:42.478	-24:14:44.55	9.8	VF	S3	0.128	2.59
ABELL 1682	3244	13:06:50.764	+46:33:19.86	9.8	VF	I3	0.226	0.00
ABELL 1689	1663	13:11:29.612	-01:20:28.69	10.7	F	I3	0.184	24.71
ABELL 1689	5004	13:11:29.606	-01:20:28.61	19.9	VF	I3	0.184	24.71
ABELL 1689	540	13:11:29.595	-01:20:28.47	10.3	F	I3	0.184	24.71
ABELL 1758	2213	13:32:42.978	+50:32:44.83	58.3	VF	S3	0.279	21.01
ABELL 1763	3591	13:35:17.957	+40:59:55.80	19.6	VF	I3	0.187	9.26
ABELL 1795 †	5289	13:48:52.829	+26:35:24.01	15.0	VF	I3	0.062	7.59
ABELL 1835	495	14:01:01.951	+02:52:43.18	19.5	F	S3	0.253	39.38
ABELL 1914	3593	14:26:01.399	+37:49:27.83	18.9	VF	I3	0.171	26.25
ABELL 1942	3290	14:38:21.878	+03:40:12.97	57.6	VF	I2	0.224	2.27
ABELL 1995	906	14:52:57.758	+58:02:51.34	0.0	F	S3	0.319	10.19
ABELL 2029 †	6101	15:10:56.163	+05:44:40.89	9.9	VF	I3	0.076	13.90
ABELL 2034	2204	15:10:11.003	+33:30:46.46	53.9	VF	I3	0.113	6.45
ABELL 2065 †	31821	15:22:29.220	+27:42:46.54	0.0	VF	I3	0.073	2.92
ABELL 2069	4965	15:24:09.181	+29:53:18.05	55.4	VF	I2	0.116	3.82
ABELL 2111	544	15:39:41.432	+34:25:12.26	10.3	F	I3	0.230	7.45
ABELL 2125	2207	15:41:14.154	+66:15:57.20	81.5	VF	I3	0.246	0.77
ABELL 2163	1653	16:15:45.705	-06:09:00.62	71.1	VF	I1	0.170	49.11
ABELL 2204 †	499	16:32:45.437	+05:34:21.05	10.1	F	S3	0.152	20.77
ABELL 2204	6104	16:32:45.428	+05:34:20.89	9.6	VF	I3	0.152	22.03
ABELL 2218	1666	16:35:50.831	+66:12:42.31	48.6	VF	I0	0.171	8.39
ABELL 2219 †	896	16:40:21.069	+46:42:29.07	42.3	F	S3	0.226	33.15
ABELL 2255	894	17:12:40.385	+64:03:50.63	39.4	F	I3	0.081	3.67
ABELL 2256 †	1386	17:03:44.567	+78:38:11.51	12.4	F	I3	0.058	4.65
ABELL 2259	3245	17:20:08.299	+27:40:11.53	10.0	VF	I3	0.164	5.37
ABELL 2261	5007	17:22:27.254	+32:07:58.60	24.3	VF	I3	0.224	17.49
ABELL 2294	3246	17:24:10.149	+85:53:09.77	10.0	VF	I3	0.178	10.35

TABLE 1 — *Continued*

Cluster	Obs.ID	R.A. hr:min:sec	Dec. $^\circ:':''$	ExpT ksec	Mode	ACIS	z	$L_{bol.}$ 10^{44} ergs s^{-1}
(1)	(2)	(3)	(4)	(5)	(6)	(7)	(8)	(9)
ABELL 2384	4202	21:52:21.178	-19:32:51.90	31.5	VF	I3	0.095	1.95
ABELL 2390 †	4193	21:53:36.825	+17:41:44.38	95.1	VF	S3	0.230	31.02
ABELL 2409	3247	22:00:52.567	+20:58:34.11	10.2	VF	I3	0.148	7.01
ABELL 2537	4962	23:08:22.313	-02:11:29.88	36.2	VF	S3	0.295	10.16
ABELL 2550	2225	23:11:35.806	-21:44:46.70	59.0	VF	S3	0.154	0.58
ABELL 2554 †	1696	23:12:19.939	-21:30:09.84	19.9	VF	S3	0.110	1.57
ABELL 2556 †	2226	23:13:01.413	-21:38:04.47	19.9	VF	S3	0.086	1.43
ABELL 2631	3248	23:37:38.560	+00:16:28.64	9.2	VF	I3	0.278	12.59
ABELL 2667	2214	23:51:39.395	-26:05:02.75	9.6	VF	S3	0.230	19.91
ABELL 2670	4959	23:54:13.687	-10:25:08.85	39.6	VF	I3	0.076	1.39
ABELL 2717	6974	00:03:11.996	-35:56:08.01	19.8	VF	I3	0.048	0.26
ABELL 2744	2212	00:14:14.396	-30:22:40.04	24.8	VF	S3	0.308	29.00
ABELL 3128 †	893	03:29:50.918	-52:34:51.04	19.6	F	I3	0.062	0.35
ABELL 3158 †	3201	03:42:54.675	-53:37:24.36	24.8	VF	I3	0.059	3.01
ABELL 3158 †	3712	03:42:54.683	-53:37:24.37	30.9	VF	I3	0.059	3.01
ABELL 3164	6955	03:46:16.839	-57:02:11.38	13.5	VF	I3	0.057	0.19
ABELL 3376	3202	06:02:05.122	-39:57:42.82	44.3	VF	I3	0.046	0.75
ABELL 3376	3450	06:02:05.162	-39:57:42.87	19.8	VF	I3	0.046	0.75
ABELL 3391 †	4943	06:26:21.511	-53:41:44.81	18.4	VF	I3	0.056	1.44
ABELL 3921	4973	22:49:57.829	-64:25:42.17	29.4	VF	I3	0.093	3.37
AC 114	1562	22:58:48.196	-34:47:56.89	72.5	F	S3	0.312	10.90
CL 0024+17	929	00:26:35.996	+17:09:45.37	39.8	F	S3	0.394	2.88
CL 1221+4918	1662	12:21:26.709	+49:18:21.60	79.1	VF	I3	0.700	8.65
CL J0030+2618	5762	00:30:34.339	+26:18:01.58	17.9	VF	I3	0.500	3.41
CL J0152-1357	913	01:52:42.141	-13:57:59.71	36.5	F	I3	0.831	13.30
CL J0542.8-4100	914	05:42:49.994	-40:59:58.50	50.4	F	I3	0.630	6.18
CL J0848+4456	1708	08:48:48.235	+44:56:16.81	61.4	VF	I1	0.574	0.62
CL J0848+4456	927	08:48:48.252	+44:56:17.13	125.1	VF	I1	0.574	0.62
CL J1113.1-2615	915	11:13:05.167	-26:15:40.43	104.6	F	I3	0.730	2.22
CL J1213+0253	4934	12:13:34.948	+02:53:45.45	18.9	VF	I3	0.409	0.00
CL J1226.9+3332	3180	12:26:58.373	+33:32:47.36	31.7	VF	I3	0.890	30.76
CL J1226.9+3332	5014	12:26:58.372	+33:32:47.18	32.7	VF	I3	0.890	30.76
CL J1641+4001	3575	16:41:53.704	+40:01:44.40	46.5	VF	I3	0.464	0.00
CL J2302.8+0844	918	23:02:48.156	+08:43:52.74	108.6	F	I3	0.730	2.93
DLS J0514-4904	4980	05:14:40.037	-49:03:15.07	19.9	VF	I3	0.091	0.68
EXO 0422-086 †	4183	04:25:51.271	-08:33:36.42	10.0	VF	I3	0.040	0.65
HERCULES A †	1625	16:51:08.161	+04:59:32.44	14.8	VF	S3	0.154	3.27
IRAS 09104+4109	509	09:13:45.481	+40:56:27.49	9.1	F	S3	0.442	0.00
LYNX E	17081	08:48:58.841	+44:51:51.14	61.4	VF	I2	1.260	0.00
LYNX E	9271	08:48:58.858	+44:51:51.46	125.1	VF	I2	1.260	0.00
MACS J0011.7-1523	3261	00:11:42.965	-15:23:20.79	21.6	VF	I3	0.360	10.75
MACS J0011.7-1523	6105	00:11:42.957	-15:23:20.46	37.3	VF	I3	0.360	10.75
MACS J0025.4-1222	3251	00:25:29.368	-12:22:38.05	19.3	VF	I3	0.584	13.00
MACS J0025.4-1222	5010	00:25:29.399	-12:22:38.10	24.8	VF	I3	0.584	13.00
MACS J0035.4-2015	3262	00:35:26.573	-20:15:46.06	21.4	VF	I3	0.364	19.79
MACS J0111.5+0855	3256	01:11:31.515	+08:55:39.21	19.4	VF	I3	0.263	0.64
MACS J0152.5-2852	3264	01:52:34.479	-28:53:38.01	17.5	VF	I3	0.341	6.33
MACS J0159.0-3412	5818	01:59:00.366	-34:13:00.23	9.4	VF	I3	0.458	18.92
MACS J0159.8-0849	3265	01:59:49.453	-08:50:00.90	17.9	VF	I3	0.405	26.31
MACS J0159.8-0849	6106	01:59:49.422	-08:50:00.42	35.3	VF	I3	0.405	26.31
MACS J0242.5-2132	3266	02:42:35.906	-21:32:26.30	11.9	VF	I3	0.314	12.74
MACS J0257.1-2325	1654	02:57:09.130	-23:26:05.85	19.8	F	I3	0.505	21.72
MACS J0257.1-2325	3581	02:57:09.152	-23:26:06.21	18.5	VF	I3	0.505	21.72
MACS J0257.6-2209	3267	02:57:41.024	-22:09:11.12	20.5	VF	I3	0.322	10.77
MACS J0308.9+2645	3268	03:08:55.927	+26:45:38.34	24.4	VF	I3	0.324	20.42
MACS J0329.6-0211	3257	03:29:41.681	-02:11:47.67	9.9	VF	I3	0.450	12.82
MACS J0329.6-0211	3582	03:29:41.688	-02:11:47.81	19.9	VF	I3	0.450	12.82
MACS J0329.6-0211	6108	03:29:41.681	-02:11:47.57	39.6	VF	I3	0.450	12.82
MACS J0404.6+1109	3269	04:04:32.491	+11:08:02.10	21.8	VF	I3	0.355	3.90
MACS J0417.5-1154	3270	04:17:34.686	-11:54:32.71	12.0	VF	I3	0.440	37.99
MACS J0429.6-0253	3271	04:29:36.088	-02:53:09.02	23.2	VF	I3	0.399	11.58
MACS J0451.9+0006	5815	04:51:54.291	+00:06:20.20	10.2	VF	I3	0.430	8.20
MACS J0455.2+0657	5812	04:55:17.426	+06:57:47.15	9.9	VF	I3	0.425	9.77
MACS J0520.7-1328	3272	05:20:42.052	-13:28:49.38	19.2	VF	I3	0.340	9.63
MACS J0547.0-3904	3273	05:47:01.582	-39:04:28.24	21.7	VF	I3	0.210	1.59
MACS J0553.4-3342	5813	05:53:27.200	-33:42:53.02	9.9	VF	I3	0.407	32.68
MACS J0717.5+3745	1655	07:17:31.654	+37:45:18.52	19.9	F	I3	0.548	46.58
MACS J0717.5+3745	4200	07:17:31.651	+37:45:18.46	59.2	VF	I3	0.548	46.58
MACS J0744.8+3927	3197	07:44:52.802	+39:27:24.41	20.2	VF	I3	0.686	24.67
MACS J0744.8+3927	3585	07:44:52.779	+39:27:24.41	19.9	VF	I3	0.686	24.67
MACS J0744.8+3927	6111	07:44:52.800	+39:27:24.81	49.5	VF	I3	0.686	24.67
MACS J0911.2+1746	3587	09:11:11.325	+17:46:31.26	17.9	VF	I3	0.541	10.52
MACS J0911.2+1746	5012	09:11:11.309	+17:46:30.92	23.8	VF	I3	0.541	10.52
MACS J0949+1708	3274	09:49:51.824	+17:07:05.62	14.3	VF	I3	0.382	19.19
MACS J1006.9+3200	5819	10:06:54.668	+32:01:34.61	10.9	VF	I3	0.359	6.06

TABLE 1 — *Continued*

Cluster	Obs.ID	R.A. hr:min:sec	Dec. ° : ′ : ″	ExpT ksec	Mode	ACIS	z	$L_{bol.}$ 10^{44} ergs s^{-1}
(1)	(2)	(3)	(4)	(5)	(6)	(7)	(8)	(9)
MACS J1105.7-1014	5817	11:05:46.462	-10:14:37.20	10.3	VF	I3	0.466	11.29
MACS J1108.8+0906	3252	11:08:55.393	+09:05:50.66	9.9	VF	I3	0.449	8.96
MACS J1108.8+0906	5009	11:08:55.402	+09:05:51.14	24.5	VF	I3	0.449	8.96
MACS J1115.2+5320	3253	11:15:15.632	+53:20:03.31	8.8	VF	I3	0.439	14.29
MACS J1115.2+5320	5008	11:15:15.646	+53:20:03.74	18.0	VF	I3	0.439	14.29
MACS J1115.2+5320	5350	11:15:15.632	+53:20:03.37	6.9	VF	I3	0.439	14.29
MACS J1115.8+0129	3275	11:15:52.048	+01:29:56.56	15.9	VF	I3	0.120	1.47
MACS J1131.8-1955	3276	11:31:56.011	-19:55:55.85	13.9	VF	I3	0.307	17.45
MACS J1149.5+2223	1656	11:49:35.856	+22:23:55.02	18.5	VF	I3	0.544	21.60
MACS J1149.5+2223	3589	11:49:35.848	+22:23:54.55	20.0	VF	I3	0.544	21.60
MACS J1206.2-0847	3277	12:06:12.276	-08:48:02.40	23.5	VF	I3	0.440	37.02
MACS J1226.8+2153	3590	12:26:51.207	+21:49:55.22	19.0	VF	I3	0.370	2.63
MACS J1311.0-0310	3258	13:11:01.665	-03:10:39.50	14.9	VF	I3	0.494	10.03
MACS J1311.0-0310	6110	13:11:01.680	-03:10:39.75	63.2	VF	I3	0.494	10.03
MACS J1319+7003	3278	13:20:08.370	+70:04:33.81	21.6	VF	I3	0.328	7.03
MACS J1427.2+4407	6112	14:27:16.175	+44:07:30.33	9.4	VF	I3	0.477	14.18
MACS J1427.6-2521	3279	14:27:39.389	-25:21:04.66	16.9	VF	I3	0.220	1.55
MACS J1621.3+3810	3254	16:21:25.552	+38:09:43.56	9.8	VF	I3	0.461	11.49
MACS J1621.3+3810	3594	16:21:25.558	+38:09:43.44	19.7	VF	I3	0.461	11.49
MACS J1621.3+3810	6109	16:21:25.535	+38:09:43.34	37.5	VF	I3	0.461	11.49
MACS J1621.3+3810	6172	16:21:25.559	+38:09:43.63	29.8	VF	I3	0.461	11.49
MACS J1731.6+2252	3281	17:31:39.902	+22:52:00.55	20.5	VF	I3	0.366	9.32
MACS J1824.3+4309	3255	18:24:18.444	+43:09:43.39	14.9	VF	I3	0.487	0.00
MACS J1931.8-2634	3282	19:31:49.656	-26:34:33.99	13.6	VF	I3	0.352	23.14
MACS J2046.0-3430	5816	20:46:00.522	-34:30:15.50	10.0	VF	I3	0.413	5.79
MACS J2049.9-3217	3283	20:49:56.245	-32:16:52.30	23.8	VF	I3	0.325	8.71
MACS J2211.7-0349	3284	22:11:45.856	-03:49:37.24	17.7	VF	I3	0.270	22.11
MACS J2214.9-1359	3259	22:14:57.467	-14:00:09.35	19.5	VF	I3	0.503	24.05
MACS J2214.9-1359	5011	22:14:57.481	-14:00:09.69	18.5	VF	I3	0.503	24.05
MACS J2228+2036	3285	22:28:33.241	+20:37:11.42	19.9	VF	I3	0.412	17.92
MACS J2229.7-2755	3286	22:29:45.358	-27:55:38.41	16.4	VF	I3	0.324	9.49
MACS J2243.3-0935	3260	22:43:21.537	-09:35:44.30	20.5	VF	I3	0.101	0.78
MACS J2245.0+2637	3287	22:45:04.547	+26:38:07.88	16.9	VF	I3	0.304	9.36
MACS J2311+0338	3288	23:11:33.213	+03:38:06.51	13.6	VF	I3	0.300	10.98
MKW3S	900	15:21:51.930	+07:42:31.97	57.3	VF	I3	0.045	1.14
MS 0016.9+1609	520	00:18:33.503	+16:26:12.99	67.4	VF	I3	0.541	32.94
MS 0302.7+1658	525	03:05:31.614	+17:10:02.06	10.0	VF	I3	0.424	0.00
MS 0440.5+0204 †	4196	04:43:09.952	+02:10:18.70	59.4	VF	S3	0.190	2.17
MS 0451.6-0305	902	04:54:11.004	-03:00:52.19	44.2	F	S3	0.539	33.32
MS 0735.6+7421	4197	07:41:44.245	+74:14:38.23	45.5	VF	S3	0.216	7.57
MS 0839.8+2938	2224	08:42:55.969	+29:27:26.97	29.8	F	S3	0.194	3.10
MS 0906.5+1110	924	09:09:12.753	+10:58:32.00	29.7	VF	I3	0.163	4.64
MS 1006.0+1202	925	10:08:47.194	+11:47:55.99	29.4	VF	I3	0.221	4.75
MS 1008.1-1224	926	10:10:32.312	-12:39:56.80	44.2	VF	I3	0.301	6.44
MS 1054.5-0321	512	10:56:58.499	-03:37:32.76	89.1	F	S3	0.830	27.22
MS 1455.0+2232	4192	14:57:15.088	+22:20:32.49	91.9	VF	I3	0.259	10.25
MS 1621.5+2640	546	16:23:35.522	+26:34:25.67	30.1	F	I3	0.426	6.49
MS 2053.7-0449	1667	20:56:21.295	-04:37:46.61	44.5	VF	I3	0.583	2.96
MS 2053.7-0449	551	20:56:21.297	-04:37:46.80	44.3	F	I3	0.583	2.96
MS 2137.3-2353	4974	21:40:15.178	-23:39:40.71	57.4	VF	S3	0.313	11.28
MS J1157.3+5531 †	4964	11:59:52.295	+55:32:05.61	75.1	VF	S3	0.081	0.12
NGC 6338 †	4194	17:15:23.036	+57:24:40.29	47.3	VF	I3	0.028	0.13
PKS 0745-191	6103	07:47:31.469	-19:17:40.01	10.3	VF	I3	0.103	18.41
RBS 0797	2202	09:47:12.971	+76:23:13.90	11.7	VF	I3	0.354	26.07
RDCS 1252-29	4198	12:52:54.221	-29:27:21.01	163.4	VF	I3	1.237	2.28
RX J0232.2-4420	4993	02:32:18.771	-44:20:46.68	23.4	VF	I3	0.284	18.17
RX J0340-4542	6954	03:40:44.765	-45:41:18.41	17.9	VF	I3	0.082	0.33
RX J0439+0520	527	04:39:02.218	+05:20:43.11	9.6	VF	I3	0.208	3.57
RX J0439.0+0715	1449	04:39:00.710	+07:16:07.65	6.3	F	I3	0.230	9.44
RX J0439.0+0715	3583	04:39:00.710	+07:16:07.33	19.2	VF	I3	0.230	9.44
RX J0528.9-3927	4994	05:28:53.039	-39:28:15.53	22.5	VF	I3	0.263	12.99
RX J0647.7+7015	3196	06:47:50.029	+70:14:49.66	19.3	VF	I3	0.584	26.48
RX J0647.7+7015	3584	06:47:50.114	+70:14:49.99	20.0	VF	I3	0.584	26.48
RX J0819.6+6336 †	2199	08:19:26.007	+63:37:26.53	14.9	F	S3	0.119	0.98
RX J0910+5422	2452	09:10:44.478	+54:22:03.77	65.3	VF	I3	1.100	1.33
RX J1053+5735	4936	10:53:39.844	+57:35:18.42	92.2	F	S3	1.140	0.00
RX J1347.5-1145	3592	13:47:30.593	-11:45:10.05	57.7	VF	I3	0.451	100.36
RX J1347.5-1145	507	13:47:30.598	-11:45:10.27	10.0	F	S3	0.451	100.36
RX J1350+6007	2229	13:50:48.038	+60:07:08.39	58.3	VF	I3	0.804	2.19
RX J1423.8+2404	1657	14:23:47.759	+24:04:40.45	18.5	VF	I3	0.545	15.84
RX J1423.8+2404	4195	14:23:47.763	+24:04:40.63	115.6	VF	S3	0.545	15.84
RX J1504.1-0248	5793	15:04:07.415	-02:48:15.70	39.2	VF	I3	0.215	34.64
RX J1525+0958	1664	15:24:39.729	+09:57:44.42	50.9	VF	I3	0.516	3.29
RX J1532.9+3021	1649	15:32:55.642	+30:18:57.69	9.4	VF	S3	0.345	20.77
RX J1532.9+3021	1665	15:32:55.641	+30:18:57.31	10.0	VF	I3	0.345	20.77

Cavagnolo et al.

TABLE 1 — *Continued*

Cluster	Obs.ID	R.A. hr:min:sec	Dec. $\circ:':''$	ExpT ksec	Mode	ACIS	z	$L_{bol.}$ 10^{44} ergs s^{-1}
(1)	(2)	(3)	(4)	(5)	(6)	(7)	(8)	(9)
RX J1716.9+6708	548	17:16:49.015	+67:08:25.80	51.7	F	I3	0.810	8.04
RX J1720.1+2638	4361	17:20:09.941	+26:37:29.11	25.7	VF	I3	0.164	11.39
RX J1720.2+3536	3280	17:20:16.953	+35:36:23.63	20.8	VF	I3	0.391	13.02
RX J1720.2+3536	6107	17:20:16.949	+35:36:23.48	33.9	VF	I3	0.391	13.02
RX J1720.2+3536	7225	17:20:16.947	+35:36:23.29	2.0	VF	I3	0.391	13.02
RX J2011.3-5725	4995	20:11:26.889	-57:25:09.08	24.0	VF	I3	0.279	2.77
RX J2129.6+0005	552	21:29:39.944	+00:05:18.83	10.0	VF	I3	0.235	12.56
S0463	6956	04:29:07.040	-53:49:38.02	29.3	VF	I3	0.099	22.19
S0463	7250	04:29:07.063	-53:49:38.11	29.1	VF	I3	0.099	22.19
TRIANG AUSTR †	1281	16:38:22.712	-64:21:19.70	11.4	F	I3	0.051	9.41
V 1121.0+2327	1660	11:20:57.195	+23:26:27.60	71.3	VF	I3	0.560	3.28
ZWCL 1215	4184	12:17:40.787	+03:39:39.42	12.1	VF	I3	0.075	3.49
ZWCL 1358+6245	516	13:59:50.526	+62:31:04.57	54.1	F	S3	0.328	12.42
ZWCL 1953	1659	08:50:06.677	+36:04:16.16	24.9	F	I3	0.380	17.11
ZWCL 3146	909	10:23:39.735	+04:11:08.05	46.0	F	I3	0.290	29.59
ZWCL 5247	539	12:34:21.928	+09:47:02.83	9.3	VF	I3	0.229	4.87
ZWCL 7160	543	14:57:15.158	+22:20:33.85	9.9	F	I3	0.258	10.14
ZWICKY 2701	3195	09:52:49.183	+51:53:05.27	26.9	VF	S3	0.210	5.19
ZwCL 1332.8+5043	5772	13:34:20.698	+50:31:04.64	19.5	VF	I3	0.620	4.46
ZwCl 0848.5+3341	4205	08:51:38.873	+33:31:08.00	11.4	VF	S3	0.371	4.58

NOTE. — (1) Cluster name, (2) CDA observation identification number, (3) R.A. of cluster center, (4) Dec. of cluster center, (5) nominal exposure time, (6) observing mode, (7) CCD location of centroid, (8) redshift, (9) NRAO absorbing Galactic neutral hydrogen column density, (10) bolometric luminosity. † indicates clusters analyzed within R_{5000} only.

TABLE 2
WEIGHTED AVERAGES FOR VARIOUS APERTURES

Aperture	[0.7-7.0] keV	[2.0$_{rest}$-7.0] keV	T_{HBR}	[0.7-7.0] keV	[2.0$_{rest}$-7.0] keV	T_{HBR}
	. . . . Without Core			. . . . With Core		
R_{2500}	4.94±0.02	6.26±0.07	1.16±0.01	4.47±0.02	5.45±0.05	1.13±0.01
R_{5000}	4.83±0.02	6.11±0.07	1.14±0.01	4.27±0.02	5.29±0.05	1.14±0.01
Simulated	3.85±0.004	4.45±0.009	1.13±0.002	. . . .	. . . .	. . . .
Control	4.78±0.004	5.14±0.008	1.00±0.001	. . . .	. . . .	. . . .

NOTE. — Quoted errors are standard deviation of the mean calculated using an unbiased estimator for weighted samples. Simulated sample has been culled to include only T_2=0.75 keV.

TABLE 3
CLUSTERS WITH $T_{HBR} > 1.1$ AT THE 1σ LEVEL.

Name	T_{HBR}	Merger	Core	T_{dec}	X-ray Morphology	Ref.
RX J1525+0958	$1.86^{+0.83}_{-0.51}$	Y	CC	$0.42^{+0.14}_{-0.08}$	Arrowhead shape w/ no visible core	none
MS 1008.1-1224 . . .	$1.59^{+0.37}_{-0.27}$	Y	NCC	$0.93^{+0.19}_{-0.14}$	Wide gas tail extending ∼550 kpc north	[1]
ABELL 2034	$1.40^{+0.14}_{-0.11}$	Y	NCC	$1.07^{+0.11}_{-0.09}$	Prominent cold front, gas tail extending south	[2]
ABELL 401	$1.37^{+0.12}_{-0.10}$	Y	NCC	$1.13^{+0.12}_{-0.10}$	Highly spherical w/ possible cold front to north	[3]
ABELL 1689	$1.36^{+0.14}_{-0.12}$	Y	NCC	$0.95^{+0.09}_{-0.07}$	Exceptionally spherical w/ bright central core	[6],[7]
RX J0439.0+0715 . .	$1.42^{+0.24}_{-0.18}$	Unknown	NCC	$0.98^{+0.11}_{-0.09}$	Bright core w/ possibly cold front to north	none
ABELL 3376	$1.33^{+0.11}_{-0.10}$	Y	NCC	$0.97^{+0.07}_{-0.07}$	Highly disturbed w/ broad gas tail to west	[4],[5]
ABELL 2255	$1.32^{+0.12}_{-0.10}$	Y	NCC	$1.48^{+0.32}_{-0.23}$	Spherical w/ compressed isophotes west of core	[8],[9]
ABELL 2218	$1.36^{+0.19}_{-0.15}$	Y	NCC	$1.39^{+0.23}_{-0.19}$	Spherical, core of cluster elongated NW-SE	[10]
ABELL 1763	$1.48^{+0.39}_{-0.26}$	Y	NCC	$0.83^{+0.17}_{-0.13}$	Elongated ENE-SSW w/ cold front to west of core	[11],[12]
MACS J2243.3-0935	$1.76^{+0.81}_{-0.55}$	Unknown	NCC	$1.73^{+0.44}_{-0.32}$	No core, highly flattened along WNW-ESE axis	none
ABELL 2069	$1.32^{+0.17}_{-0.14}$	Y	NCC	$1.00^{+0.18}_{-0.14}$	No core, highly elongated NNW-SSE	[13]
ABELL 2384	$1.31^{+0.16}_{-0.14}$	Unknown	CC	$0.59^{+0.03}_{-0.03}$	Gas tail extending 1.1 Mpc from core	none
ABELL 168	$1.31^{+0.16}_{-0.14}$	Y	NCC	$1.16^{+0.14}_{-0.10}$	Highly disrupted and irregular	[14],[15]
ABELL 209	$1.38^{+0.28}_{-0.22}$	Y	NCC	$1.08^{+0.22}_{-0.17}$	Asymmetric core structure w/ possible cold front	[16]
ABELL 665	$1.29^{+0.15}_{-0.13}$	Y	NCC	$1.14^{+0.19}_{-0.15}$	Wide, broad gas tail extending north w/ prominent cold front	[17]
1E0657-56	$1.21^{+0.06}_{-0.05}$	Y	NCC	$1.04^{+0.10}_{-0.08}$	The famous "Bullet Cluster"	[18]
MACS J0547.0-3904	$1.51^{+0.50}_{-0.36}$	Unknown	NCC	$0.79^{+0.11}_{-0.09}$	Bright core w/ gas spur extending NW	none
ZWCL 1215	$1.31^{+0.21}_{-0.18}$	Unknown	NCC	$0.95^{+0.15}_{-0.13}$	No core, flattened along NE-SW axis	none
ABELL 1204	$1.26^{+0.17}_{-0.14}$	Unknown	NCC	$0.96^{+0.05}_{-0.05}$	Highly spherical w/ bright centralized core	none
MKW3S	$1.17^{+0.05}_{-0.05}$	Y	CC	$0.87^{+0.02}_{-0.02}$	High mass group, egg shaped w/ bright core	[19]
MACS J2311+0338 .	$1.54^{+0.68}_{-0.42}$	Unknown	NCC	$0.69^{+0.20}_{-0.15}$	Elongated N-S w/ disc-like core elongated toward gas clump	none
ABELL 267	$1.33^{+0.27}_{-0.21}$	Unknown	NCC	$1.09^{+0.20}_{-0.16}$	Elongated NNE-SSW w/ cold front to north	none
RX J1720.1+2638 . .	$1.22^{+0.12}_{-0.11}$	Y	CC	$0.73^{+0.04}_{-0.04}$	Highly spherical w/ bright peaky core and cold front	[20]
ABELL 907	$1.20^{+0.09}_{-0.08}$	Unknown	CC	$0.77^{+0.03}_{-0.03}$	NW-SW elongation and western cold front	none
ABELL 514	$1.26^{+0.19}_{-0.15}$	Y	NCC	$1.56^{+1.07}_{-0.40}$	Very diffuse and disrupted	[21]
ABELL 1651	$1.24^{+0.16}_{-0.13}$	Y	NCC	$1.07^{+0.10}_{-0.08}$	Spherical w/ compressed isophotes to SW	[22]
3C 28.0	$1.23^{+0.14}_{-0.12}$	Y	CC	$0.54^{+0.03}_{-0.03}$	Obvious merger w/ ∼1 Mpc gas tail	[23]
MACS J1427.6-2521	$1.80^{+1.13}_{-0.69}$	Unknown	NCC	$0.85^{+0.19}_{-0.14}$	Highly spherical w/ bright peaky core	none

NOTE. — Clusters ordered by lower limit of T_{HBR}. [1] Ettori & Lombardi (2003), [2] Kempner et al. (2003), [3] Yuan et al. (2005), [4] Markevitch et al. (1998), [5] Bagchi et al. (2006), [6] Teague et al. (1990), [7] Andersson & Madejski (2004), [8] Burns et al. (1995), [9] Feretti et al. (1997), [10] Girardi et al. (1997), [11] Dahle et al. (2002), [12] Smith et al. (2005), [13] Gioia et al. (1982), [14] Hallman & Markevitch (2004), [15] Yang et al. (2004), [16] Mercurio et al. (2003), [17] Gómez et al. (2000), [18] Tucker et al. (1998), [19] Krempec-Krygier & Krygier (1999), [20] Mazzotta et al. (2001), [21] Govoni et al. (2001), [22] Bliton et al. (1998), [23] Gutierrez & Krawczynski (2005)

TABLE 4
SUMMARY OF EXCISED R_{2500} SPECTRAL FITS

Cluster	R_{CORE} kpc	R_{2500} kpc	N_{HI} 10^{20} cm^{-2}	T_{77} keV	T_{27} keV	T_{HBR}	Z_{77} $Z_\odot$	$\chi^2_{red,77}$	$\chi^2_{red,27}$	% Source
(1)	(2)	(3)	(4)	(5)	(6)	(7)	(8)	(9)	(10)	(11)
1E0657 56 †	69	687	6.53	$11.99^{+0.27}_{-0.26}$	$14.54^{+0.67}_{-0.53}$	$1.21^{+0.06}_{-0.05}$	$0.29^{+0.03}_{-0.02}$	1.24	1.11	92
1RXS J2129.4-0741 †	68	504	4.36	$8.22^{+1.18}_{-0.95}$	$8.10^{+1.47}_{-1.10}$	$0.99^{+0.23}_{-0.18}$	$0.43^{+0.18}_{-0.17}$	1.07	1.05	80
2PIGG J0011.5-2850	70	547	2.18	$5.15^{+0.25}_{-0.24}$	$6.20^{+0.79}_{-0.65}$	$1.20^{+0.16}_{-0.14}$	$0.26^{+0.09}_{-0.08}$	1.09	1.00	70
2PIGG J2227.0-3041	70	378	1.11	$2.80^{+0.15}_{-0.14}$	$2.97^{+0.34}_{-0.27}$	$1.06^{+0.11}_{-0.08}$	$0.35^{+0.08}_{-0.08}$	1.16	1.15	69
3C 220.1	70	437	1.91	$9.26^{+14.71}_{-3.98}$	$8.00^{+17.66}_{-4.03}$	$0.86^{+1.49}_{-0.29}$	$0.00^{+0.52}_{-0.00}$	1.15	1.39	61
3C 28.0	70	420	5.71	$5.53^{+0.29}_{-0.27}$	$6.81^{+0.71}_{-0.60}$	$1.23^{+0.14}_{-0.12}$	$0.30^{+0.08}_{-0.07}$	0.98	0.88	87
3C 295	69	466	1.35	$5.16^{+0.42}_{-0.38}$	$5.93^{+0.84}_{-0.69}$	$1.15^{+0.19}_{-0.16}$	$0.38^{+0.12}_{-0.11}$	0.91	0.93	79
3C 388	70	419	6.11	$3.23^{+0.23}_{-0.21}$	$3.26^{+0.49}_{-0.37}$	$1.01^{+0.17}_{-0.13}$	$0.51^{+0.16}_{-0.14}$	0.95	0.95	68
4C 55.16	70	425	4.00	$4.98^{+0.17}_{-0.17}$	$5.54^{+0.40}_{-0.36}$	$1.11^{+0.09}_{-0.08}$	$0.49^{+0.07}_{-0.07}$	0.89	0.80	58
ABELL 0068	69	652	4.60	$9.01^{+1.53}_{-1.14}$	$9.13^{+2.60}_{-1.71}$	$1.01^{+0.34}_{-0.23}$	$0.46^{+0.24}_{-0.22}$	1.15	1.13	79
ABELL 0168 †	69	382	3.27	$2.56^{+0.11}_{-0.08}$	$3.36^{+0.37}_{-0.35}$	$1.31^{+0.16}_{-0.14}$	$0.29^{+0.06}_{-0.04}$	1.07	1.03	40
ABELL 0209 †	70	609	1.68	$7.30^{+0.59}_{-0.51}$	$10.07^{+1.91}_{-1.41}$	$1.38^{+0.28}_{-0.22}$	$0.23^{+0.10}_{-0.09}$	1.12	1.11	82
ABELL 0267 †	69	545	2.74	$6.70^{+0.56}_{-0.47}$	$8.88^{+1.68}_{-1.27}$	$1.33^{+0.27}_{-0.21}$	$0.32^{+0.11}_{-0.11}$	1.18	1.15	82
ABELL 0370	71	517	3.37	$7.35^{+0.72}_{-0.84}$	$10.35^{+1.89}_{-2.27}$	$1.41^{+0.29}_{-0.35}$	$0.45^{+0.06}_{-0.23}$	1.08	1.04	39
ABELL 0383	69	424	4.07	$4.91^{+0.29}_{-0.27}$	$5.42^{+0.74}_{-0.59}$	$1.10^{+0.16}_{-0.13}$	$0.44^{+0.11}_{-0.11}$	0.97	0.90	64
ABELL 0399	70	546	$7.57^{+0.71}_{-0.71}$	$7.95^{+0.35}_{-0.31}$	$8.87^{+0.55}_{-0.50}$	$1.12^{+0.08}_{-0.08}$	$0.30^{+0.05}_{-0.05}$	1.12	0.99	82
ABELL 0401	70	643	12.48	$6.37^{+0.19}_{-0.19}$	$8.71^{+0.72}_{-0.61}$	$1.37^{+0.12}_{-0.10}$	$0.26^{+0.06}_{-0.06}$	1.44	1.05	78
ABELL 0478	70	597	30.90	$7.30^{+0.26}_{-0.24}$	$8.62^{+0.58}_{-0.54}$	$1.18^{+0.09}_{-0.08}$	$0.45^{+0.06}_{-0.05}$	1.05	0.95	91
ABELL 0514	70	495	3.14	$3.60^{+0.18}_{-0.18}$	$4.55^{+0.63}_{-0.50}$	$1.26^{+0.16}_{-0.12}$	$0.30^{+0.09}_{-0.08}$	1.08	0.97	56
ABELL 0520	69	576	$1.06^{+1.06}_{-1.05}$	$9.29^{+0.67}_{-0.60}$	$9.88^{+0.85}_{-0.73}$	$1.06^{+0.12}_{-0.10}$	$0.37^{+0.07}_{-0.07}$	1.11	1.04	87
ABELL 0521	69	535	6.17	$7.03^{+0.59}_{-0.53}$	$8.39^{+1.62}_{-1.22}$	$1.19^{+0.25}_{-0.20}$	$0.39^{+0.13}_{-0.12}$	1.10	1.15	49
ABELL 0586	70	635	4.71	$6.47^{+0.55}_{-0.47}$	$8.06^{+1.46}_{-1.11}$	$1.25^{+0.25}_{-0.19}$	$0.56^{+0.17}_{-0.16}$	0.91	0.81	82
ABELL 0611	69	524	4.99	$7.06^{+0.55}_{-0.48}$	$7.97^{+1.09}_{-0.91}$	$1.13^{+0.18}_{-0.15}$	$0.35^{+0.11}_{-0.10}$	0.97	0.98	54
ABELL 0665	69	618	4.24	$7.45^{+0.38}_{-0.34}$	$9.61^{+1.02}_{-0.85}$	$1.29^{+0.15}_{-0.13}$	$0.31^{+0.06}_{-0.07}$	1.02	0.93	87
ABELL 0697	70	611	3.34	$9.52^{+0.87}_{-0.76}$	$12.24^{+2.05}_{-1.63}$	$1.29^{+0.25}_{-0.20}$	$0.37^{+0.12}_{-0.11}$	1.08	1.02	89
ABELL 0773	69	614	1.46	$7.83^{+0.66}_{-0.57}$	$9.75^{+1.65}_{-1.27}$	$1.25^{+0.24}_{-0.19}$	$0.44^{+0.12}_{-0.12}$	1.06	1.09	84
ABELL 0781	69	661	1.90	$5.81^{+1.01}_{-0.79}$	$7.50^{+3.57}_{-1.81}$	$1.29^{+0.65}_{-0.36}$	$0.31^{+0.20}_{-0.20}$	1.38	1.61	74
ABELL 0907	70	488	5.69	$5.59^{+0.18}_{-0.18}$	$6.69^{+0.47}_{-0.42}$	$1.20^{+0.09}_{-0.08}$	$0.42^{+0.06}_{-0.05}$	1.13	0.99	88
ABELL 0963	70	543	1.39	$6.73^{+0.32}_{-0.30}$	$6.98^{+0.66}_{-0.57}$	$1.04^{+0.11}_{-0.10}$	$0.29^{+0.07}_{-0.08}$	1.06	1.02	64
ABELL 1063S	70	650	1.77	$11.96^{+0.88}_{-0.79}$	$13.70^{+1.68}_{-1.38}$	$1.15^{+0.16}_{-0.14}$	$0.38^{+0.09}_{-0.09}$	1.02	0.98	90
ABELL 1204	70	419	1.44	$3.63^{+0.18}_{-0.16}$	$4.58^{+0.57}_{-0.45}$	$1.26^{+0.17}_{-0.14}$	$0.31^{+0.09}_{-0.09}$	1.06	0.90	88
ABELL 1423	70	614	1.60	$6.01^{+0.75}_{-0.64}$	$7.53^{+2.35}_{-1.55}$	$1.25^{+0.42}_{-0.29}$	$0.30^{+0.18}_{-0.17}$	0.87	0.65	78
ABELL 1651	70	595	2.02	$6.26^{+0.30}_{-0.27}$	$7.78^{+0.90}_{-0.76}$	$1.24^{+0.16}_{-0.13}$	$0.42^{+0.09}_{-0.09}$	1.19	1.20	86
ABELL 1682	70	624	1.10	$7.06^{+1.76}_{-1.26}$	$10.30^{+8.85}_{-3.42}$	$1.46^{+1.31}_{-0.55}$	$0.60^{+0.40}_{-0.33}$	1.19	1.33	64
ABELL 1689 †	70	681	1.87	$9.48^{+0.38}_{-0.35}$	$12.89^{+1.23}_{-1.01}$	$1.36^{+0.14}_{-0.12}$	$0.36^{+0.06}_{-0.05}$	1.13	1.02	91
ABELL 1758	70	573	1.09	$12.14^{+1.15}_{-0.92}$	$11.16^{+3.08}_{-2.14}$	$0.92^{+0.27}_{-0.19}$	$0.56^{+0.13}_{-0.13}$	1.21	1.09	58
ABELL 1763	69	562	0.82	$7.78^{+0.67}_{-0.60}$	$11.49^{+2.89}_{-1.84}$	$1.48^{+0.39}_{-0.25}$	$0.25^{+0.11}_{-0.10}$	1.12	0.92	84
ABELL 1835	69	571	2.36	$9.77^{+0.57}_{-0.52}$	$11.00^{+1.23}_{-1.03}$	$1.13^{+0.14}_{-0.12}$	$0.31^{+0.08}_{-0.07}$	0.98	1.02	86
ABELL 1914	70	698	0.97	$9.62^{+0.55}_{-0.49}$	$11.42^{+1.26}_{-1.06}$	$1.19^{+0.15}_{-0.13}$	$0.30^{+0.08}_{-0.07}$	1.07	1.03	92
ABELL 1942	70	474	2.75	$4.77^{+0.38}_{-0.35}$	$5.49^{+0.98}_{-0.74}$	$1.15^{+0.22}_{-0.18}$	$0.33^{+0.12}_{-0.14}$	1.06	1.04	70
ABELL 1995	70	366	1.44	$8.37^{+0.70}_{-0.61}$	$9.23^{+1.44}_{-1.13}$	$1.10^{+0.20}_{-0.16}$	$0.39^{+0.12}_{-0.11}$	1.02	0.96	74
ABELL 2034	69	594	1.58	$7.15^{+0.23}_{-0.22}$	$10.02^{+0.92}_{-0.75}$	$1.40^{+0.11}_{-0.11}$	$0.32^{+0.05}_{-0.05}$	1.22	1.00	84
ABELL 2069	69	623	1.97	$6.50^{+0.33}_{-0.29}$	$8.61^{+1.02}_{-0.84}$	$1.32^{+0.14}_{-0.14}$	$0.26^{+0.08}_{-0.07}$	1.04	0.96	71
ABELL 2111	69	592	2.20	$7.13^{+1.29}_{-0.95}$	$11.10^{+4.67}_{-3.05}$	$1.56^{+0.48}_{-0.48}$	$0.13^{+0.19}_{-0.13}$	1.06	0.88	76
ABELL 2125	69	370	2.75	$2.88^{+0.30}_{-0.27}$	$3.76^{+0.98}_{-0.65}$	$1.31^{+0.37}_{-0.26}$	$0.31^{+0.18}_{-0.16}$	1.26	1.30	61
ABELL 2163	69	751	12.04	$19.20^{+0.87}_{-0.80}$	$21.30^{+1.77}_{-1.47}$	$1.11^{+0.11}_{-0.09}$	$0.10^{+0.06}_{-0.06}$	1.37	1.26	90
ABELL 2204	70	574	5.84	$8.65^{+0.58}_{-0.52}$	$10.57^{+1.48}_{-1.23}$	$1.22^{+0.19}_{-0.16}$	$0.37^{+0.10}_{-0.09}$	0.95	1.00	90
ABELL 2218	70	557	3.12	$7.35^{+0.39}_{-0.35}$	$10.03^{+1.26}_{-0.98}$	$1.36^{+0.19}_{-0.15}$	$0.22^{+0.07}_{-0.06}$	1.01	0.90	87
ABELL 2255	70	571	2.53	$6.12^{+0.20}_{-0.19}$	$8.10^{+0.66}_{-0.58}$	$1.32^{+0.12}_{-0.10}$	$0.30^{+0.06}_{-0.06}$	1.13	0.95	76
ABELL 2259	70	481	3.70	$5.18^{+0.46}_{-0.39}$	$6.40^{+1.33}_{-0.95}$	$1.24^{+0.28}_{-0.21}$	$0.41^{+0.14}_{-0.14}$	1.05	1.01	85
ABELL 2261	70	577	3.31	$7.63^{+0.47}_{-0.43}$	$9.30^{+1.21}_{-0.91}$	$1.22^{+0.18}_{-0.15}$	$0.36^{+0.08}_{-0.08}$	0.99	0.95	90
ABELL 2294	69	572	6.10	$9.98^{+1.43}_{-1.12}$	$11.07^{+3.19}_{-2.11}$	$1.11^{+0.36}_{-0.25}$	$0.53^{+0.21}_{-0.21}$	1.07	0.95	82
ABELL 2384	69	436	2.99	$4.75^{+0.22}_{-0.20}$	$6.22^{+0.72}_{-0.60}$	$1.31^{+0.16}_{-0.14}$	$0.23^{+0.07}_{-0.07}$	1.06	0.92	81
ABELL 2409	69	512	6.72	$5.94^{+0.43}_{-0.38}$	$6.77^{+0.99}_{-0.82}$	$1.14^{+0.19}_{-0.16}$	$0.37^{+0.13}_{-0.11}$	1.13	0.96	88
ABELL 2537	68	497	4.26	$8.40^{+0.76}_{-0.68}$	$7.81^{+1.15}_{-0.93}$	$0.93^{+0.16}_{-0.13}$	$0.40^{+0.13}_{-0.13}$	0.91	0.84	46
ABELL 2550	69	349	2.03	$2.06^{+0.12}_{-0.11}$	$2.17^{+0.46}_{-0.33}$	$1.05^{+0.23}_{-0.17}$	$0.33^{+0.09}_{-0.08}$	1.26	1.11	34
ABELL 2631	70	631	3.74	$7.06^{+1.06}_{-0.84}$	$7.83^{+2.18}_{-1.45}$	$1.11^{+0.35}_{-0.24}$	$0.34^{+0.19}_{-0.18}$	0.97	0.88	83
ABELL 2667	69	524	1.64	$6.75^{+0.48}_{-0.43}$	$7.45^{+1.06}_{-0.88}$	$1.10^{+0.18}_{-0.15}$	$0.36^{+0.11}_{-0.11}$	1.17	1.08	76
ABELL 2670	69	451	2.88	$3.95^{+0.14}_{-0.12}$	$4.65^{+0.42}_{-0.36}$	$1.18^{+0.11}_{-0.10}$	$0.42^{+0.08}_{-0.06}$	1.13	1.07	70
ABELL 2717	69	298	1.12	$2.63^{+0.17}_{-0.16}$	$3.17^{+0.58}_{-0.43}$	$1.21^{+0.23}_{-0.18}$	$0.48^{+0.13}_{-0.10}$	0.88	0.87	55
ABELL 2744	68	620	1.82	$9.18^{+0.68}_{-0.60}$	$10.20^{+1.38}_{-1.10}$	$1.11^{+0.17}_{-0.14}$	$0.24^{+0.10}_{-0.09}$	0.99	0.90	67
ABELL 3164	69	433	2.55	$2.83^{+0.53}_{-0.26}$	$3.81^{+1.38}_{-1.47}$	$1.35^{+1.28}_{-0.52}$	$0.39^{+0.33}_{-0.21}$	0.88	0.94	29
ABELL 3376 †	69	463	5.21	$4.48^{+0.11}_{-0.12}$	$5.95^{+0.47}_{-0.42}$	$1.33^{+0.11}_{-0.10}$	$0.39^{+0.05}_{-0.08}$	1.16	1.09	63

TABLE 4 — *Continued*

Cluster	R_{CORE} kpc	R_{2500} kpc	N_{HI} 10^{20} cm^{-2}	T_{77} keV	T_{27} keV	T_{HBR}	Z_{77} $Z_{\odot}$	$\chi^2_{red,77}$	$\chi^2_{red,27}$	% Source
(1)	(2)	(3)	(4)	(5)	(6)	(7)	(8)	(9)	(10)	(11)
ABELL 3921	70	535	3.07	$5.70^{+0.24}_{-0.23}$	$6.65^{+0.65}_{-0.54}$	$1.17^{+0.12}_{-0.11}$	$0.31^{+0.08}_{-0.07}$	1.02	0.96	77
AC 114	69	528	1.44	$7.53^{+0.49}_{-0.44}$	$8.30^{+1.03}_{-0.85}$	$1.10^{+0.15}_{-0.13}$	$0.26^{+0.08}_{-0.09}$	1.07	1.06	55
CL 0024+17	70	417	4.36	$6.03^{+1.66}_{-1.10}$	$7.18^{+7.91}_{-3.16}$	$1.19^{+1.35}_{-0.57}$	$0.60^{+0.37}_{-0.33}$	1.00	1.44	37
CL 1221+4918	68	427	1.44	$6.62^{+1.24}_{-0.99}$	$7.11^{+1.73}_{-1.31}$	$1.07^{+0.33}_{-0.25}$	$0.34^{+0.20}_{-0.18}$	0.94	0.93	62
CL J0030+2618	69	753	4.10	$4.63^{+2.72}_{-1.32}$	$5.18^{+8.29}_{-1.96}$	$1.12^{+1.91}_{-0.53}$	$0.26^{+0.75}_{-0.26}$	1.00	1.23	37
CL J0152-1357	69	375	1.45	$7.33^{+2.78}_{-1.77}$	$7.31^{+3.43}_{-2.02}$	$1.00^{+0.60}_{-0.49}$	$0.00^{+0.24}_{-0.00}$	0.89	1.00	36
CL J0542.8-4100	68	427	3.59	$6.07^{+1.47}_{-1.05}$	$6.29^{+2.14}_{-1.41}$	$1.04^{+0.43}_{-0.29}$	$0.16^{+0.23}_{-0.16}$	1.04	0.91	66
CL J0848+4456 †	68	306	2.53	$4.53^{+1.57}_{-1.13}$	$5.52^{+3.28}_{-1.74}$	$1.22^{+0.84}_{-0.49}$	$0.00^{+0.45}_{-0.00}$	0.92	0.93	58
CL J1113.1-2615	69	417	5.51	$4.19^{+1.61}_{-1.02}$	$4.10^{+2.47}_{-1.44}$	$0.98^{+0.70}_{-0.42}$	$0.46^{+0.63}_{-0.44}$	1.01	1.08	23
CL J1213+0253	69	362	1.78	$4.83^{+3.25}_{-1.65}$	$5.05^{+5.43}_{-2.32}$	$1.05^{+1.33}_{-0.60}$	$0.06^{+0.95}_{-0.06}$	0.48	0.62	56
CL J1226.9+3332 †	70	450	1.37	$11.81^{+2.25}_{-1.70}$	$11.29^{+2.45}_{-1.77}$	$0.96^{+0.28}_{-0.20}$	$0.21^{+0.21}_{-0.21}$	0.81	0.86	86
CL J1641+4001	69	234	1.09	$3.29^{+0.93}_{-0.54}$	$5.75^{+3.80}_{-2.01}$	$1.75^{+1.26}_{-0.59}$	$0.77^{+0.92}_{-0.53}$	1.63	1.77	74
CL J2302.8+0844	69	493	5.05	$4.25^{+1.17}_{-1.32}$	$4.67^{+2.00}_{-1.80}$	$1.10^{+0.56}_{-0.54}$	$0.13^{+0.33}_{-0.13}$	0.89	0.97	50
DLS J0514-4904	69	486	2.52	$4.62^{+0.53}_{-0.47}$	$6.14^{+2.08}_{-1.34}$	$1.33^{+0.48}_{-0.32}$	$0.37^{+0.24}_{-0.20}$	1.04	1.12	54
MACS J0011.7-1523 †	69	452	2.08	$6.49^{+0.48}_{-0.43}$	$6.76^{+0.81}_{-0.66}$	$1.04^{+0.15}_{-0.12}$	$0.30^{+0.10}_{-0.09}$	0.86	0.90	87
MACS J0025.4-1222 †	69	454	2.72	$6.33^{+0.85}_{-0.70}$	$6.01^{+1.05}_{-0.85}$	$0.95^{+0.21}_{-0.17}$	$0.37^{+0.16}_{-0.15}$	0.90	0.92	80
MACS J0035.4-2015	69	527	1.55	$7.46^{+0.79}_{-0.66}$	$9.31^{+1.75}_{-1.29}$	$1.25^{+0.27}_{-0.21}$	$0.33^{+0.12}_{-0.12}$	0.94	0.93	90
MACS J0111.5+0855	69	417	4.18	$4.11^{+1.61}_{-1.05}$	$3.72^{+3.08}_{-1.29}$	$0.91^{+0.83}_{-0.39}$	$0.11^{+0.59}_{-0.11}$	0.68	0.65	49
MACS J0152.5-2852	69	440	1.46	$5.64^{+0.89}_{-0.70}$	$7.24^{+2.57}_{-1.59}$	$1.28^{+0.50}_{-0.32}$	$0.22^{+0.17}_{-0.17}$	1.10	1.02	84
MACS J0159.0-3412	69	549	1.54	$10.90^{+4.77}_{-2.53}$	$14.65^{+12.31}_{-5.39}$	$1.34^{+1.27}_{-0.35}$	$0.26^{+0.35}_{-0.26}$	0.87	0.92	81
MACS J0159.8-0849 †	69	587	2.01	$9.16^{+0.71}_{-0.63}$	$9.83^{+1.13}_{-0.96}$	$1.07^{+0.15}_{-0.13}$	$0.30^{+0.09}_{-0.09}$	1.08	1.09	90
MACS J0242.5-2132	69	497	2.71	$5.58^{+0.63}_{-0.52}$	$6.26^{+1.38}_{-0.99}$	$1.12^{+0.28}_{-0.21}$	$0.34^{+0.16}_{-0.15}$	1.03	0.83	87
MACS J0257.1-2325 †	70	579	2.09	$9.25^{+1.28}_{-1.01}$	$10.16^{+1.95}_{-1.54}$	$1.10^{+0.26}_{-0.21}$	$0.14^{+0.12}_{-0.12}$	0.99	1.08	84
MACS J0257.6-2209	68	540	2.02	$8.02^{+1.12}_{-0.88}$	$8.17^{+1.92}_{-1.30}$	$1.02^{+0.28}_{-0.21}$	$0.30^{+0.16}_{-0.17}$	1.12	1.26	84
MACS J0308.9+2645	69	539	11.88	$10.54^{+1.28}_{-1.07}$	$11.38^{+2.16}_{-1.66}$	$1.08^{+0.24}_{-0.19}$	$0.28^{+0.13}_{-0.14}$	0.97	1.01	87
MACS J0329.6-0211 †	71	419	6.21	$6.30^{+0.47}_{-0.41}$	$7.50^{+0.83}_{-0.69}$	$1.19^{+0.16}_{-0.13}$	$0.41^{+0.10}_{-0.09}$	1.10	1.17	86
MACS J0404.6+1109	71	473	14.96	$5.77^{+1.14}_{-0.88}$	$6.15^{+2.00}_{-1.30}$	$1.07^{+0.41}_{-0.28}$	$0.24^{+0.22}_{-0.20}$	0.85	0.78	73
MACS J0417.5-1154	70	430	4.00	$11.07^{+1.98}_{-1.49}$	$14.90^{+5.03}_{-3.24}$	$1.35^{+0.51}_{-0.34}$	$0.33^{+0.19}_{-0.19}$	1.07	0.97	94
MACS J0429.6-0253	68	495	5.70	$5.66^{+0.64}_{-0.54}$	$6.71^{+1.26}_{-0.98}$	$1.19^{+0.26}_{-0.21}$	$0.35^{+0.14}_{-0.13}$	1.21	1.12	82
MACS J0451.9+0006	69	440	7.65	$5.80^{+1.46}_{-1.03}$	$7.02^{+3.29}_{-1.80}$	$1.21^{+0.64}_{-0.38}$	$0.51^{+0.33}_{-0.29}$	1.25	1.35	83
MACS J0455.2+0657	68	461	10.45	$7.25^{+2.04}_{-1.33}$	$8.25^{+3.98}_{-2.10}$	$1.14^{+0.64}_{-0.36}$	$0.56^{+0.37}_{-0.33}$	0.83	0.94	82
MACS J0520.7-1328	69	492	8.88	$6.35^{+0.81}_{-0.67}$	$8.22^{+2.18}_{-1.45}$	$1.29^{+0.38}_{-0.27}$	$0.43^{+0.17}_{-0.16}$	1.23	1.38	86
MACS J0547.0-3904	69	363	4.08	$3.58^{+0.44}_{-0.37}$	$5.41^{+1.67}_{-1.18}$	$1.51^{+0.50}_{-0.36}$	$0.09^{+0.15}_{-0.09}$	1.16	1.42	75
MACS J0553.4-3342	69	663	2.88	$13.14^{+3.82}_{-2.50}$	$13.86^{+6.45}_{-3.44}$	$1.05^{+0.58}_{-0.33}$	$0.57^{+0.35}_{-0.33}$	0.80	0.76	87
MACS J0717.5+3745 †	70	565	6.75	$12.77^{+1.16}_{-1.00}$	$13.21^{+1.58}_{-1.29}$	$1.03^{+0.16}_{-0.13}$	$0.30^{+0.10}_{-0.10}$	0.93	0.90	88
MACS J0744.8+3927 †	71	539	4.66	$8.09^{+0.77}_{-0.66}$	$8.77^{+1.04}_{-0.87}$	$1.08^{+0.16}_{-0.14}$	$0.32^{+0.10}_{-0.10}$	1.14	1.18	82
MACS J0911.2+1746 †	69	518	3.55	$7.51^{+1.27}_{-0.99}$	$7.17^{+1.60}_{-1.20}$	$0.95^{+0.27}_{-0.20}$	$0.21^{+0.17}_{-0.16}$	0.93	0.84	78
MACS J0949+1708	69	556	3.17	$9.16^{+1.53}_{-1.18}$	$9.11^{+2.27}_{-1.55}$	$0.99^{+0.30}_{-0.20}$	$0.37^{+0.20}_{-0.20}$	0.89	0.84	89
MACS J1006.9+3200	69	491	1.83	$7.89^{+2.78}_{-1.74}$	$8.05^{+5.70}_{-2.45}$	$1.02^{+0.81}_{-0.38}$	$0.15^{+0.35}_{-0.15}$	1.84	1.15	76
MACS J1105.7-1014	70	481	4.58	$7.54^{+2.29}_{-1.51}$	$7.78^{+3.93}_{-1.97}$	$1.03^{+0.61}_{-0.33}$	$0.22^{+0.29}_{-0.22}$	1.17	1.27	81
MACS J1108.8+0906 †	71	471	2.52	$6.52^{+0.94}_{-0.82}$	$7.31^{+1.89}_{-1.29}$	$1.12^{+0.33}_{-0.24}$	$0.29^{+0.18}_{-0.17}$	0.95	0.80	80
MACS J1115.2+5320 †	70	527	0.98	$8.91^{+1.42}_{-1.12}$	$9.58^{+2.36}_{-1.62}$	$1.08^{+0.32}_{-0.24}$	$0.37^{+0.20}_{-0.18}$	0.93	0.88	75
MACS J1115.8+0129	69	448	4.36	$6.78^{+1.17}_{-0.91}$	$8.27^{+3.27}_{-2.16}$	$1.22^{+0.53}_{-0.36}$	$0.07^{+0.21}_{-0.07}$	1.00	0.97	65
MACS J1131.8-1955	70	576	4.49	$8.64^{+1.23}_{-0.97}$	$11.01^{+3.61}_{-2.10}$	$1.27^{+0.46}_{-0.28}$	$0.42^{+0.17}_{-0.17}$	1.00	1.00	87
MACS J1149.5+2223 †	69	505	2.32	$7.65^{+0.89}_{-0.75}$	$8.13^{+1.36}_{-1.04}$	$1.06^{+0.22}_{-0.17}$	$0.20^{+0.12}_{-0.11}$	1.00	1.09	87
MACS J1206.2-0847	70	519	4.15	$10.21^{+1.19}_{-0.97}$	$12.51^{+2.44}_{-1.87}$	$1.23^{+0.28}_{-0.22}$	$0.33^{+0.13}_{-0.13}$	0.96	1.05	93
MACS J1226.8+2153	70	469	1.82	$4.21^{+1.07}_{-0.80}$	$5.02^{+3.29}_{-1.52}$	$1.19^{+0.84}_{-0.43}$	$0.23^{+0.38}_{-0.23}$	1.02	0.81	67
MACS J1311.0-0310 †	69	425	2.18	$5.76^{+0.51}_{-0.42}$	$5.91^{+0.73}_{-0.62}$	$1.03^{+0.15}_{-0.13}$	$0.39^{+0.13}_{-0.11}$	0.96	0.98	72
MACS J1319+7003	69	476	1.53	$7.99^{+2.08}_{-1.43}$	$10.62^{+7.35}_{-3.72}$	$1.33^{+0.98}_{-0.47}$	$0.30^{+0.29}_{-0.28}$	1.25	1.24	74
MACS J1427.2+4407	70	467	1.41	$9.80^{+3.81}_{-2.53}$	$10.35^{+6.30}_{-3.26}$	$1.06^{+0.43}_{-0.00}$	$0.00^{+0.34}_{-0.00}$	0.67	0.50	84
MACS J1427.6-2521	70	409	6.11	$4.66^{+0.95}_{-0.72}$	$8.37^{+5.00}_{-2.96}$	$1.80^{+1.13}_{-0.69}$	$0.18^{+0.27}_{-0.18}$	1.19	1.39	68
MACS J1621.3+3810 †	69	505	1.07	$7.12^{+0.66}_{-0.55}$	$7.09^{+0.92}_{-0.75}$	$1.00^{+0.13}_{-0.13}$	$0.34^{+0.11}_{-0.11}$	0.93	0.86	73
MACS J1731.6+2252	70	500	6.48	$7.45^{+1.32}_{-0.99}$	$10.99^{+4.67}_{-2.46}$	$1.48^{+0.68}_{-0.38}$	$0.35^{+0.19}_{-0.17}$	1.20	1.07	84
MACS J1931.8-2634	70	535	9.13	$6.97^{+0.72}_{-0.61}$	$7.72^{+1.31}_{-0.99}$	$1.11^{+0.22}_{-0.17}$	$0.27^{+0.11}_{-0.12}$	0.95	0.86	90
MACS J2046.0-3430	70	370	4.98	$4.64^{+1.18}_{-0.82}$	$5.49^{+2.29}_{-1.47}$	$1.18^{+0.58}_{-0.38}$	$0.20^{+0.32}_{-0.20}$	0.89	1.11	82
MACS J2049.9-3217	69	523	5.99	$6.83^{+0.84}_{-0.69}$	$8.94^{+2.08}_{-1.48}$	$1.31^{+0.34}_{-0.25}$	$0.43^{+0.17}_{-0.15}$	0.99	0.92	83
MACS J2211.7-0349	70	663	5.86	$11.30^{+1.46}_{-1.17}$	$13.82^{+3.54}_{-2.41}$	$1.22^{+0.35}_{-0.27}$	$0.15^{+0.13}_{-0.14}$	1.24	1.26	88
MACS J2214.9-1359 †	70	531	3.32	$9.78^{+1.38}_{-1.09}$	$10.45^{+2.19}_{-1.56}$	$1.07^{+0.27}_{-0.20}$	$0.23^{+0.14}_{-0.14}$	0.99	1.06	87
MACS J2228+2036	70	546	4.52	$7.86^{+1.08}_{-0.85}$	$9.17^{+2.05}_{-1.46}$	$1.17^{+0.31}_{-0.22}$	$0.39^{+0.16}_{-0.15}$	0.99	1.00	88
MACS J2229.7-2755	69	466	1.34	$5.01^{+0.50}_{-0.43}$	$5.79^{+1.11}_{-0.86}$	$1.16^{+0.25}_{-0.20}$	$0.55^{+0.19}_{-0.18}$	1.05	1.08	85
MACS J2243.3-0935	70	550	4.31	$4.09^{+0.51}_{-0.45}$	$7.20^{+3.17}_{-2.12}$	$1.76^{+0.81}_{-0.55}$	$0.03^{+0.15}_{-0.03}$	1.17	0.92	51
MACS J2245.0+2637	70	452	5.50	$6.06^{+0.63}_{-0.54}$	$6.76^{+1.24}_{-0.93}$	$1.12^{+0.24}_{-0.18}$	$0.60^{+0.20}_{-0.18}$	0.94	1.09	88
MACS J2311+0338	69	348	5.23	$8.14^{+1.45}_{-1.16}$	$12.53^{+5.10}_{-2.93}$	$1.54^{+0.68}_{-0.42}$	$0.46^{+0.18}_{-0.20}$	1.07	1.15	88
MKW3S	69	338	3.05	$3.91^{+0.06}_{-0.06}$	$4.58^{+0.18}_{-0.18}$	$1.17^{+0.05}_{-0.05}$	$0.34^{+0.03}_{-0.04}$	1.38	0.97	86

TABLE 4 — *Continued*

Cluster	R_{CORE} kpc	R_{2500} kpc	N_{HI} 10^{20} cm^{-2}	T_{77} keV	T_{27} keV	T_{HBR}	Z_{77} $Z_{\odot}$	$\chi^2_{red,77}$	$\chi^2_{red,27}$	% Source
(1)	(2)	(3)	(4)	(5)	(6)	(7)	(8)	(9)	(10)	(11)
MS 0016.9+1609	69	549	4.06	$8.94^{+0.71}_{-0.62}$	$9.78^{+1.09}_{-0.90}$	$1.09^{+0.15}_{-0.13}$	$0.29^{+0.09}_{-0.08}$	0.91	0.88	83
MS 0302.7+1658	68	354	10.95	$3.27^{+1.05}_{-0.64}$	$2.60^{+1.23}_{-0.55}$	$0.80^{+0.45}_{-0.23}$	$0.81^{+1.56}_{-0.73}$	1.14	1.12	70
MS 0451.6-0305	69	514	5.68	$8.90^{+0.85}_{-0.72}$	$10.43^{+1.59}_{-1.26}$	$1.17^{+0.21}_{-0.17}$	$0.37^{+0.11}_{-0.11}$	1.00	0.93	60
MS 0735.6+7421	69	491	3.40	$5.55^{+0.57}_{-0.22}$	$6.34^{+0.11}_{-0.50}$	$1.14^{+0.11}_{-0.19}$	$0.35^{+0.07}_{-0.06}$	1.05	1.05	62
MS 0839.8+2938	70	415	3.92	$4.68^{+0.52}_{-0.29}$	$5.05^{+0.82}_{-0.65}$	$1.08^{+0.15}_{-0.12}$	$0.46^{+0.13}_{-0.12}$	0.90	0.87	60
MS 0906.5+1110	70	616	3.60	$5.38^{+0.33}_{-0.77}$	$6.76^{+0.92}_{-0.77}$	$1.26^{+0.19}_{-0.16}$	$0.27^{+0.09}_{-0.09}$	1.21	1.08	75
MS 1006.0+1202	69	557	3.63	$5.61^{+0.51}_{-0.43}$	$7.48^{+1.66}_{-1.22}$	$1.33^{+0.32}_{-0.24}$	$0.24^{+0.11}_{-0.12}$	1.30	1.34	75
MS 1008.1-1224	69	549	6.71	$5.65^{+0.49}_{-0.43}$	$9.01^{+1.95}_{-1.38}$	$1.59^{+0.37}_{-0.27}$	$0.26^{+0.11}_{-0.10}$	1.21	0.98	78
MS 1054.5-0321	69	535	3.69	$9.38^{+1.72}_{-1.34}$	$9.91^{+2.66}_{-1.77}$	$1.06^{+0.34}_{-0.24}$	$0.13^{+0.17}_{-0.13}$	1.02	1.03	41
MS 1455.0+2232	70	436	3.35	$4.77^{+0.13}_{-0.13}$	$5.37^{+0.36}_{-0.06}$	$1.13^{+0.08}_{-0.06}$	$0.44^{+0.05}_{-0.05}$	1.29	1.10	90
MS 1621.5+2640	69	515	3.59	$6.11^{+0.95}_{-0.76}$	$6.22^{+1.56}_{-1.10}$	$1.02^{+0.30}_{-0.24}$	$0.40^{+0.23}_{-0.21}$	1.02	1.21	68
MS 2053.7-0449 †	69	538	5.16	$3.66^{+0.81}_{-0.60}$	$4.07^{+1.23}_{-0.83}$	$1.11^{+0.42}_{-0.29}$	$0.39^{+0.38}_{-0.33}$	0.97	1.07	58
MS 2137.3-2353	69	501	3.40	$6.01^{+0.52}_{-0.46}$	$7.48^{+1.68}_{-1.09}$	$1.24^{+0.29}_{-0.20}$	$0.45^{+0.14}_{-0.14}$	1.12	1.25	55
PKS 0745-191	69	651	40.80	$8.13^{+0.39}_{-0.34}$	$9.68^{+0.83}_{-0.72}$	$1.19^{+0.12}_{-0.10}$	$0.38^{+0.06}_{-0.06}$	1.02	0.98	89
RBS 0797	70	494	2.22	$7.68^{+0.92}_{-0.77}$	$9.05^{+1.80}_{-1.33}$	$1.18^{+0.27}_{-0.21}$	$0.32^{+0.14}_{-0.13}$	1.07	1.06	89
RDCS 1252-29	68	264	6.06	$4.25^{+1.82}_{-1.14}$	$4.47^{+2.16}_{-1.29}$	$1.05^{+0.68}_{-0.41}$	$0.79^{+1.01}_{-0.62}$	1.07	1.17	50
RX J0232.2-4420	69	569	2.53	$7.83^{+0.77}_{-0.68}$	$9.92^{+2.11}_{-1.44}$	$1.27^{+0.30}_{-0.21}$	$0.36^{+0.12}_{-0.13}$	1.13	1.09	85
RX J0340-4542	69	395	1.63	$3.16^{+0.38}_{-0.35}$	$2.80^{+0.94}_{-0.57}$	$0.89^{+0.32}_{-0.21}$	$0.62^{+0.31}_{-0.25}$	1.27	1.22	43
RX J0439+0520	69	454	10.02	$4.60^{+0.64}_{-0.59}$	$4.95^{+1.28}_{-0.88}$	$1.08^{+0.32}_{-0.24}$	$0.44^{+0.29}_{-0.24}$	1.03	1.14	77
RX J0439.0+0715 †	69	533	11.16	$5.63^{+0.36}_{-0.32}$	$8.02^{+1.25}_{-0.93}$	$1.42^{+0.24}_{-0.18}$	$0.32^{+0.10}_{-0.08}$	1.28	1.16	82
RX J0528.9-3927	69	641	2.36	$7.89^{+0.96}_{-0.76}$	$8.91^{+2.30}_{-1.42}$	$1.13^{+0.32}_{-0.19}$	$0.27^{+0.14}_{-0.14}$	0.92	0.93	83
RX J0647.7+7015 †	69	513	5.18	$11.28^{+1.85}_{-1.45}$	$11.01^{+2.17}_{-1.63}$	$0.98^{+0.25}_{-0.17}$	$0.20^{+0.17}_{-0.17}$	1.02	1.00	80
RX J0910+5422 †	70	235	2.07	$4.53^{+3.02}_{-1.70}$	$5.98^{+5.30}_{-2.49}$	$1.32^{+1.46}_{-0.00}$	$0.00^{+0.73}_{-0.00}$	0.90	0.71	31
RX J1053+5735	71	241	0.59	$7.03^{+17.25}_{-3.46}$	$5.06^{+12.74}_{-2.48}$	$0.72^{+2.53}_{-0.50}$	$0.55^{+2.26}_{-0.55}$	1.48	1.27	16
RX J1347.5-1145 †	68	607	4.89	$14.62^{+0.97}_{-0.79}$	$16.62^{+1.54}_{-1.24}$	$1.14^{+0.13}_{-0.09}$	$0.32^{+0.08}_{-0.07}$	1.12	1.12	93
RX J1350+6007	68	320	1.77	$4.48^{+2.32}_{-1.49}$	$5.31^{+3.02}_{-2.07}$	$1.19^{+0.91}_{-0.61}$	$0.13^{+1.23}_{-0.13}$	0.82	0.72	57
RX J1423.8+2404 †	70	423	2.65	$6.64^{+0.38}_{-0.34}$	$7.01^{+0.59}_{-0.51}$	$1.06^{+0.11}_{-0.09}$	$0.37^{+0.07}_{-0.07}$	1.02	0.98	86
RX J1504.1-0248	69	628	6.27	$8.00^{+0.27}_{-0.24}$	$8.92^{+0.52}_{-0.46}$	$1.11^{+0.08}_{-0.07}$	$0.40^{+0.04}_{-0.05}$	1.29	1.25	91
RX J1525+0958	71	399	2.96	$3.67^{+0.60}_{-0.44}$	$6.70^{+2.72}_{-1.57}$	$1.83^{+0.80}_{-0.48}$	$0.68^{+0.36}_{-0.29}$	1.27	0.93	78
RX J1532.9+3021 †	69	458	2.21	$6.03^{+0.42}_{-0.38}$	$6.95^{+0.88}_{-0.72}$	$1.15^{+0.17}_{-0.14}$	$0.42^{+0.11}_{-0.10}$	0.94	1.05	73
RX J1716.9+6708	68	466	3.71	$5.71^{+1.47}_{-1.06}$	$5.77^{+1.88}_{-1.28}$	$1.01^{+0.42}_{-0.29}$	$0.68^{+0.42}_{-0.35}$	0.79	0.74	55
RX J1720.1+2638	70	510	4.02	$6.37^{+0.28}_{-0.26}$	$7.78^{+0.69}_{-0.61}$	$1.22^{+0.12}_{-0.11}$	$0.35^{+0.07}_{-0.06}$	1.10	1.02	90
RX J1720.2+3536 †	70	453	3.35	$7.21^{+3.13}_{-0.46}$	$6.97^{+0.76}_{-0.59}$	$0.97^{+0.13}_{-0.10}$	$0.41^{+0.16}_{-0.10}$	1.12	1.09	85
RX J2011.3-5725	70	399	4.76	$3.94^{+0.54}_{-0.37}$	$4.40^{+1.20}_{-0.81}$	$1.12^{+0.43}_{-0.33}$	$0.34^{+0.21}_{-0.18}$	0.94	1.09	76
RX J2129.6+0005	70	690	4.30	$5.91^{+0.54}_{-0.47}$	$7.02^{+1.30}_{-0.99}$	$1.19^{+0.25}_{-0.23}$	$0.45^{+0.15}_{-0.15}$	1.21	1.07	80
S0463 †	69	415	1.06	$3.10^{+0.29}_{-0.25}$	$3.10^{+0.66}_{-0.53}$	$1.00^{+0.23}_{-0.19}$	$0.24^{+0.14}_{-0.11}$	1.10	1.07	47
V 1121.0+2327	71	426	1.30	$3.60^{+0.62}_{-0.46}$	$4.08^{+1.09}_{-0.80}$	$1.13^{+0.36}_{-0.24}$	$0.36^{+0.29}_{-0.24}$	1.21	1.19	66
ZWCL 1215	69	392	1.76	$6.62^{+0.39}_{-0.36}$	$8.67^{+1.29}_{-1.06}$	$1.31^{+0.21}_{-0.19}$	$0.29^{+0.09}_{-0.09}$	1.17	1.04	88
ZWCL 1358+6245	69	530	1.94	$10.66^{+1.48}_{-1.13}$	$10.19^{+4.83}_{-2.24}$	$0.96^{+0.47}_{-0.23}$	$0.47^{+0.19}_{-0.19}$	1.08	1.04	55
ZWCL 1953	69	732	3.10	$7.37^{+1.00}_{-0.78}$	$10.44^{+3.25}_{-2.20}$	$1.42^{+0.48}_{-0.33}$	$0.19^{+0.13}_{-0.13}$	0.84	0.78	74
ZWCL 3146	70	722	2.70	$7.48^{+0.32}_{-0.30}$	$8.61^{+0.66}_{-0.58}$	$1.15^{+0.10}_{-0.09}$	$0.31^{+0.05}_{-0.06}$	1.03	0.98	86
ZWCL 5247	69	609	1.70	$5.06^{+0.85}_{-0.64}$	$5.91^{+2.09}_{-1.30}$	$1.17^{+0.46}_{-0.30}$	$0.22^{+0.21}_{-0.19}$	0.83	0.72	74
ZWCL 7160	70	637	3.10	$4.53^{+0.40}_{-0.35}$	$5.16^{+1.01}_{-0.77}$	$1.14^{+0.24}_{-0.19}$	$0.40^{+0.15}_{-0.14}$	0.94	0.92	80
ZWICKY 2701	69	445	0.83	$5.21^{+0.34}_{-0.30}$	$5.68^{+0.85}_{-0.66}$	$1.09^{+0.18}_{-0.14}$	$0.43^{+0.13}_{-0.11}$	0.89	0.94	57
ZwCL 1332.8+5043	71	616	1.10	$3.62^{+3.46}_{-1.20}$	$3.84^{+5.93}_{-1.48}$	$1.06^{+1.93}_{-0.54}$	$0.76^{+12.45}_{-0.76}$	0.24	0.29	48
ZwCl 0848.5+3341	70	497	1.12	$6.83^{+2.18}_{-1.33}$	$7.24^{+5.11}_{-2.26}$	$1.06^{+0.82}_{-0.39}$	$0.56^{+0.54}_{-0.45}$	0.82	0.93	37

NOTE. — Note: '77' refers to 0.7-7.0 keV band, '27' refers to 2.0_{rest}-7.0 keV band. (1) Cluster name, (2) excluded core region in kpc, (3) R_{2500} in kpc, (3) absorbing, Galactic neutral hydrogen column density, (4,5) best-fit MeKaL temperatures, (6) best-fit 77 MeKaL abundance, (7) $T_{0.7-7.0}/T_{2.0-7.0}$ also called T_{HBR}, (8,9) reduced χ^2 statistics, (10) percent of emission attributable to source. † indicates cluster with multiple independent, simultaneously fit spectra.

TABLE 5
SUMMARY OF EXCISED R$_{5000}$ SPECTRAL FITS

Cluster	R$_{CORE}$	R$_{5000}$	N$_{HI}$	T$_{77}$	T$_{27}$	T$_{HBR}$	Z$_{77}$	$\chi^2_{red,77}$	$\chi^2_{red,27}$	% Source
	kpc	kpc	10^{20} cm^{-2}	keV	keV		Z$_\odot$			
(1)	(2)	(3)	(4)	(5)	(6)	(7)	(8)	(9)	(10)	(11)
1E0657 56 †	69	486	6.53	$11.81^{+0.29}_{-0.27}$	$14.13^{+0.58}_{-0.53}$	$1.20^{+0.06}_{-0.05}$	$0.29^{+0.03}_{-0.03}$	1.22	1.10	95
1RXS J2129.4-0741 †	68	358	4.36	$8.47^{+1.31}_{-1.04}$	$8.57^{+1.73}_{-1.27}$	$1.01^{+0.26}_{-0.19}$	$0.51^{+0.20}_{-0.19}$	1.16	1.27	87
2PIGG J0011.5-2850	70	387	2.18	$5.25^{+0.29}_{-0.27}$	$6.21^{+0.83}_{-0.68}$	$1.18^{+0.17}_{-0.14}$	$0.23^{+0.09}_{-0.08}$	1.08	1.01	78
2PIGG J0311.8-2655	69	320	1.46	$3.35^{+0.25}_{-0.22}$	$3.67^{+0.71}_{-0.54}$	$1.10^{+0.25}_{-0.21}$	$0.33^{+0.13}_{-0.11}$	1.03	1.10	51
2PIGG J2227.0-3041	70	267	1.11	$2.81^{+0.16}_{-0.15}$	$2.99^{+0.36}_{-0.28}$	$1.06^{+0.14}_{-0.11}$	$0.35^{+0.11}_{-0.08}$	1.14	1.10	77
3C 220.1	70	308	1.91	$7.81^{+7.50}_{-3.00}$	$7.49^{+11.53}_{-3.50}$	$0.96^{+0.77}_{-0.38}$	$0.00^{+0.56}_{-0.00}$	0.79	0.76	64
3C 28.0	70	297	5.71	$5.18^{+0.28}_{-0.27}$	$7.11^{+1.15}_{-0.90}$	$1.37^{+0.23}_{-0.19}$	$0.30^{+0.09}_{-0.07}$	0.96	0.77	90
3C 295	69	329	1.35	$5.35^{+0.48}_{-0.41}$	$8.06^{+2.35}_{-1.52}$	$1.51^{+0.46}_{-0.31}$	$0.29^{+0.12}_{-0.10}$	1.01	1.07	86
3C 388	70	297	6.11	$3.27^{+0.24}_{-0.21}$	$3.44^{+0.73}_{-0.51}$	$1.05^{+0.24}_{-0.17}$	$0.43^{+0.16}_{-0.13}$	1.09	1.04	76
4C 55.16	70	300	4.00	$4.88^{+0.16}_{-0.16}$	$5.11^{+0.44}_{-0.39}$	$1.05^{+0.10}_{-0.09}$	$0.52^{+0.07}_{-0.07}$	0.93	0.85	71
ABELL 0013	70	404	2.03	$6.84^{+0.56}_{-0.36}$	$9.29^{+1.37}_{-1.08}$	$1.36^{+0.21}_{-0.17}$	$0.55^{+0.10}_{-0.12}$	1.14	1.10	56
ABELL 0068	69	460	4.60	$9.72^{+1.82}_{-1.36}$	$10.89^{+5.21}_{-2.85}$	$1.12^{+0.58}_{-0.33}$	$0.41^{+0.24}_{-0.23}$	1.08	1.03	87
ABELL 0119	69	399	3.30	$5.86^{+0.28}_{-0.27}$	$6.20^{+0.74}_{-0.59}$	$1.06^{+0.14}_{-0.11}$	$0.44^{+0.10}_{-0.10}$	0.98	0.89	75
ABELL 0168 †	69	270	3.27	$2.56^{+0.13}_{-0.10}$	$3.37^{+0.48}_{-0.41}$	$1.32^{+0.20}_{-0.17}$	$0.32^{+0.07}_{-0.05}$	1.03	0.97	44
ABELL 0209 †	70	430	1.68	$7.32^{+0.65}_{-0.56}$	$10.05^{+2.33}_{-1.58}$	$1.37^{+0.34}_{-0.24}$	$0.21^{+0.11}_{-0.10}$	1.07	1.15	88
ABELL 0267 †	69	385	2.74	$6.46^{+0.51}_{-0.45}$	$7.46^{+1.22}_{-0.91}$	$1.15^{+0.21}_{-0.16}$	$0.37^{+0.12}_{-0.11}$	1.18	1.29	88
ABELL 0370	71	365	3.37	$8.74^{+0.98}_{-0.83}$	$10.15^{+2.17}_{-1.52}$	$1.16^{+0.28}_{-0.21}$	$0.37^{+0.14}_{-0.13}$	1.05	1.02	50
ABELL 0383	69	299	4.07	$4.95^{+0.30}_{-0.28}$	$5.92^{+1.05}_{-0.85}$	$1.20^{+0.22}_{-0.18}$	$0.43^{+0.12}_{-0.11}$	1.12	1.10	75
ABELL 0399	70	386	$8.33^{+0.82}_{-0.80}$	$7.93^{+0.38}_{-0.35}$	$8.86^{+0.67}_{-0.59}$	$1.12^{+0.10}_{-0.09}$	$0.32^{+0.06}_{-0.05}$	1.06	0.96	87
ABELL 0401	70	454	12.48	$6.54^{+0.22}_{-0.20}$	$9.37^{+0.91}_{-0.74}$	$1.43^{+0.15}_{-0.12}$	$0.29^{+0.07}_{-0.07}$	1.53	1.10	85
ABELL 0478	70	422	30.90	$7.27^{+0.26}_{-0.25}$	$8.19^{+0.56}_{-0.50}$	$1.13^{+0.09}_{-0.08}$	$0.47^{+0.06}_{-0.06}$	1.02	0.93	95
ABELL 0514	70	350	3.14	$3.85^{+0.27}_{-0.25}$	$4.92^{+1.02}_{-0.76}$	$1.28^{+0.28}_{-0.21}$	$0.29^{+0.12}_{-0.11}$	1.00	1.01	58
ABELL 0520	69	408	$1.14^{+1.16}_{-1.14}$	$9.15^{+0.73}_{-0.63}$	$10.43^{+1.41}_{-1.06}$	$1.14^{+0.18}_{-0.14}$	$0.36^{+0.07}_{-0.07}$	1.12	1.01	91
ABELL 0521	69	378	6.17	$7.31^{+0.79}_{-0.64}$	$9.01^{+3.73}_{-1.87}$	$1.23^{+0.53}_{-0.28}$	$0.48^{+0.17}_{-0.16}$	1.11	0.95	55
ABELL 0586	70	449	4.71	$6.43^{+0.55}_{-0.49}$	$8.06^{+1.51}_{-1.14}$	$1.25^{+0.26}_{-0.20}$	$0.50^{+0.15}_{-0.15}$	0.88	0.81	87
ABELL 0611	69	369	4.99	$6.79^{+0.51}_{-0.46}$	$6.88^{+1.23}_{-0.95}$	$1.01^{+0.20}_{-0.16}$	$0.32^{+0.15}_{-0.10}$	1.04	1.07	67
ABELL 0644	69	411	6.31	$7.81^{+0.20}_{-0.19}$	$8.08^{+0.44}_{-0.39}$	$1.03^{+0.06}_{-0.06}$	$0.42^{+0.05}_{-0.04}$	1.15	1.05	92
ABELL 0665	69	437	4.24	$7.35^{+0.40}_{-0.37}$	$10.43^{+1.76}_{-1.31}$	$1.42^{+0.25}_{-0.19}$	$0.29^{+0.07}_{-0.07}$	1.07	0.94	91
ABELL 0697	70	433	3.34	$9.78^{+0.99}_{-0.85}$	$14.71^{+4.47}_{-2.90}$	$1.50^{+0.48}_{-0.32}$	$0.48^{+0.13}_{-0.13}$	1.06	0.95	93
ABELL 0773	69	434	1.46	$8.08^{+0.74}_{-0.65}$	$11.24^{+2.84}_{-1.94}$	$1.39^{+0.37}_{-0.26}$	$0.37^{+0.12}_{-0.12}$	1.03	0.96	89
ABELL 0907	70	345	5.69	$5.60^{+0.19}_{-0.18}$	$6.26^{+0.49}_{-0.44}$	$1.12^{+0.10}_{-0.09}$	$0.46^{+0.06}_{-0.06}$	1.17	1.02	92
ABELL 0963	70	385	1.39	$6.97^{+0.35}_{-0.32}$	$7.65^{+1.00}_{-0.82}$	$1.10^{+0.15}_{-0.13}$	$0.29^{+0.08}_{-0.07}$	1.13	1.12	74
ABELL 1063S	70	458	1.77	$11.94^{+0.91}_{-0.80}$	$14.04^{+1.83}_{-1.47}$	$1.18^{+0.18}_{-0.15}$	$0.38^{+0.10}_{-0.09}$	1.01	0.98	94
ABELL 1068	70	304	0.71	$4.67^{+0.18}_{-0.18}$	$5.49^{+0.71}_{-0.58}$	$1.18^{+0.16}_{-0.13}$	$0.37^{+0.06}_{-0.06}$	0.92	0.91	77
ABELL 1201	69	401	1.85	$5.74^{+0.44}_{-0.40}$	$5.99^{+1.39}_{-0.95}$	$1.04^{+0.26}_{-0.18}$	$0.35^{+0.13}_{-0.11}$	1.06	1.10	50
ABELL 1204	70	295	1.44	$3.67^{+0.18}_{-0.16}$	$4.72^{+0.75}_{-0.57}$	$1.29^{+0.21}_{-0.17}$	$0.32^{+0.09}_{-0.09}$	1.11	0.92	92
ABELL 1361	70	316	2.18	$5.14^{+1.00}_{-0.74}$	$7.24^{+8.23}_{-2.78}$	$1.41^{+1.62}_{-0.58}$	$0.29^{+0.31}_{-0.27}$	1.10	0.82	61
ABELL 1423	70	435	1.60	$6.04^{+0.82}_{-0.68}$	$7.93^{+4.09}_{-2.20}$	$1.31^{+0.70}_{-0.39}$	$0.33^{+0.20}_{-0.17}$	0.95	0.91	84
ABELL 1651	70	421	2.02	$6.30^{+0.32}_{-0.28}$	$7.46^{+0.99}_{-0.81}$	$1.18^{+0.17}_{-0.14}$	$0.44^{+0.09}_{-0.09}$	1.13	1.17	91
ABELL 1664	70	291	8.47	$4.26^{+0.30}_{-0.26}$	$4.91^{+1.05}_{-0.80}$	$1.15^{+0.26}_{-0.20}$	$0.31^{+0.12}_{-0.11}$	1.07	1.08	70
ABELL 1689 †	70	480	1.87	$9.76^{+0.40}_{-0.38}$	$12.97^{+1.25}_{-1.05}$	$1.33^{+0.14}_{-0.12}$	$0.35^{+0.06}_{-0.05}$	1.14	1.04	94
ABELL 1758	70	406	1.09	$9.66^{+0.79}_{-0.64}$	$9.90^{+1.22}_{-1.89}$	$1.02^{+0.15}_{-0.21}$	$0.48^{+0.11}_{-0.11}$	1.03	0.96	68
ABELL 1763	69	396	0.82	$7.74^{+0.73}_{-0.64}$	$12.56^{+6.70}_{-3.12}$	$1.62^{+0.88}_{-0.42}$	$0.22^{+0.11}_{-0.12}$	1.16	1.02	89
ABELL 1795	69	449	1.22	$6.05^{+0.15}_{-0.15}$	$6.85^{+0.42}_{-0.38}$	$1.13^{+0.07}_{-0.07}$	$0.33^{+0.04}_{-0.05}$	1.19	1.03	93
ABELL 1835	69	404	2.36	$9.55^{+0.58}_{-0.51}$	$11.99^{+1.96}_{-1.44}$	$1.26^{+0.22}_{-0.17}$	$0.35^{+0.07}_{-0.08}$	0.91	0.88	91
ABELL 1914	70	494	0.97	$9.73^{+0.58}_{-0.51}$	$11.97^{+1.90}_{-1.40}$	$1.23^{+0.21}_{-0.16}$	$0.32^{+0.08}_{-0.07}$	1.11	1.03	95
ABELL 1942	70	334	2.75	$4.96^{+0.45}_{-0.39}$	$5.94^{+2.24}_{-0.99}$	$1.20^{+0.46}_{-0.25}$	$0.37^{+0.15}_{-0.14}$	1.04	0.87	77
ABELL 1995	70	260	1.44	$8.50^{+0.83}_{-0.71}$	$9.41^{+1.87}_{-1.32}$	$1.11^{+0.24}_{-0.18}$	$0.33^{+0.13}_{-0.12}$	1.05	1.02	81
ABELL 2029	69	434	3.26	$8.20^{+0.32}_{-0.29}$	$9.90^{+0.90}_{-0.73}$	$1.21^{+0.12}_{-0.10}$	$0.40^{+0.06}_{-0.06}$	1.07	1.03	94
ABELL 2034	69	420	1.58	$7.35^{+0.26}_{-0.24}$	$9.96^{+1.09}_{-0.84}$	$1.36^{+0.16}_{-0.13}$	$0.34^{+0.05}_{-0.05}$	1.17	1.02	90
ABELL 2065	70	370	2.96	$5.75^{+0.19}_{-0.17}$	$6.39^{+0.46}_{-0.41}$	$1.11^{+0.09}_{-0.08}$	$0.28^{+0.05}_{-0.05}$	1.11	1.01	89
ABELL 2069	69	441	1.97	$6.33^{+0.36}_{-0.32}$	$8.29^{+1.36}_{-1.02}$	$1.31^{+0.23}_{-0.18}$	$0.24^{+0.08}_{-0.08}$	1.14	1.15	78
ABELL 2111	69	418	2.20	$5.74^{+1.43}_{-0.97}$	$7.18^{+6.73}_{-2.52}$	$1.25^{+1.21}_{-0.49}$	$0.16^{+0.30}_{-0.16}$	1.06	0.97	74
ABELL 2125	69	262	2.75	$3.09^{+0.37}_{-0.31}$	$3.69^{+1.99}_{-0.81}$	$1.19^{+0.66}_{-0.29}$	$0.36^{+0.25}_{-0.20}$	1.25	1.22	68
ABELL 2163	69	531	12.04	$18.78^{+0.89}_{-0.83}$	$19.49^{+2.03}_{-1.86}$	$1.04^{+0.12}_{-0.11}$	$0.09^{+0.06}_{-0.05}$	1.33	1.25	93
ABELL 2204 †	70	406	5.84	$9.35^{+0.43}_{-0.41}$	$10.18^{+0.95}_{-0.77}$	$1.09^{+0.11}_{-0.10}$	$0.37^{+0.07}_{-0.07}$	0.95	0.97	86
ABELL 2218	70	394	3.12	$7.37^{+0.40}_{-0.37}$	$9.36^{+1.42}_{-1.07}$	$1.27^{+0.20}_{-0.16}$	$0.22^{+0.07}_{-0.06}$	1.00	0.91	91
ABELL 2219	70	463	1.76	$12.60^{+0.65}_{-0.61}$	$12.54^{+1.52}_{-1.21}$	$1.00^{+0.13}_{-0.11}$	$0.31^{+0.07}_{-0.07}$	1.02	0.98	81
ABELL 2255	70	404	2.53	$6.37^{+0.24}_{-0.23}$	$7.70^{+0.79}_{-0.69}$	$1.21^{+0.13}_{-0.12}$	$0.34^{+0.06}_{-0.06}$	0.93	0.84	81
ABELL 2256	69	423	4.05	$5.66^{+0.19}_{-0.17}$	$7.30^{+0.69}_{-0.63}$	$1.29^{+0.13}_{-0.12}$	$0.31^{+0.07}_{-0.07}$	1.61	1.44	79
ABELL 2259	70	339	3.70	$5.07^{+0.46}_{-0.40}$	$5.49^{+1.29}_{-0.91}$	$1.08^{+0.27}_{-0.20}$	$0.40^{+0.16}_{-0.14}$	0.92	0.92	90
ABELL 2261	70	408	3.31	$7.86^{+0.51}_{-0.47}$	$9.84^{+1.94}_{-1.30}$	$1.25^{+0.26}_{-0.18}$	$0.40^{+0.09}_{-0.09}$	0.98	0.95	94
ABELL 2294	69	404	6.10	$10.49^{+1.75}_{-1.30}$	$12.33^{+5.72}_{-3.05}$	$1.18^{+0.58}_{-0.33}$	$0.57^{+0.25}_{-0.24}$	1.16	1.08	88

TABLE 5 — *Continued*

Cluster	R_{CORE} kpc	R_{5000} kpc	N_{HI} 10^{20} cm^{-2}	T_{77} keV	T_{27} keV	T_{HBR}	Z_{77} $Z_\odot$	$\chi^2_{red,77}$	$\chi^2_{red,27}$	% Source
(1)	(2)	(3)	(4)	(5)	(6)	(7)	(8)	(9)	(10)	(11)
ABELL 2384	69	309	2.99	$4.53^{+0.22}_{-0.21}$	$6.78^{+1.13}_{-0.89}$	$1.50^{+0.26}_{-0.21}$	$0.15^{+0.07}_{-0.06}$	0.99	0.88	86
ABELL 2390	69	447	6.71	$10.85^{+0.34}_{-0.31}$	$10.53^{+0.62}_{-0.53}$	$0.97^{+0.06}_{-0.06}$	$0.35^{+0.05}_{-0.04}$	1.15	1.03	81
ABELL 2409	69	362	6.72	$5.93^{+0.45}_{-0.39}$	$5.87^{+0.95}_{-0.76}$	$0.99^{+0.18}_{-0.14}$	$0.35^{+0.13}_{-0.11}$	1.05	0.76	92
ABELL 2537	68	351	4.26	$8.83^{+0.20}_{-0.74}$	$7.83^{+1.54}_{-1.16}$	$0.89^{+0.15}_{-0.15}$	$0.39^{+0.14}_{-0.14}$	0.93	0.83	59
ABELL 2550	69	247	2.03	$2.12^{+0.11}_{-0.11}$	$2.56^{+0.69}_{-0.49}$	$1.21^{+0.24}_{-0.24}$	$0.36^{+0.15}_{-0.08}$	1.34	1.14	47
ABELL 2554	70	398	2.04	$5.35^{+0.45}_{-0.40}$	$6.46^{+1.93}_{-1.24}$	$1.21^{+0.37}_{-0.25}$	$0.35^{+0.15}_{-0.13}$	0.93	0.79	40
ABELL 2556	70	323	2.02	$3.57^{+0.16}_{-0.15}$	$4.07^{+0.56}_{-0.46}$	$1.14^{+0.16}_{-0.14}$	$0.36^{+0.07}_{-0.07}$	0.99	0.95	58
ABELL 2631	70	446	3.74	$7.18^{+1.18}_{-0.94}$	$9.18^{+3.17}_{-1.96}$	$1.28^{+0.49}_{-0.32}$	$0.34^{+0.20}_{-0.19}$	1.03	0.99	89
ABELL 2667	69	371	1.64	$6.68^{+0.48}_{-0.43}$	$7.35^{+1.27}_{-1.05}$	$1.10^{+0.21}_{-0.17}$	$0.41^{+0.12}_{-0.12}$	1.05	0.95	84
ABELL 2670	69	319	2.88	$3.96^{+0.13}_{-0.13}$	$4.75^{+0.50}_{-0.41}$	$1.20^{+0.13}_{-0.11}$	$0.45^{+0.08}_{-0.07}$	1.16	1.09	80
ABELL 2717	69	210	1.12	$2.59^{+0.17}_{-0.16}$	$3.18^{+0.59}_{-0.44}$	$1.23^{+0.24}_{-0.19}$	$0.53^{+0.14}_{-0.12}$	0.90	0.95	67
ABELL 2744	68	439	1.82	$9.82^{+0.89}_{-0.77}$	$11.21^{+2.76}_{-1.81}$	$1.14^{+0.30}_{-0.26}$	$0.30^{+0.12}_{-0.12}$	0.88	0.73	74
ABELL 3128	69	305	1.59	$3.04^{+0.23}_{-0.21}$	$3.48^{+0.73}_{-0.54}$	$1.14^{+0.26}_{-0.19}$	$0.33^{+0.13}_{-0.10}$	1.05	1.13	64
ABELL 3158 †	70	381	1.60	$5.08^{+0.08}_{-0.08}$	$6.26^{+0.26}_{-0.24}$	$1.23^{+0.05}_{-0.05}$	$0.40^{+0.03}_{-0.03}$	1.15	0.97	89
ABELL 3164	69	306	2.55	$2.40^{+0.65}_{-0.48}$	$3.19^{+5.68}_{-1.41}$	$1.33^{+2.39}_{-0.64}$	$0.23^{+0.32}_{-0.19}$	1.29	1.59	30
ABELL 3376 †	69	327	5.21	$4.44^{+0.14}_{-0.13}$	$5.94^{+0.55}_{-0.47}$	$1.34^{+0.13}_{-0.11}$	$0.36^{+0.06}_{-0.06}$	1.18	1.13	65
ABELL 3391	69	397	5.46	$5.72^{+0.31}_{-0.28}$	$6.44^{+0.80}_{-0.66}$	$1.13^{+0.15}_{-0.13}$	$0.11^{+0.08}_{-0.07}$	1.00	0.97	67
ABELL 3921	70	378	3.07	$5.69^{+0.25}_{-0.24}$	$6.74^{+0.71}_{-0.58}$	$1.18^{+0.14}_{-0.11}$	$0.34^{+0.08}_{-0.07}$	0.93	0.85	84
AC 114	69	373	1.44	$7.75^{+0.56}_{-0.50}$	$9.76^{+2.28}_{-1.55}$	$1.26^{+0.31}_{-0.22}$	$0.36^{+0.11}_{-0.10}$	1.01	0.95	63
CL 0024+17	70	296	4.36	$4.75^{+1.07}_{-0.76}$	$7.14^{+5.42}_{-2.83}$	$1.50^{+1.19}_{-0.64}$	$0.58^{+0.35}_{-0.30}$	1.07	0.97	44
CL 1221+4918	68	300	1.44	$6.73^{+1.29}_{-1.02}$	$7.60^{+4.33}_{-2.01}$	$1.13^{+0.68}_{-0.34}$	$0.32^{+0.20}_{-0.19}$	0.92	0.69	73
CL J0030+2618	69	532	4.10	$4.48^{+2.43}_{-1.40}$	$3.77^{+9.73}_{-1.96}$	$0.84^{+2.22}_{-0.51}$	$0.00^{+0.37}_{-0.00}$	1.01	0.85	51
CL J0152-1357	69	266	1.45	$7.20^{+7.14}_{-2.48}$	$6.07^{+6.16}_{-2.51}$	$0.84^{+1.20}_{-0.45}$	$0.00^{+0.63}_{-0.00}$	2.97	3.26	49
CL J0542.8-4100	68	300	3.59	$5.65^{+1.21}_{-0.90}$	$5.93^{+3.52}_{-1.76}$	$1.05^{+0.66}_{-0.35}$	$0.25^{+0.24}_{-0.22}$	0.67	0.58	72
CL J0848+4456 †	68	215	2.53	$3.73^{+1.47}_{-0.85}$	$4.96^{+2.82}_{-1.81}$	$1.33^{+0.92}_{-0.57}$	$0.17^{+0.98}_{-0.17}$	0.87	0.82	64
CL J1113.1-2615	69	295	5.51	$4.74^{+1.52}_{-0.98}$	$4.79^{+1.15}_{-1.26}$	$1.01^{+0.40}_{-0.34}$	$0.53^{+0.37}_{-0.37}$	1.02	1.01	32
CL J1226.9+3332 †	70	316	1.37	$13.02^{+2.69}_{-2.00}$	$12.33^{+2.78}_{-2.13}$	$0.95^{+0.23}_{-0.22}$	$0.18^{+0.23}_{-0.18}$	0.75	0.80	91
CL J2302.8+0844	69	347	5.05	$5.94^{+1.73}_{-1.86}$	$6.58^{+8.08}_{-2.67}$	$1.11^{+1.40}_{-0.57}$	$0.10^{+0.29}_{-0.10}$	0.94	1.01	56
DLS J0514-4904	69	344	2.52	$4.94^{+0.61}_{-0.55}$	$6.26^{+2.33}_{-1.30}$	$1.27^{+0.50}_{-0.23}$	$0.35^{+0.27}_{-0.23}$	0.86	1.03	63
EXO 0422-086	70	294	6.22	$3.41^{+0.14}_{-0.13}$	$3.44^{+0.37}_{-0.31}$	$1.01^{+0.12}_{-0.10}$	$0.37^{+0.08}_{-0.08}$	0.96	0.93	80
HERCULES A	69	313	$1.49^{+2.01}_{-1.49}$	$5.28^{+0.60}_{-0.50}$	$4.50^{+0.88}_{-0.65}$	$0.85^{+0.19}_{-0.15}$	$0.42^{+0.15}_{-0.14}$	0.98	0.98	70
LYNX E †	68	185	2.53	$4.14^{+1.31}_{-1.38}$	$3.06^{+3.86}_{-0.70}$	$0.74^{+1.31}_{-0.30}$	$3.10^{+33.81}_{-2.93}$	0.27	0.44	66
MACS J0011.7-1523 †	69	320	2.08	$6.73^{+0.55}_{-0.47}$	$7.27^{+0.99}_{-0.74}$	$1.08^{+0.17}_{-0.13}$	$0.27^{+0.10}_{-0.09}$	0.90	0.95	92
MACS J0025.4-1222 †	69	321	2.72	$6.65^{+1.07}_{-0.85}$	$6.31^{+1.38}_{-1.02}$	$0.95^{+0.26}_{-0.19}$	$0.39^{+0.20}_{-0.19}$	0.66	0.75	86
MACS J0035.4-2015	69	373	1.55	$7.72^{+0.88}_{-0.74}$	$9.39^{+1.91}_{-1.35}$	$1.22^{+0.28}_{-0.21}$	$0.39^{+0.14}_{-0.13}$	1.02	1.05	94
MACS J0111.5+0855	69	294	4.18	$4.12^{+1.60}_{-1.04}$	$4.16^{+2.96}_{-1.44}$	$1.01^{+0.82}_{-0.43}$	$0.00^{+0.43}_{-0.00}$	0.79	1.23	62
MACS J0152.5-2852	69	311	1.46	$5.75^{+1.05}_{-0.78}$	$7.70^{+3.21}_{-1.89}$	$1.34^{+0.61}_{-0.38}$	$0.28^{+0.22}_{-0.21}$	0.84	0.58	90
MACS J0159.0-3412	69	388	1.54	$10.99^{+5.87}_{-2.95}$	$12.74^{+12.45}_{-4.72}$	$1.16^{+1.29}_{-0.53}$	$0.50^{+0.52}_{-0.50}$	1.35	1.34	85
MACS J0159.8-0849 †	69	414	2.01	$9.36^{+0.77}_{-0.67}$	$10.37^{+1.29}_{-1.04}$	$1.11^{+0.17}_{-0.14}$	$0.29^{+0.09}_{-0.09}$	1.05	1.01	94
MACS J0242.5-2132	69	351	2.71	$5.48^{+0.62}_{-0.51}$	$5.99^{+2.04}_{-1.19}$	$1.09^{+0.39}_{-0.24}$	$0.32^{+0.16}_{-0.15}$	1.08	1.06	92
MACS J0257.1-2325 †	70	409	2.09	$9.42^{+1.37}_{-1.05}$	$10.76^{+2.05}_{-1.69}$	$1.14^{+0.27}_{-0.22}$	$0.14^{+0.13}_{-0.13}$	1.03	1.13	90
MACS J0257.6-2209	68	382	2.02	$8.09^{+1.10}_{-0.88}$	$7.90^{+1.64}_{-1.20}$	$0.98^{+0.24}_{-0.18}$	$0.41^{+0.19}_{-0.18}$	1.13	1.24	90
MACS J0308.9+2645	69	381	11.88	$10.64^{+1.38}_{-1.14}$	$11.12^{+2.23}_{-1.68}$	$1.05^{+0.24}_{-0.19}$	$0.37^{+0.15}_{-0.15}$	0.96	0.97	92
MACS J0329.6-0211 †	71	296	6.21	$6.44^{+0.50}_{-0.45}$	$7.55^{+0.88}_{-0.73}$	$1.17^{+0.16}_{-0.14}$	$0.40^{+0.10}_{-0.09}$	1.12	1.16	91
MACS J0404.6+1109	71	334	14.96	$6.90^{+2.01}_{-1.29}$	$7.40^{+3.63}_{-1.93}$	$1.07^{+0.61}_{-0.34}$	$0.22^{+0.27}_{-0.22}$	0.96	0.92	80
MACS J0417.5-1154	70	303	4.00	$10.44^{+2.08}_{-1.56}$	$14.46^{+5.92}_{-3.41}$	$1.39^{+0.63}_{-0.39}$	$0.41^{+0.23}_{-0.21}$	1.10	1.17	96
MACS J0429.6-0253	68	349	5.70	$5.96^{+0.72}_{-0.60}$	$7.48^{+2.65}_{-1.64}$	$1.26^{+0.47}_{-0.30}$	$0.34^{+0.15}_{-0.14}$	1.02	0.78	89
MACS J0451.9+0006	69	312	7.65	$5.76^{+1.77}_{-1.11}$	$6.68^{+4.50}_{-1.94}$	$1.16^{+0.86}_{-0.40}$	$0.47^{+0.46}_{-0.38}$	1.03	1.33	89
MACS J0455.2+0657	68	326	10.45	$6.99^{+2.27}_{-1.44}$	$8.35^{+5.66}_{-2.49}$	$1.19^{+0.90}_{-0.43}$	$0.48^{+0.35}_{-0.31}$	1.04	1.24	88
MACS J0520.7-1328	69	347	8.88	$6.77^{+1.01}_{-0.79}$	$9.41^{+3.38}_{-1.91}$	$1.39^{+0.53}_{-0.33}$	$0.33^{+0.16}_{-0.16}$	1.22	1.33	91
MACS J0547.0-3904	69	256	4.08	$3.70^{+0.44}_{-0.37}$	$5.82^{+2.97}_{-1.66}$	$1.57^{+0.82}_{-0.48}$	$0.24^{+0.21}_{-0.17}$	1.14	1.21	83
MACS J0553.4-3342	69	470	2.88	$13.90^{+5.89}_{-3.28}$	$14.59^{+11.16}_{-4.72}$	$1.05^{+0.92}_{-0.42}$	$0.38^{+0.39}_{-0.38}$	1.22	1.10	91
MACS J0717.5+3745 †	70	400	6.75	$13.30^{+1.44}_{-1.21}$	$12.82^{+1.70}_{-1.39}$	$0.96^{+0.17}_{-0.14}$	$0.32^{+0.12}_{-0.13}$	0.91	0.87	91
MACS J0744.8+3927 †	71	379	4.66	$8.58^{+0.85}_{-0.73}$	$9.32^{+1.20}_{-0.96}$	$1.09^{+0.18}_{-0.15}$	$0.30^{+0.11}_{-0.11}$	1.14	1.19	89
MACS J0911.2+1746 †	69	367	3.55	$7.71^{+1.55}_{-1.16}$	$7.88^{+2.11}_{-1.44}$	$1.02^{+0.34}_{-0.24}$	$0.22^{+0.20}_{-0.20}$	0.77	0.77	85
MACS J0949+1708	69	395	3.17	$8.94^{+1.57}_{-1.20}$	$10.29^{+5.60}_{-2.41}$	$1.15^{+0.66}_{-0.31}$	$0.48^{+0.23}_{-0.22}$	0.74	0.58	93
MACS J1006.9+3200	69	348	1.83	$7.03^{+2.66}_{-1.64}$	$6.53^{+4.61}_{-2.11}$	$0.93^{+0.74}_{-0.37}$	$0.18^{+0.45}_{-0.18}$	1.64	1.53	81
MACS J1105.7-1014	70	341	4.58	$7.73^{+2.85}_{-1.73}$	$6.61^{+3.02}_{-1.79}$	$0.86^{+0.50}_{-0.30}$	$0.20^{+0.32}_{-0.20}$	1.27	1.08	87
MACS J1108.8+0906 †	71	331	2.52	$6.80^{+1.21}_{-0.93}$	$7.52^{+2.39}_{-1.53}$	$1.11^{+0.40}_{-0.27}$	$0.24^{+0.20}_{-0.19}$	1.08	1.01	86
MACS J1115.2+5320 †	70	373	0.98	$9.58^{+1.85}_{-1.37}$	$9.80^{+2.74}_{-1.81}$	$1.02^{+0.35}_{-0.24}$	$0.37^{+0.22}_{-0.21}$	0.94	0.91	82
MACS J1115.8+0129	69	317	4.36	$6.82^{+1.15}_{-0.88}$	$9.39^{+4.77}_{-2.84}$	$1.38^{+0.74}_{-0.45}$	$0.07^{+0.19}_{-0.07}$	0.94	0.85	77
MACS J1131.8-1955	70	408	4.49	$8.64^{+1.32}_{-1.03}$	$9.45^{+2.52}_{-1.68}$	$1.09^{+0.34}_{-0.23}$	$0.49^{+0.19}_{-0.19}$	1.07	1.02	91
MACS J1149.5+2223 †	69	359	2.32	$7.72^{+0.94}_{-0.79}$	$8.36^{+1.51}_{-1.14}$	$1.08^{+0.24}_{-0.18}$	$0.25^{+0.12}_{-0.13}$	0.87	0.94	75
MACS J1206.2-0847	70	368	4.15	$9.98^{+1.27}_{-1.01}$	$11.93^{+2.56}_{-1.88}$	$1.20^{+0.30}_{-0.22}$	$0.32^{+0.14}_{-0.14}$	1.02	1.15	95

TABLE 5 — *Continued*

Cluster	R_{CORE} kpc	R_{5000} kpc	N_{HI} 10^{20} cm^{-2}	T_{77} keV	T_{27} keV	T_{HBR}	Z_{77} $Z_\odot$	$\chi^2_{red,77}$	$\chi^2_{red,27}$	% Source
(1)	(2)	(3)	(4)	(5)	(6)	(7)	(8)	(9)	(10)	(11)
MACS J1226.8+2153	70	333	1.82	$4.86^{+1.58}_{-1.08}$	$5.84^{+3.45}_{-2.14}$	$1.20^{+0.81}_{-0.51}$	$0.00^{+0.28}_{-0.00}$	1.32	1.36	78
MACS J1311.0-0310 †	69	300	2.18	$5.73^{+0.46}_{-0.40}$	$5.92^{+0.70}_{-0.60}$	$1.03^{+0.15}_{-0.13}$	$0.44^{+0.12}_{-0.12}$	0.93	1.00	83
MACS J1319+7003	69	337	1.53	$8.08^{+2.14}_{-1.56}$	$10.12^{+5.50}_{-2.78}$	$1.25^{+0.76}_{-0.42}$	$0.10^{+0.25}_{-0.10}$	1.00	1.07	82
MACS J1427.2+4407	70	331	1.41	$8.61^{+4.04}_{-2.23}$	$8.83^{+5.55}_{-2.81}$	$1.03^{+0.80}_{-0.42}$	$0.14^{+0.36}_{-0.14}$	0.68	0.58	90
MACS J1427.6-2521	70	289	6.11	$4.43^{+0.86}_{-0.64}$	$5.54^{+3.81}_{-1.77}$	$1.25^{+0.89}_{-0.44}$	$0.21^{+0.26}_{-0.21}$	1.08	1.15	79
MACS J1621.3+3810 †	69	357	1.07	$7.49^{+0.73}_{-0.63}$	$7.75^{+1.12}_{-0.89}$	$1.03^{+0.18}_{-0.15}$	$0.35^{+0.13}_{-0.12}$	0.98	0.92	82
MACS J1731.6+2252	70	353	6.48	$8.19^{+1.88}_{-1.31}$	$10.50^{+4.76}_{-2.46}$	$1.28^{+0.65}_{-0.36}$	$0.49^{+0.27}_{-0.25}$	1.16	0.98	87
MACS J1824.3+4309	68	246	4.52	$4.13^{+1.87}_{-1.01}$	$4.76^{+10.39}_{-1.86}$	$1.15^{+2.57}_{-0.53}$	$0.76^{+2.14}_{-0.75}$	0.52	0.13	78
MACS J1931.8-2634	70	377	9.13	$6.85^{+0.73}_{-0.61}$	$6.86^{+1.58}_{-1.15}$	$1.00^{+0.25}_{-0.19}$	$0.23^{+0.12}_{-0.11}$	1.02	1.07	94
MACS J2046.0-3430	70	263	4.98	$5.02^{+1.95}_{-1.04}$	$6.23^{+2.57}_{-2.30}$	$1.24^{+0.70}_{-0.53}$	$0.23^{+0.55}_{-0.23}$	1.10	1.14	89
MACS J2049.9-3217	69	371	5.99	$7.88^{+1.22}_{-0.98}$	$11.48^{+4.02}_{-2.42}$	$1.46^{+0.56}_{-0.36}$	$0.37^{+0.18}_{-0.23}$	0.94	0.90	89
MACS J2211.7-0349	70	469	5.86	$11.13^{+1.45}_{-1.15}$	$13.77^{+3.49}_{-2.40}$	$1.24^{+0.35}_{-0.25}$	$0.18^{+0.14}_{-0.14}$	1.33	1.34	93
MACS J2214.9-1359 †	70	376	3.32	$9.87^{+1.54}_{-1.17}$	$9.97^{+2.17}_{-1.50}$	$1.01^{+0.27}_{-0.19}$	$0.31^{+0.17}_{-0.17}$	1.03	1.01	92
MACS J2228+2036	70	387	4.52	$7.79^{+1.14}_{-0.90}$	$10.04^{+3.96}_{-2.25}$	$1.29^{+0.54}_{-0.32}$	$0.41^{+0.18}_{-0.17}$	0.84	0.96	92
MACS J2229.7-2755	69	330	1.34	$5.25^{+0.54}_{-0.46}$	$6.07^{+1.76}_{-1.18}$	$1.16^{+0.36}_{-0.25}$	$0.59^{+0.20}_{-0.19}$	0.98	1.02	91
MACS J2243.3-0935	70	389	4.31	$5.15^{+0.65}_{-0.54}$	$8.81^{+4.31}_{-2.67}$	$1.71^{+0.86}_{-0.55}$	$0.05^{+0.17}_{-0.05}$	1.38	1.27	66
MACS J2245.0+2637	70	320	5.50	$6.05^{+0.66}_{-0.56}$	$7.05^{+1.31}_{-1.08}$	$1.17^{+0.25}_{-0.21}$	$0.64^{+0.21}_{-0.20}$	0.78	0.95	92
MACS J2311+0338	69	247	5.23	$7.60^{+1.60}_{-1.19}$	$11.76^{+8.05}_{-3.81}$	$1.55^{+1.11}_{-0.56}$	$0.44^{+0.24}_{-0.22}$	1.21	0.96	92
MKW3S	69	239	3.05	$3.93^{+0.06}_{-0.06}$	$4.58^{+0.19}_{-0.17}$	$1.17^{+0.05}_{-0.05}$	$0.35^{+0.02}_{-0.03}$	1.28	0.93	88
MS 0016.9+1609	69	388	4.06	$9.11^{+0.79}_{-0.68}$	$11.73^{+2.98}_{-1.84}$	$1.29^{+0.35}_{-0.22}$	$0.32^{+0.10}_{-0.09}$	0.91	0.92	88
MS 0440.5+0204	70	477	9.10	$5.99^{+0.91}_{-0.73}$	$4.45^{+1.61}_{-1.37}$	$0.74^{+0.29}_{-0.25}$	$0.66^{+0.32}_{-0.29}$	0.89	0.74	28
MS 0451.6-0305	69	363	5.68	$9.25^{+0.89}_{-0.77}$	$11.55^{+2.88}_{-1.91}$	$1.25^{+0.33}_{-0.23}$	$0.42^{+0.12}_{-0.11}$	0.95	0.94	71
MS 0735.6+7421	69	347	3.40	$5.54^{+0.24}_{-0.23}$	$6.47^{+0.75}_{-0.65}$	$1.17^{+0.14}_{-0.12}$	$0.35^{+0.07}_{-0.07}$	1.09	1.08	74
MS 0839.8+2938	70	293	3.92	$4.63^{+0.30}_{-0.28}$	$4.64^{+0.94}_{-0.71}$	$1.00^{+0.21}_{-0.16}$	$0.49^{+0.13}_{-0.13}$	0.97	0.91	69
MS 0906.5+1110	70	436	3.60	$5.56^{+0.34}_{-0.31}$	$6.94^{+1.23}_{-0.92}$	$1.25^{+0.23}_{-0.18}$	$0.34^{+0.10}_{-0.10}$	1.20	0.97	82
MS 1006.0+1202	69	393	3.63	$5.79^{+0.54}_{-0.46}$	$7.76^{+2.25}_{-1.56}$	$1.34^{+0.41}_{-0.29}$	$0.28^{+0.12}_{-0.12}$	1.22	1.24	82
MS 1008.1-1224	69	388	6.71	$5.76^{+0.56}_{-0.47}$	$9.88^{+2.54}_{-1.70}$	$1.72^{+0.47}_{-0.33}$	$0.24^{+0.11}_{-0.11}$	1.29	1.08	83
MS 1054.5-0321	69	378	3.69	$9.75^{+1.69}_{-1.28}$	$14.17^{+12.06}_{-4.93}$	$1.45^{+1.26}_{-0.54}$	$0.16^{+0.16}_{-0.16}$	1.05	0.85	51
MS 1455.0+2232	70	308	3.35	$4.81^{+0.13}_{-0.13}$	$5.81^{+0.42}_{-0.36}$	$1.21^{+0.09}_{-0.08}$	$0.46^{+0.05}_{-0.05}$	1.34	1.12	94
MS 1621.5+2640	69	363	3.59	$5.72^{+0.90}_{-0.72}$	$5.10^{+2.04}_{-1.27}$	$0.89^{+0.38}_{-0.25}$	$0.37^{+0.23}_{-0.21}$	1.00	0.98	74
MS 2053.7-0449 †	69	381	5.16	$4.68^{+1.04}_{-0.75}$	$5.37^{+1.73}_{-1.19}$	$1.15^{+0.45}_{-0.31}$	$0.26^{+0.26}_{-0.24}$	0.99	0.94	65
MS 2137.3-2353	69	355	3.40	$6.00^{+0.55}_{-0.47}$	$7.56^{+2.79}_{-1.46}$	$1.26^{+0.48}_{-0.26}$	$0.35^{+0.13}_{-0.12}$	1.08	1.28	69
MS J1157.3+5531	70	272	1.22	$3.28^{+0.36}_{-0.32}$	$10.57^{+6.42}_{-3.33}$	$3.22^{+1.99}_{-1.06}$	$0.76^{+0.30}_{-0.19}$	1.22	1.15	37
NGC 6338	70	254	2.60	$2.34^{+0.08}_{-0.07}$	$3.03^{+0.30}_{-0.24}$	$1.29^{+0.14}_{-0.11}$	$0.24^{+0.04}_{-0.03}$	1.06	1.00	54
PKS 0745-191	69	460	40.80	$8.30^{+0.39}_{-0.36}$	$9.69^{+0.84}_{-0.73}$	$1.17^{+0.12}_{-0.11}$	$0.42^{+0.06}_{-0.07}$	1.01	0.97	93
RBS 0797	70	350	2.22	$7.63^{+0.94}_{-0.77}$	$8.62^{+2.60}_{-1.69}$	$1.13^{+0.37}_{-0.25}$	$0.25^{+0.13}_{-0.13}$	1.06	0.83	93
RDCS 1252-29	68	188	6.06	$4.63^{+2.39}_{-1.41}$	$4.94^{+9.84}_{-2.82}$	$1.07^{+2.20}_{-0.69}$	$1.14^{+2.11}_{-0.83}$	1.36	0.28	60
RX J0232.2-4420	69	402	2.53	$7.92^{+0.85}_{-0.74}$	$10.54^{+2.53}_{-1.74}$	$1.33^{+0.35}_{-0.25}$	$0.38^{+0.13}_{-0.13}$	1.05	0.98	91
RX J0340-4542	69	279	1.63	$3.10^{+0.43}_{-0.38}$	$2.75^{+1.15}_{-0.67}$	$0.89^{+0.39}_{-0.24}$	$0.63^{+0.39}_{-0.28}$	1.22	1.30	48
RX J0439+0520	69	322	10.02	$4.67^{+0.58}_{-0.47}$	$5.37^{+2.03}_{-1.24}$	$1.15^{+0.46}_{-0.29}$	$0.36^{+0.22}_{-0.20}$	0.91	0.81	85
RX J0439.0+0715 †	69	376	11.16	$5.65^{+0.38}_{-0.34}$	$8.21^{+1.29}_{-0.96}$	$1.45^{+0.25}_{-0.19}$	$0.34^{+0.09}_{-0.09}$	1.32	1.14	87
RX J0528.9-3927	69	452	2.36	$7.96^{+1.01}_{-0.81}$	$9.84^{+2.92}_{-1.81}$	$1.24^{+0.40}_{-0.28}$	$0.26^{+0.14}_{-0.15}$	0.96	1.04	88
RX J0647.7+7015 †	69	362	5.18	$11.46^{+2.05}_{-1.58}$	$11.18^{+2.46}_{-1.77}$	$0.98^{+0.28}_{-0.20}$	$0.24^{+0.18}_{-0.20}$	1.00	0.92	88
RX J0819.6+6336	70	308	4.11	$3.92^{+0.46}_{-0.40}$	$3.24^{+1.26}_{-0.66}$	$0.83^{+0.34}_{-0.19}$	$0.16^{+0.17}_{-0.14}$	1.00	1.00	50
RX J0910+5422 †	70	165	2.07	$4.08^{+3.11}_{-1.34}$	$5.00^{+5.09}_{-2.03}$	$1.23^{+1.56}_{-0.64}$	$0.43^{+1.89}_{-0.43}$	0.64	0.56	42
RX J1347.5-1145 †	68	431	4.89	$15.12^{+1.03}_{-0.86}$	$17.32^{+1.73}_{-1.40}$	$1.15^{+0.14}_{-0.11}$	$0.33^{+0.07}_{-0.08}$	1.12	1.11	96
RX J1350+6007	68	227	1.77	$4.22^{+3.13}_{-1.53}$	$3.29^{+10.52}_{-1.93}$	$0.78^{+2.56}_{-0.54}$	$0.63^{+5.75}_{-0.63}$	1.00	0.14	66
RX J1423.8+2404 †	70	301	2.65	$6.90^{+0.39}_{-0.37}$	$7.19^{+0.59}_{-0.52}$	$1.04^{+0.10}_{-0.09}$	$0.38^{+0.07}_{-0.08}$	0.94	0.90	90
RX J1504.1-0248	69	445	6.27	$8.02^{+0.58}_{-0.52}$	$8.52^{+0.94}_{-0.50}$	$1.06^{+0.08}_{-0.07}$	$0.39^{+0.04}_{-0.05}$	1.25	1.17	95
RX J1532.9+3021 †	69	323	2.21	$6.06^{+0.43}_{-0.39}$	$7.20^{+0.94}_{-0.77}$	$1.19^{+0.18}_{-0.15}$	$0.46^{+0.10}_{-0.11}$	0.92	1.02	83
RX J1716.9+6708	68	328	3.71	$6.51^{+1.79}_{-1.24}$	$6.21^{+4.03}_{-2.26}$	$0.95^{+0.67}_{-0.39}$	$0.56^{+0.39}_{-0.32}$	0.84	0.92	63
RX J1720.1+2638	70	361	4.02	$6.33^{+0.29}_{-0.25}$	$7.71^{+0.84}_{-0.72}$	$1.22^{+0.14}_{-0.12}$	$0.37^{+0.07}_{-0.07}$	1.04	0.96	94
RX J1720.2+3536 †	70	320	3.35	$7.34^{+0.59}_{-0.50}$	$7.40^{+0.86}_{-0.71}$	$1.01^{+0.14}_{-0.12}$	$0.43^{+0.11}_{-0.11}$	1.03	0.94	91
RX J2011.3-5725	70	283	4.76	$4.10^{+0.47}_{-0.39}$	$3.93^{+0.98}_{-0.70}$	$0.96^{+0.26}_{-0.20}$	$0.41^{+0.24}_{-0.20}$	0.95	1.08	84
RX J2129.6+0005	70	488	4.30	$6.01^{+0.55}_{-0.46}$	$7.19^{+1.68}_{-1.21}$	$1.20^{+0.30}_{-0.22}$	$0.51^{+0.16}_{-0.15}$	1.29	1.34	87
S0463 †	69	294	1.06	$3.26^{+0.33}_{-0.38}$	$3.92^{+1.16}_{-0.94}$	$1.20^{+0.38}_{-0.32}$	$0.23^{+0.18}_{-0.15}$	1.08	1.08	54
TRIANG AUSTR	70	516	13.27	$9.37^{+0.32}_{-0.30}$	$14.68^{+1.18}_{-1.08}$	$1.57^{+0.14}_{-0.13}$	$0.09^{+0.04}_{-0.04}$	0.01	1.89	88
V 1121.0+2327	71	302	1.30	$4.17^{+0.78}_{-0.60}$	$4.70^{+3.00}_{-1.17}$	$1.13^{+0.75}_{-0.32}$	$0.46^{+0.36}_{-0.28}$	1.09	0.87	74
ZWCL 1215	69	277	1.76	$6.63^{+0.45}_{-0.40}$	$7.64^{+1.34}_{-1.00}$	$1.15^{+0.22}_{-0.17}$	$0.37^{+0.11}_{-0.11}$	1.10	1.04	91
ZWCL 1358+6245	69	375	1.94	$9.70^{+1.16}_{-0.94}$	$9.04^{+2.09}_{-1.46}$	$0.93^{+0.24}_{-0.18}$	$0.57^{+0.19}_{-0.19}$	1.03	0.90	65
ZWCL 1953	69	517	3.10	$8.28^{+1.25}_{-0.96}$	$15.12^{+11.45}_{-5.45}$	$1.83^{+1.41}_{-0.69}$	$0.20^{+0.14}_{-0.15}$	0.87	0.74	82
ZWCL 3146	70	512	2.70	$7.46^{+0.32}_{-0.30}$	$8.99^{+0.94}_{-0.78}$	$1.21^{+0.14}_{-0.12}$	$0.31^{+0.06}_{-0.05}$	1.06	0.97	91
ZWCL 5247	69	430	1.70	$4.89^{+0.86}_{-0.65}$	$4.39^{+2.30}_{-1.21}$	$0.90^{+0.50}_{-0.27}$	$0.37^{+0.30}_{-0.25}$	1.09	0.93	78
ZWCL 7160	70	451	3.10	$4.64^{+0.41}_{-0.37}$	$6.82^{+2.26}_{-1.44}$	$1.47^{+0.50}_{-0.33}$	$0.36^{+0.14}_{-0.14}$	0.94	0.76	87

Cavagnolo et al.

TABLE 5 — *Continued*

Cluster	R_{CORE} kpc	R_{5000} kpc	N_{HI} 10^{20} cm^{-2}	T_{77} keV	T_{27} keV	T_{HBR}	Z_{77} $Z_\odot$	$\chi^2_{red,77}$	$\chi^2_{red,27}$	% Source
(1)	(2)	(3)	(4)	(5)	(6)	(7)	(8)	(9)	(10)	(11)
ZWICKY 2701	69	315	0.83	$5.08^{+0.32}_{-0.30}$	$4.96^{+0.87}_{-0.69}$	$0.98^{+0.18}_{-0.15}$	$0.45^{+0.13}_{-0.11}$	0.95	0.76	70
ZwCL 1332.8+5043	71	434	1.10	$3.82^{+3.34}_{-1.42}$	$2.86^{+3.96}_{-1.21}$	$0.75^{+1.23}_{-0.42}$	$0.16^{+4.75}_{-0.16}$	0.71	0.95	60
ZwCl 0848.5+3341	70	350	1.12	$6.54^{+2.04}_{-1.27}$	$6.41^{+3.79}_{-1.88}$	$0.98^{+0.66}_{-0.34}$	$0.59^{+0.59}_{-0.48}$	0.89	1.01	47

NOTE. — Note: '77' refers to 0.7-7.0 keV band, '27' refers to 2.0_{rest}-7.0 keV band. (1) Cluster name, (2) excluded core region in kpc, (3) R_{5000} in kpc, (3) absorbing, Galactic neutral hydrogen column density, (4,5) best-fit MeKaL temperatures, (6) best-fit 77 MeKaL abundance, (7) $T_{0.7-7.0}/T_{2.0-7.0}$ also called T_{HBR}, (8,9) reduced χ^2 statistics, (10) percent of emission attributable to source. † indicates cluster with multiple independent, simultaneously fit spectra.